CHARACTERIZATION OF THE SOLUTE TRANSPORT PROPERTIES OF THE ACTIVE LAYERS OF POLYAMIDE THIN FILM COMPOSITE MEMBRNES

Jingbo Wang

A dissertation submitted to the faculty at the University of North Carolina at Chapel Hill in partial fulfillment of the requirements for the degree of Doctor of Philosophy in the Department of Environmental Sciences and Engineering in the Gillings School of Global Public Health.

Chapel Hill
2018

Approved by:

Orlando Coronell

Michael Aitken

David Couper

Rene Lopez

Jill Stewart

ABSTRACT

Jingbo Wang: Characterization of the Solute Transport Properties of the Active Layers of Polyamide Thin Film Composite Membranes
(Under the direction of Orlando Coronell)

The overall objective of this study was to elucidate which parameter among solute partitioning, solute diffusion, and active layer thickness accounts for the differences in solute permeability among polyamide active layers of thin film composite (TFC) membranes. To accomplish the overall goal of this project, the following specific objectives were pursued: (i) to develop a method to measure solute partition coefficient (K_S) from aqueous solution into polyamide active layer of TFC membranes; (ii) to quantify the solute partition (K_S) and diffusion coefficient (D_S) inside polyamide active layers of TFC membranes with a broad range of performance levels; (iii) to determining which parameter among solute partition coefficient (K_S), solute diffusion coefficient (D_S) and active layer thickness (δ) accounts for the most difference in solute permeation among TFC membranes with a broad range of performance levels.

The following major conclusions were drawn through this dissertation: (i) for all membranes, the partition coefficients of all inorganic salts and small acids obtained experimentally were lower than 1 and the partition coefficient did not differ much among different TFC membranes; (ii) for all membranes tested, Donnan theory provided an appropriate theoretical framework to predict the effect of pH on salt partitioning and salt rejection; (iii) changes in salt rejection with feed solution pH are primarily driven by changes in salt partitioning with likely minimal (or absent) changes in salt diffusion; (iv) geometrical properties of active layers (thickness, pore volume fraction, roughness) do not account for the differences in

salt permeability observed among membranes, and (v) the differences in salt permeability observed among membranes are mainly due to the differences in both salt partition and diffusion coefficients in active layers.

ACKNOWLEDGEMENTS

I would like to express my sincerest appreciation to my advisor, Dr. Orlando Coronell. Thank you for your support, patience, attention to detail, and demand for excellence. You have been sharing your expertise and wisdom through guiding and mentoring. It was such a pleasure to have you as my Ph.D. advisor.

I would like to express my gratitude to Dr. Mike Aitken, Dr. Rene Lopez, Dr. Jill Stewart and Dr. David Couper for being part of my PhD committee. You have always been so willing to help me throughout my PhD study by offering insightful feedback and encouragement. I cannot thank you enough for your assistance and support. I am honored to have you as members of my committee.

To the members of my American family, the Coronell Group (former and current members), thank you for making my graduate school experience such a pleasant journey full of love and laughter. Special thanks to Lin Lin, Tony Perry, Panitan Jutaporn, Josh Powella, Ariel Atkinson, Ryan Kingsbury, Kasia Grzebyk and Mikayla Armstrong, for your assistance on experiments and insightful discussions, for all the company and support in labs even at nights and weekends.

Also, I would like to thank Dr. Tom Clegg, Dr. Grayson Rich, Dr. Carrie Donley, and Wallace Ambrose, for your generous help with carrying out all the characterization experiments.

I would like to acknowledge the faculty and staff within the Department of Environmental Sciences and Engineering, most notably Rebecca Gunn, Dr. Glenn Walters, Jac

Whaley, Wake Harper. My graduate school has been so much happier and easier with your unwavering support.

I want to acknowledge my dearest parents and friends. None of this would be possible without your love and support. Thank you for helping me survive, thrive and become a doctor.

TABLE OF CONTENTS

LIST OF TABLES xi

LIST OF FIGURES xii

LIST OF ABBREVIATIONS xv

CHAPTER 1 - INTRODUCTION 1

1.1 Background and Motivation 1

1.1.1 The importance and structure of polyamide reverse osmosis and nanofiltration membranes 1

1.1.2 Mechanisms of water and solute permeation through TFC membranes 2

1.1.3 State of art of measurements of partition and diffusion coefficients in polyamide active layer 4

1.1.4 Gaps in the literature regarding the mechanisms of solute transport through polyamide active layers 5

1.2 Objectives 7

1.2.1 Overall research goal 7

1.2.2 Specific objectives 7

1.3 Dissertation organization 8

REFERENCES 10

CHAPTER 2 – PARTITIONING OF ALKALI METAL SALTS AND BORIC ACID FROM AQUEOUS PHASE INTO THE POLYAMIDE ACTIVE LAYERS OF REVERSE OSMOSIS MEMBRANES 12

2.1 Introduction 12

2.2 Materials and Methods 14

2.2.1 Chemicals and solutions 14

2.2.2 Membranes 14

2.2.3 Membrane sample preparation 15

2.2.4 Measurement of areal mass of active layer and change in areal mass of the active layer when exposed to test solutions 15

2.2.5 Partitioning tests 16

2.2.6 QCM analyses 17

2.2.7 Theoretical estimation of partition coefficients 18

2.3 Results and discussion 19

2.3.1 Measured changes in areal mass of coated QCM sensors during partitioning tests 19

2.3.2 Estimation of solute partition coefficients in polyamide 20

2.3.3 Estimation of net solute partition coefficients in active layer 30

2.3.4 Effect of bulk solution pH on salt partitioning 33

2.3.5 Comparison of experimental solute partitioning values to values predicted using the Donnan and Manning theories 34

2.4 Conclusion 37

2.5 Acknowledgments 38

REFERENCES 39

CHAPTER 3 – EFFECT OF FEED WATER PH ON PARTITIONING OF ALKALI METAL SALTS FROM AQUEOUS PHASE INTO THE POLYAMIDE ACTIVE LAYERS OF REVERSE OSMOSIS MEMBRANES 43

3.1 Introduction 43

3.2 Materials and Methods 45

3.2.1 Chemicals and solutions 45

3.2.2 Membranes 45

3.2.3 Membrane sample preparation 46

3.2.4 QCM analyses 46

3.2.5 Evaluation of Partitioning at pH 5.3 47

3.2.6 Evaluation of pH effect on salt partitioning 48

3.2.7 Calculation of partition coefficients in active layers 49

3.2.8 Prediction of effect of pH on salt partition coefficient in active layers 53

3.2.9 Membrane performance tests 54

3.2.10 Prediction of effect of pH on salt rejection 55

3.3 Results and Discussion 56

3.3.1 Partitioning at pH 5.3 56

3.3.2 Effect of pH on NaCl partitioning 58

3.3.3 Effect of pH on the partitioning of other chloride salts of alkali metals 63

3.3.4 Donnan theory prediction of the effect of pH on salt rejection 65

3.4 Conclusion 67

3.5 Acknowledgements 68

REFERENCES 69

CHAPTER 4 – RELATIVE IMPORTANCE OF GEOMETRICAL AND INTRINSIC SALT TRANSPORT PROPERTIES OF ACTIVE LAYERS IN THE SALT REJECTION BY POLYAMIDE THIN-FILM COMPOSITE MEMBRANES 75

4.1 Introduction 75

4.2 Materials and Methods 77

4.2.1 Salts and feed waters 77

4.2.2 Membranes and membrane sample preparation 77

4.2.3 Salt permeation tests 78

4.2.4 Transmission electron microscopy analyses 81

4.2.5 Atomic force microscopy analyses 81

4.2.6 Quartz crystal microbalance analyses 81

4.2.7 Calculation of void fractions of active layers 82

4.2.8 Calculation of active layer thickness 82

4.2.9 Pore diameter measurements 84

4.2.10 Calculation of salt partition coefficients 84

4.2.11 Statistical correlation analyses 85

4.3 Results and discussion 86

4.3.1 Correlation between solute permeation coefficient and geometrical properties of active layer. 86

4.3.2 Correlation between solute permeation coefficient and salt permeability 91

4.3.3 Salt partition and diffusion coefficients in the active layer 92

4.3.4 Correlation between salt permeability and salt partition and diffusion coefficients. 94

4.3.5 Correlation between solute permeation coefficient and water permeance in the active layer 97

4.4 Conclusion 98

4.5 Acknowledgment 99

REFERENCES 101

CHAPTER 5 - CONCLUSIONS 105

CHAPTER 6 - FUTURE WORK 108

APPENDIX A: SUPPORTING INFORMATION FOR CHAPTER 2 110

REFERENCES 134

APPENDIX B: SUPPORTING INFORMATION FOR CHAPTER 3 136

APPENDIX C: SUPPORTING INFORMATION FOR CHAPTER 4 141

REFERENCES 153

LIST OF TABLES

Table 2.1. Summary of partition coefficients (K_p and K_{net}) of CsCl, RbCl, KCl, NaCl, LiCl and boric acid in the polyamide active layer of the SWC4+ membrane at pH=5.3. Scenarios A and B assume unhydrated and hydrated solutes, respectively, in the polyamide phase. Reported values and uncertainties correspond to the average and standard deviation of triplicate samples. 31

Table 3.1. Summary of salts and pH conditions evaluated for each membrane in partitioning tests. 48

Table 3.2. Summary of partition coefficients [a] of CsCl, RbCl, KCl, NaCl and LiCl in the polyamide active layer of SWC4+, XLE, ESPA3, NF90, and TFC membranes at pH 5.3. Scenarios A and B assume unhydrated and hydrated solutes in the polyamide phase, respectively. 56

Table 3.3. Measured layer thicknesses, charge densities and void fractions for membrane active layers. Reported values and uncertainties correspond to the average and standard deviation of duplicate samples. 61

Table 4.1. Geometric and solute transport properties of membrane active layers: total thickness (δ_{AL}), top film thickness (δ_{TF}), pore volume fraction (f), mean pore diameter (d), surface roughness (σ), solute permeation coefficient (B), salt partition coefficient in the active layer polymer (K_p), salt diffusion coefficient in the active layer polymer assuming complete interconnectivity among pores ($D_{p,Cl}$), salt partition coefficient in the active layer (K_{AL}), salt diffusion coefficient in the active layer (D_{AL}) and water permeability coefficient (A). All the salt properties correspond to NaCl properties unless otherwise specified. Uncertainties represent standard deviations between duplicate or triplicate samples. The values of geometric properties of XLE, ESPA3, and NF90 have been reproduced from reference 31 since the membranes were the same used in that study. 88

LIST OF FIGURES

Figure 2.1. Representative results for the increase in the areal mass of a coated QCM sensor when exposed to a sequence of (a) NaCl and (b) boric acid solutions (pH=5.3) with increasing solute concentration. The polyamide active layer coating the sensor was that of the SWC4+ membrane. 21

Figure 2.2. Partition coefficient in the polyamide phase of the active layer (K_p) as a function of solute concentration in bulk solution ($C_{S,bulk}$) assuming that solutes in the polyamide active layer (a) are unhydrated (Scenario A) and (b, c) have the same hydration number as in bulk solution (Scenario B). Panels (a) and (b) present results for all solutes at pH=5.3. Panel (c) presents results for NaCl at pH=5.3 and 8.0 obtained during the same experimental run,and includes predictions of K_p at pH=8.0 (empty symbols) based on the experimental results at pH=5.3 and Donnan exclusion theory. Partition coefficients were calculated based on the areal mass changes (Δm) measured for the coated sensors when exposed to test solutions. Δm values for boric acid, LiCl, NaCl, KCl, RbCl, and CsCl were above the limit of quantification (33 ng.cm^{-2}, see SI) for $C_{S,bulk} \geq$ 0.1, 0.3, 0.2, 0.05, 0.005, and 0.005 M, respectively. At $C_{S,bulk} > C_{FC}$ = 0.061 M it is ensured that 95% or more of any measured Δm is due to mobile salt partitioned into the active layer, and not excess cations saturating negative fixed charges. The relatively high K_p calculated for RbCl and CsCl at $C_{S,bulk}$ = 0.005 and 0.01 M were likely the result of counter-ions neutralizing additional fixed charges in polyamide not neutralized with the reference 1 mM solutions (see main text). Note that the NaCl partitioning results at pH=5.3 in panels (a) and (c) are different by 17% on average. This is likely the result of a 2.5 year storage time of the coated sensors (in the original plastic storage boxes) between the experiments in the two panels. 29

Figure 2.3. Parity plot comparing experimentally-determined salt partition coefficients in the polyamide phase (K_p) of the active layer of the SWC4+ membrane with predictions of Donnan-Manning theory when using (a) ion hydration numbers (n) equal to those in bulk solution (Scenario B), and (b) ion hydration numbers fitted to maximize agreement between experimental results and Donnan-Manning predictions..... 36

Figure 3.1. Representative $\Delta m_{XCl,AL}$ results for the increase in the areal mass of a coated QCM sensor when exposed to 1 M NaCl solution at pH 5.3. Data shown corresponds to sensors coated with the polyamide active layers of the (a) ESPA3 and (b) NF90 membranes. Each bar in each panel corresponds to independent tests performed with the same set of sensors; the sensors were unmounted from the QCM, rinsed, dried, and remounted on the QCM in between tests. In each panel, from left to right, bars correspond to data obtained when the sensors were exposed to (1) pH=5.3, (2) pH=5.3 after exposure to pH 8.0, (3) pH=5.3 after exposure to pH 10.5, and (4) pH=5.3 after tests (1) through (3). 52

Figure 3.2. Partition coefficient of NaCl in the polyamide phase (K_p) of representative active layer samples from (a) SWC4+ (b) XLE (c) ESPA3 (d) NF90 and (e) TFC membranes as a function of solute concentration in bulk solution ($C_{S,bulk}$) assuming that solutes in polyamide have the same hydration number as in bulk solution (Scenario B). All panels present results at pH 5.3 and 10.5 (solid symbols) obtained during the same experimental run, and include predictions of K_p at pH 10.5 (empty symbols) based on the experimental results at pH 5.3 and Donnan theory (Equation 11). Only mass changes greater than the limit of quantification (LOQ = 33 ng.cm^{-2}) from QCM tests were used for calculations, which correspond to $C_{S,bulk}$ > 0.1M in this set of experiments.[7,32] 60

Figure 3.3. Partition coefficient of NaCl in polyamide phase of representative active layer samples (K_p) from (a) XLE (b) ESPA3 (c) NF90 (d) SWC4+ and (e) TFC membranes as a function of solute concentration in bulk solution ($C_{S,bulk}$) assuming that solutes in the polyamide layer have the same hydration number as in bulk solution (Scenario B). All panels present results at pH 5.3 and 8.0 (solid symbols) obtained during the same experimental run, and include predictions of K_p at pH 8.0 (empty symbols) based on the experimental results at pH 5.3 and Donnan exclusion theory. 63

Figure 3.4. Partition coefficient in the polyamide phase (K_p) of XLE membrane as a function of solute concentration in bulk solution ($C_{S,bulk}$) assuming that solutes in the polyamide layer have the same hydration number as in bulk solution (Scenario B). Panels (a), (b), (c) and (d) present results for LiCl, KCl, RbCl, and CsCl, respectively. All panels present results at pH 5.3 and 10.5 obtained during the same experimental run, and include predictions of K_p at pH 10.5 (empty symbols) based on the experimental results at pH 5.3 and Donnan exclusion theory. Partition coefficients were calculated based on the areal mass changes ($\Delta m_{XCl,AL}$) measured for the coated sensors when exposed to test solutions..... 65

Figure 3.5. Rejection of sodium chloride (NaCl) as a function of pH by the (a) SWC4+, (b) XLE, (c) ESPA3, (d) NF90 and (e) TFC membranes. Red and green indicate pH values of 5.3 and 10.5, respectively. Continuous lines correspond to model fitting results, and dashed lines correspond to model predictions. A summary of fitted and predicted model parameters is presented in Table 3.4. 67

Figure 4.1. Schematic of cross-flow membrane filtration system used in permeation tests. Solid lines, dot-dashed lines, and dashed lines represent feed water lines, permeate lines and membranes, respectively. 81

Figure 4.2. Representative cross-sectional TEM image of a polyamide thin-film composite membrane. The image shown corresponds to that of a sample of the homemade TFC membrane. The red lines outline the perimeter of the active layer. The dense top film is delimited by the membrane surface (top red line) and the first set of pores from the surface (blue line). 84

Figure 4.3. Solute permeation coefficient of NaCl (B) as a function of geometrical properties of the active layer including (a) thickness, (b) surface roughness, (c) pore fraction and (d) pore diameter In panel (a), results for total thickness (δ_{AL}) and top film thickness (δ_{TF}) are presented. Values and error bars for δ represent average and standard deviation of duplicate samples, respectively. Values and error bars for B, σ, f, and d represent average and standard deviation of triplicate samples, respectively. 90

Figure 4.4. Salt diffusive permeation coefficient of NaCl (B) as a function of salt permeability (P_S). Values and error bars for B and P_S represent average and standard deviation of triplicate samples, respectively. Values and error bars represent average and standard deviation, respectively, for triplicate samples. 92

Figure 4.5. Salt permeability of NaCl (P_S) as a function of (a) salt partition coefficient in the active layer polymer assuming salt was not hydrated during partitioning ($K_{p,\ unhydrated}$) and assuming salt was fully hydrated during partitioning ($K_{p,\ hydrated}$), and (b) salt diffusion coefficient calculated with unhydrated partition coefficient ($D_{p,\ unhydrated}$) and salt diffusion coefficient calculated with hydrated partition coefficient ($D_{p,\ hydrated}$). Values and error bars represent average and standard deviation, respectively, for triplicate samples. 95

Figure 4.6. Salt permeability of NaCl (P_S) as a function of (a) salt partition coefficient in the whole active layer assuming salt was not hydrated during partitioning ($K_{AL,\ unhydrated}$) and assuming salt was fully hydrated during partitioning ($K_{AL,\ hydrated}$), and (b) salt diffusion coefficient calculated with unhydrated partition coefficient ($D_{AL,\ unhydrated}$) and salt diffusion coefficient calculated with hydrated partition coefficient ($D_{AL,\ hydrated}$). Values and error bars represent average and standard deviation, respectively, for triplicate samples. 97

Figure 4.7. Solute permeation coefficient of NaCl (B) as a function of water permeability coefficient (A). Values and error bars represent average and standard deviation, respectively, for triplicate samples..... 98

LIST OF ABBREVIATIONS

AFM	Atomic force microscopy
AL	active layer
CsCl	cesium chloride
DMF	dimethylformamide
KCl	potassium chloride
LiCl	lithium chloride
NaCl	sodium chloride
NF	nanofiltration
QCM	quartz crystal microbalance
RBS	Rutherford backscattering spectrometry
RO	reverse osmosis
RbCl	rubidium chloride
SS	stainless steel
TEM	transmission electron microscopy
TFC	thin-film composite

CHAPTER 1 - INTRODUCTION

1.1 Background and Motivation

1.1.1 The importance and structure of polyamide reverse osmosis and nanofiltration membranes

The growing demands of municipalities, industry, and agriculture for potable water have provoked a water deficit that threatens global energy, food, and economic security. Limited freshwater access, contamination of existing water sources and severe droughts highlight the need to expand water supply portfolios that take advantage of treating impaired supply sources such as seawater, brackish water, and wastewater effluent. Membrane separation processes, such as reverse osmosis (RO) and nanofiltration (NF), which have the capability to remove a broad range of contaminants (e.g., inorganic salts, small organics) from water, offer promising low-energy solutions for desalination and wastewater treatment. [1–5]

Most commercial RO/NF membranes have a thin-film composite (TFC) structure. The top selective layer (~20-200 nm), which is referred to as the active layer, is based on a fully aromatic polyamide formed by interfacial polymerization of *meta*-phenylenediamine (MPD) and trimesoyl chloride (TMC).[3,6,7] The porous support layers are consist of an intermediate polysulfone layer (~20-50 μm) and a polyester backing layer (~50-150 μm).[3,6] The highly cross-linked top layer constitutes the main barrier to water and solute transport, while the other two layers mainly provide stronger mechanical support to the active layer. The active layer removes contaminants in the source water through a combination of size exclusion, electrostatic repulsion, and the relatively low permeation of contaminants through the membrane compared to water.[6]

1.1.2 Mechanisms of water and solute permeation through TFC membranes

As effective and efficient as current membrane technologies are, there is always a continued need to expand and improve their capabilities with growing needs and applications. [4,8–10]. A fundamental understanding of the mechanism plays a crucial role in guiding intelligent membrane material modifications and process optimization.[11,12] Current transport models assume that water and solute permeation are controlled by the interactions between the permeating molecule and the active layer.[13–16] The solution-diffusion model is the most widely accepted theory assuming a solution-diffusion permeation mechanism. In this model, the active layer is assumed to be a dense uniform layer, and both water and solute permeate through the active layer in three steps: (1) water and solutes partition into the active layer at the interface between the feed water (the water that needs to be treated) and the active layer, (2) water and solutes diffuse through the active layer, and (3) water and solutes partition out of the active layer to the permeate (purified water) side.[14–17] The performance of a TFC membrane can be evaluated by water productivity (measured as water flux) and contaminant removal rate (measured as solute rejection).

In the solution diffusion model, water flux, J_V (m.d^{-1}), is expressed as

$$J_V = A\,(\Delta p - \Delta\pi) \quad , \tag{1.1}$$

where A (m.d^{-1}.psi^{-1}), is the water permeability coefficient of the active layer, Δp (psi) is the applied trans-membrane pressure, and $\Delta\pi$ (psi) is the trans-membrane osmotic pressure.

Solute rejection R (unitless) can be calculated as

$$\mathrm{R} = 1 - \frac{C_P}{C_F} \quad , \tag{1.2}$$

where C_p (M) and C_F (M) are the solute concentrations in the permeate and feed water,

respectively. Solute passage through the membrane, J_S (mol.m^{-2}.d^{-1}), can be calculated from[16,18,19]

$$J_s = J_V C_p = B\,(C_w - C_P) + \bar{\alpha} J_V C_w \quad , \tag{1.3}$$

where C_w (M) is the solute concentration in the feed side next to the membrane wall, B (m.d^{-1}) is the diffusive permeation coefficient, and $\bar{\alpha}$ (unitless) is the advective transport coefficient. In Equation 1.3, the solute diffusive permeation coefficient, B, is defined as

$$B = \frac{D_S K_S}{\delta} \quad , \tag{1.4}$$

where D_S (m^2.d^{-1}) is the solute diffusion coefficient inside the active layer, K_S (unitless) is the solute partition coefficient at the membrane-feed interface, and δ (m) is the active layer thickness.

In Equation 1.3, the solute concentration next to the membrane wall, C_w, is higher than that in the bulk feed, C_F, because of concentration polarization.[20] At steady state, C_F, C_p, and C_w are related by[20]

$$\frac{C_w - C_P}{C_F - C_P} = \exp\left(\frac{J_V}{k}\right) \quad , \tag{1.5}$$

where k (m.d^{-1}) is the solute mass transfer coefficient in the concentration polarization layer. Combining Equations 1.2, 1.3, and 1.5 yields

$$R = 1 - \frac{C_P}{C_F} = \frac{(1-\bar{\alpha})J_V}{(B+\bar{\alpha}J_V)\exp\left(\frac{J_V}{k}\right)+(1-\bar{\alpha})J_V} \quad , \tag{1.6}$$

where C_p, C_F, and J_v can be measured from experiments, and $\bar{\alpha}$, B and k can be obtained by fitting C_p, C_F, and J_v data.

The key membrane properties that affect membrane performance in terms of solute rejection are the solute partition coefficient, diffusion coefficient and active layer thickness. The

ability to quantify these parameters and evaluate the relative importance of these properties to salt rejection would help to advance the fundamental understanding of solute transport mechanism through the membrane.

1.1.3 State of art of measurements of partition and diffusion coefficients in polyamide active layer

In spite of the importance of the solute partition and diffusion coefficients in active layers in understanding what contributes to the variance in contaminant rejection for two different membranes, neither property has been thoroughly characterized in literature. Given that the time scale of diffusion of solutes through active layers is very short (on the order of microseconds), measuring diffusion coefficients in polyamide active layers represents a substantial experimental challenge, and to our knowledge, there are no reported experimental methods to measure D_S in aromatic polyamide active layers, except for an electrochemical method[21] applicable only to redox couples, which are not contaminants of common interest in water purification.

Regarding the measurement of partition coefficients, standard methods used for relatively thick films, such as solute desorption,[22,23] are not applicable to polyamide active layers because of their extreme thinness. Nevertheless, two methods have been reported to measure partition coefficients in polyamide active layers. One of these methods was developed for organic solutes (e.g., urea, hydroquinone), and uses attenuated total reflection Fourier transform infrared spectroscopy (ATR-FTIR) for sample analyses.[24–26] The second method was developed for solutes containing relatively heavy elements (e.g., arsenic, iodine), and is based on Rutherford backscattering spectrometry (RBS) measurements.[27,28] Neither of these two methods is applicable to the inorganic, low-molecular weight contaminants of common interest in water purification applications (e.g., seawater desalination, softening) such as sodium chloride (NaCl), boric acid (H_3BO_3), or hardness (i.e., calcium, Ca^{2+}, and magnesium, Mg^{2+}). Specifically, the

ATR-FTIR method is not applicable because the calculation of partition coefficient is based on the intensities of the solute bands in the spectra of the bare and polyamide-covered crystals but only solutes that preferentially partition into the membrane, such as aromatics and large alcohols, yield to the highest quality data that could be used in calculations. The measurements with the inorganic solutes and thinner NF membranes were substantially more difficult and only rough estimates and general trends can be obtained.[16] Further, the RBS method is not applicable because inorganic contaminants of common interest (e.g., NaCl, H_3BO_3, Ca^{2+}) are relatively light and are not easily detected by RBS in the concentrations that they would exist in the active layer.[12,13]

Therefore, there is a need to develop an experimental method to quantify the partition coefficients (K_S) of inorganic solutes of common interest into active layers of the whole spectrum of TFC membranes. Given that B can be easily obtained experimentally,[17] the ability to measure K_S would also enable the calculation of D_S from Equation 4, thus providing a complete picture of the mechanisms controlling the permeation of inorganic contaminants of common concern through TFC membranes.

Note that the main reason for the very limited amount of studies on solute portioning and diffusion in a membrane active layer is the experimental challenges in characterizing material properties occurring in the bulk region of the active layers. Nanoscale spatial resolution is required to probe the bulk region of the active layer.

1.1.4 Gaps in the literature regarding the mechanisms of solute transport through polyamide active layers

Based on the background discussed in Sections 1.1.1-1.1.3, the following gaps exist in the literature that must be overcome to achieve a more complete understanding of the

mechanisms of solute transport through the polyamide active layers of TFC membranes:

(1) There are very few experimental measurements of solute partitioning in polyamide active layers available;

(2) There is no accurate, reliable experimental method in the literature to measure solute partition coefficients, especially the inorganic solutes of common concern in water treatment processes;

(3) There is no literature that reported solute diffusion coefficients in the polyamide active layers;

(4) It is unknown what is the relative contribution of solute partition coefficient (K_S), solute diffusion coefficient (D_S) and active layer thickness (δ) to the different solute rejection between any two polyamide membranes;

1.2 Objectives

1.2.1 Overall research goal

The research goal of this project was to evaluate which among solute partitioning, solute diffusion, and active layer thickness accounts for the variance in solute permeability among polyamide active layers of thin film composite membranes.

1.2.2 Specific objectives

To achieve the overall research goal, the following specific objectives were pursued:

(1) Develop a method to measure the solute partition coefficient (K_S) from aqueous solution into the polyamide active layer of TFC membranes.

(2) Quantify the solute partition (K_S) and diffusion coefficient (D_S) inside polyamide active layers of TFC membranes with a broad range of performance levels;

(3) Determine which parameter among solute partition coefficient (K_S), solute diffusion coefficient (D_S) and active layer thickness (δ) accounts for the most difference in solute permeation among TFC membranes with a broad range of performance levels.

1.3 Dissertation organization

This dissertation comprises six chapters. Chapter 1 introduces the background and motivations of this research, setting the framework for the following chapters. Chapters 2-4 offers detailed research descriptions to address the overall and specific goals of the dissertation and each chapter is independently comprehensive with introductions, materials and methods, results and discussion, conclusions, acknowledgements, and reference sections. Chapters 2-4 are briefly described below:

Chapter 2: This chapter addresses specific objective 1. In this chapter, a bench-top method was developed to determine solute partition coefficients into the polyamide active layers of RO membranes. The method used a quartz crystal microbalance (QCM) to measure the change in the mass of the active layer caused by the uptake of the partitioned solutes. The detailed measurement method and data analysis were provided. The method was evaluated using several inorganic salts (alkali metal salts of chloride) and a weak acid of common concern in water desalination (boric acid). The seawater RO SWC4+ membrane was used as a model membrane for all the tests. The range of all measured partition coefficients were reported. Results were also compared and discussed with experimental values reported in the literature, as well as values predicted with Donnan and Manning theories.

Chapter 3: This chapter addresses specific objective 2. Solute partitioning and the effect of feed solution pH on partitioning were more thoroughly characterized in this work. I performed a comprehensive characterization of the partitioning of chloride salts of alkali metals (LiCl, NaCl, KCl, RbCl and CsCl) from the aqueous phase into the polyamide active layers of five polyamide TFC membranes, including one prepared in-house and four commercial membranes (SWC4+, XLE, ESPA3 and NF90), at three pH levels (5.3, 8.0 and 10.5). I also evaluated the

effect that pH has on the partitioning of alkali metal salts, and whether the pH dependence of salt partitioning and rejection are consistent with predictions from Donnan exclusion theory. The range of all measured partition coefficients were reported. Results were compared among different TFC membranes. I also evaluated whether Donnan theory provided an appropriate theoretical framework to predict the effect of pH on salt partitioning (evaluated for all chloride salts of alkali metals) and salt rejection (evaluated for NaCl). Then a conclusion was drawn regarding whether the changes in salt rejection with feed solution pH are primarily driven by changes in salt partitioning or changes in salt diffusion.

Chapter 4: This chapter addresses specific objective 3. In this chapter, I investigated what contributed to the difference in salt rejections of TFC membranes with fully aromatic polyamide active layers. Five membranes (the same membranes used in Chapter 3) including four commercial membranes (SWC4+, XLE, ESPA3 and NF90) and one fabricated in-house were studied in this work. For each membrane, membrane performance (water flux and salt rejection), diffusion coefficient and membrane active layer thickness were quantified and reported. Salt partition coefficients of each membrane were used from the measurements in Chapter 3. Through statistical analyses, conclusions were drawn regarding the relative contribution of these parameters to the difference in solute rejection among TFC membranes tested.

Chapter 5 summarizes the results from Chapters 2-4 and provides overall conclusions. Chapter 6 suggests future avenues of research to extend this work. The appendices following Chapter 6 includes more experimental details and supporting information referenced in Chapters 2-4.

REFERENCES

(1) Nicolaisen, B. Developments in membrane technology for water treatment. *Desalination* **2003**, *153* (1–3), 355–360.

(2) Malaeb, L.; Ayoub, G. M. Reverse osmosis technology for water treatment: State of the art review. *Desalination* **2011**, *267* (1), 1–8.

(3) Petersen, R. J. Composite reverse osmosis and nanofiltration membranes. *J. Membr. Sci.* **1993**, *83* (1), 81–150.

(4) Lee, K. P.; Arnot, T. C.; Mattia, D. A review of reverse osmosis membrane materials for desalination-Development to date and future potential. *J. Membr. Sci.* **2011**, *370* (1–2), 1–22.

(5) Pendergast, M. M.; Hoek, E. M. V. A review of water treatment membrane nanotechnologies. *Energy Environ. Sci.* **2011**, *4* (6), 1946–1971.

(6) Bellona, C.; Drewes, J. E.; Xu, P.; Amy, G. Factors affecting the rejection of organic solutes during NF/RO treatment - A literature review. *Water Res.* **2004**, *38* (12), 2795–2809.

(7) Xie, W.; Geise, G. M.; Freeman, B. D.; Lee, H.-S.; Byun, G.; McGrath, J. E. Polyamide interfacial composite membranes prepared from m-phenylene diamine, trimesoyl chloride and a new disulfonated diamine. *J. Membr. Sci.* **2012**, *403–404*, 152–161.

(8) Ulbricht, M. Advanced functional polymer membranes. *Polymer (Guildf).* **2006**, *47* (7), 2217–2262.

(9) Takht Ravanchi, M.; Kaghazchi, T.; Kargari, A. Application of membrane separation processes in petrochemical industry: a review. *Desalination* **2009**, *235* (1–3), 199–244.

(10) San Roman, M. F.; Bringas, E.; Ibanez, R.; Ortiz, I. Liquid membrane technology: Fundamentals and review of its applications. *J. Chem. Technol. Biotechnol.* **2010**, *85* (1), 2–10.

(11) Dworecki, K.; Ślęzak, A.; Ornal-Węsik, B.; Wąsik, S. Effect of hydrodynamic instabilities on solute transport in a membrane system. *J. Membr. Sci.* **2005**, *265* (1–2), 94–100.

(12) Wang, J.; Dlamini, D. S.; Mishra, A. K.; Theresa, M.; Pendergast, M.; Wong, M. C. Y.; Mamba, B. B.; Freger, V.; Verliefde, A. R. D.; Hoek, E. M. V. A critical review of transport through osmotic membranes. *J. Membr. Sci.* **2014**, *454*, 516–537.

(13) Bowen, W. R.; Welfoot, J. S. Modelling the performance of membrane nanofiltration-critical assessment and model development. *Chem. Eng. Sci.* **2002**, *57* (7), 1121–1137.

(14) Paul, D. R. Reformulation of the solution-diffusion theory of reverse osmosis. *J. Membr. Sci.* **2004**, *241* (2), 371–386.

(15) Szymczyk, A.; Fievet, P. Investigating transport properties of nanofiltration membranes by means of a steric, electric and dielectric exclusion model. *J. Membr. Sci.* **2005**, *252* (1–2), 77–88.

(16) Wijmans, J. G.; Baker, R. W. The solution-diffusion model: a review. *J. Membr. Sci.* **1995**, *107* (1–2), 1–21.

(17) Lin, L.; Feng, C.; Lopez, R.; Coronell, O. Identifying facile and accurate methods to measure the thickness of the active layers of thin-film composite membranes – a comparison of seven characterization techniques. *J. Membr. Sci.* **2015**, *498*, 167–179.

(18) Urama, R. I.; Mariñas, B. J. Mechanistic interpretation of solute permeation through a fully aromatic polyamide reverse osmosis membrane. *J. Membr. Sci.* **1997**, *123* (2), 267–280.

(19) Coronell, O.; Mi, B.; Mariñas, B. J.; Cahill, D. G. Modeling the effect of charge density in the active layers of reverse osmosis and nanofiltration membranes on the rejection of arsenic(III) and potassium iodide. *Environ. Sci. Technol.* **2013**, *47* (1), 420–428.

(20) Matthiasson, E.; Sivik, B. Concentration polarization and fouling. *Desalination* **1980**, *35*, 59–103.

(21) Bason, S.; Oren, Y.; Freger, V. Characterization of ion transport in thin films using electrochemical impedance spectroscopyII: Examination of the polyamide layer of RO membranes. *J. Membr. Sci.* **2007**, *302* (1–2), 10–19.

(22) Geise, G. M.; Freeman, B. D.; Paul, D. R. Sodium chloride diffusion in sulfonated polymers for membrane applications. *J. Membr. Sci.* **2013**, *427*, 186–196.

(23) Lonsdale, H. K.; Merten, U.; Riley, R. L.; Jay, J. Transport properties of cellulose acetate osmotic membranes. *J. Appl. Polym. Sci.* **1965**, *9*, 1341–1362.

(24) Freger, V.; Ben-David, A. Use of attenuated total reflection infrared spectroscopy for analysis of partitioning of solutes between thin films and solution. *Anal. Chem.* **2005**, *77* (18), 6019–6025.

(25) Ben-David, A.; Oren, Y.; Freger, V. Thermodynamic factors in partitioning and rejection of organic compounds by polyamide composite membranes. *Environ. Sci. Technol.* **2006**, *40* (22), 7023–7028.

(26) Bendavid, a; Bason, S.; Jopp, J.; Oren, Y.; Freger, V. Partitioning of organic solutes between water and polyamide layer of RO and NF membranes: Correlation to rejection. *J. Membr. Sci.* **2006**, *281* (1–2), 480–490.

(27) Mi, B.; Mariñas, B. J.; Cahill, D. G. RBS characterization of arsenic(III) partitioning from aqueous phase into the active layers of thin-film composite NF/RO membranes. *Environ. Sci. Technol.* **2007**, *41* (9), 3290–3295.

(28) Zhang, X.; Cahill, D. G.; Coronell, O.; Mariñas, B. J. Partitioning of salt ions in FT30 reverse osmosis membranes. *Appl. Phys. Lett.* **2007**, *91* (18), 181904.

CHAPTER 2 – PARTITIONING OF ALKALI METAL SALTS AND BORIC ACID FROM AQUEOUS PHASE INTO THE POLYAMIDE ACTIVE LAYERS OF REVERSE OSMOSIS MEMBRANES [*]

2.1 Introduction

Reverse osmosis (RO) membranes have the capability of removing a broad range of contaminants (e.g., inorganic salts, small organics) from water, and are among the most promising processes for clean water production from impaired sources such as seawater and treated wastewater.[1] Most commercial RO membranes have a thin-film composite (TFC) structure with a polyamide active layer (~20-200 nm) which constitutes the main barrier to water and solute transport, an intermediate polysulfone support layer (~20-50 μm), and a polyester backing layer (~50-150 μm).[2]

Within the framework of solution-diffusion theory, solute permeation through the active layer is the result of solute partitioning into the active layer, diffusion through the active layer, and partitioning out of the active layer.[3,4] The permeability of the active layer material to solutes (P_S, $m^2 \cdot s^{-1}$) is a function of the solute partition coefficient between water and active layer (K_S, unitless) and the solute diffusion coefficient within the active layer (D_S, $m^2 \cdot s^{-1}$) as given by

$$P_S = K_S D_S \quad . \tag{2.1}$$

Therefore, the ability to quantify K_S and D_S is essential to understand from a fundamental

[*] This chapter previously appeared as an article in the *Environmental Science and Technology*. The original citation is as follows: Wang, J.; Kingsbury, R.; Perry, L.; Coronell, O., Partitioning of Alkali Metal Salts and Boric Acid from Aqueous Phase into the Polyamide Active Layers of Reverse Osmosis Membranes. *Environmental Science & Technology.* **2017**, 51 (4), 2295–2303.

perspective the mechanisms of contaminant permeation through RO membranes, and ultimately enable construction of predictive transport models. Being able to quantify K_S and D_S would also facilitate the development of improved active layer materials for specific applications, as it would enable the identification of the transport property that must be targeted for modification in the active layer to improve performance (i.e., K_S, D_S, or both).

While P_S can be easily obtained from permeation tests and measurements of active layer thickness,[5] independent measurements of K_S and D_S remain challenging. Given that the time scale of diffusion of solutes through active layers is very short ($<10^{-2}$ seconds), to our knowledge, there are no reported methods to measure D_S in active layers (except for an electrochemical method[6] applicable only to redox couples, which are not contaminants of common interest in water purification).

Regarding the measurement of K_S, standard methods used for relatively thick films, such as solute desorption,[7,8] are not applicable to polyamide active layers because of their extreme thinness. Nevertheless, two methods have been reported to measure K_S in polyamide active layers. One of these methods was developed for organic solutes (e.g., urea, hydroquinone), and uses attenuated total reflection Fourier transform infrared spectroscopy (ATR-FTIR) for sample analyses.[9–11] The second method was developed for solutes containing relatively heavy elements (e.g., arsenic, iodine), and uses Rutherford backscattering spectrometry (RBS) as an analytical technique.[12,13] Neither of these two methods is applicable to the inorganic, low-molecular weight contaminants of common interest in water purification applications (e.g., NaCl, boric acid, or hardness (Ca^{2+}, Mg^{2+})). Therefore, there is a need to develop an experimental method to quantify K_S into active layers for inorganic solutes of common interest. Given that P_S can be easily obtained experimentally,[5] the ability to measure K_S would also enable the calculation of D_S from

Equation 1, providing a complete picture of the mechanisms controlling the permeation of inorganic contaminants through RO membranes.

Accordingly, the objective of this study was to develop a method to measure the partition coefficients of inorganic solutes. We developed the method using chloride salts of alkali metals and boron (a weak acid) as model contaminants, and a seawater RO membrane with a polyamide active layer as a model membrane. We present method development and implementation, data analyses and interpretation, comparison of results with those reported in the literature for the RBS-based methods, and comparison of experimental results to predictions by the Donnan-Manning theory.[14–16]

2.2 Materials and Methods

2.2.1 Chemicals and solutions

Chloride salts of alkali metals (CsCl, RbCl, KCl, NaCl, and LiCl) and boric acid (H_3BO_3) were used as test solutes in partitioning tests. Hydrochloric acid (HCl) was used for pH adjustment to pH=5.3 at which 99.99% of boric acid exists as a neutral solute (pK_a=9.27[17]). Alkali metal hydroxide (CsOH, RbOH, KOH, NaOH, and LiOH) solutions at pH=10.5 were used to fully hydrate the active layers prior to partitioning tests as described below. All chemicals used to prepare test solutions were ACS grade with 99% or greater purity (Fisher Scientific, Pittsburgh, PA).

2.2.2 Membranes

The seawater reverse osmosis SWC4+ membrane (Hydranautics, Oceanside, CA) was used for all solute partitioning tests. The SWC4+ membrane has an uncoated aromatic polyamide active layer, as confirmed by ATR-FTIR analysis.[18] Membrane coupons (2.5×5.0 cm^2) were cut

from flat sheets provided by the manufacturer, thoroughly rinsed with ultrapure water (>18 MΩ.cm), and stored in ultrapure water in amber glass bottles until used.

2.2.3 Membrane sample preparation

The polyamide active layer was isolated from membrane coupons onto three 5 MHz quartz crystal microbalance (QCM) sensors. The isolation of the polyamide active layer enabled the performance of partitioning measurements in the absence of potential artifacts that could be caused by the presence of the much thicker polysulfone support and polyester backing layers. The polyamide area isolated on each sensor was 1.54 cm^2. The active layer isolation procedure was described in detail in our previous work,[19] is based on a protocol proposed by Freger,[20] and has been successfully applied in different studies.[21–23] It has been shown that characterization results for bulk active layer properties using isolated active layers are equivalent to corresponding results for active layers in intact membranes.[5,6,19,24,25] In brief, the polyester backing layer was first peeled off manually, leaving behind the composite of polysulfone support layer and polyamide active layer. Then, the polyamide-polysulfone composite was placed against the surface of the QCM sensor with the polyamide side facing the sensor, and the polysulfone layer was dissolved using dimethylformamide (DMF). Next, the QCM sensor coated with the polyamide active layer was air dried, rinsed with ultrapure water, dried with ultrapure nitrogen gas, and stored in a sealed plastic box until use.

2.2.4 Measurement of areal mass of active layer and change in areal mass of the active layer when exposed to test solutions

QCM analyses were used to measure the areal mass of active layers isolated on QCM sensors (m_{AL}, ng.cm^{-2}) and the change in areal mass (Δm, ng.cm^{-2}) of the active layers when exposed to test solutions during partitioning tests. For each sensor, the m_{AL} value was obtained as

the difference between QCM measurements for the sensor exposed to air before and after active layer isolation. Also for each sensor, Δm values were obtained as the difference between QCM measurements for the coated sensor exposed to ultrapure water and to aqueous solutions containing the solute of interest (see next section). The m_{AL} values were used to obtain the thicknesses of the active layers isolated on QCM sensors, and the m_{AL} and Δm values were used to calculate partition coefficients as described in the Results and Discussion section. Only mass changes greater than the limit of quantification (LOQ=33 ng.cm^{-2}, see Supporting Information (SI)) were used for calculations.[26] All values and corresponding errors reported in this manuscript correspond to the average and standard deviation, respectively, of measurements from the triplicate coated sensors.

2.2.5 Partitioning tests

Partitioning tests at pH=5.3 were performed for all solutes. We chose pH=5.3 because it is relevant for scaling prevention applications,[27,28] and because at pH values below ≈5.5 aromatic polyamide active layers have been shown[29,30] to have relatively low (<0.1M) charge density. The latter allows for the detection of mass increases that are specifically due to salt partitioning (not neutralization of charged sites) at lower salt concentrations in solution. Tests were performed by exposing the coated sensors to the following series of solutions: (1) ultrapure water, (2) a test solution (pH=5.3) containing the solute of interest at a concentration of 0.001 M, (3) test solutions (pH=5.3) at the remaining solute concentrations of interest, in order of ascending concentration (0.005, 0.01, 0.05, 0.1, 0.2, 0.3, 0.4, 0.6, 0.8 and 1 M for salts and 0.005, 0.01, 0.05, 0.1, 0.2, 0.3, 0.4, 0.5, 0.6 and 0.7 M for boric acid), and (4) ultrapure water. The final exposure of the coated sensor to ultrapure water served to verify the stability of the baseline reading of the QCM throughout the experiment. Prior to measuring Δm for any given alkali

metal, the active layers were hydrated to their fullest extent by exposing the coated sensors first to ultrapure water and then three times to an alkaline (pH=10.5) solution of the corresponding metal hydroxide and to ultrapure water. In previous work, this procedure was shown to result in maximum hydration,[25] and therefore to ensure that there are no artifacts in mass measurement related to loss or absorption of water. For partitioning tests with boric acid, LiOH was used as the metal hydroxide solution. For data analysis, the concentration of negative fixed charges in the active layer at pH=5.3 was needed and measured as C_{FC}= 0.061±0.018 M using the procedure described in detail elsewhere[25] and in the SI. The concentration of positive fixed charges in the active layer of the SWC4+ membrane was previously shown to be negligible.[30]

A second set of tests was performed with the same set of coated sensors to evaluate the effect of pH on salt partitioning. NaCl was used as the representative salt and partitioning was evaluated at pH=5.3 and 8.0. We chose pH=8.0 as the second pH because it is relevant for seawater desalination and boron removal applications.[31] Tests were performed in the same manner as described above with the exception that in steps 2 and 3, solutions at pH=5.3 and 8.0 were used sequentially at each salt concentration in solution. This allowed for a direct comparison of partitioning at both pH values. For data analysis, the concentrations of negative fixed charges in the active layer at pH=5.3 and 8.0 were needed and measured as C_{FC}= 0.063±0.003 M and 0.198±0.051 M, respectively, using the same procedure as above.

2.2.6 QCM analyses

QCM tests were performed with a Q-Sense E4 quartz crystal microbalance (Biolin Scientific, Lithicum Heights, MD), which has a mass sensitivity on the order of a few ng.cm^{-2} and the capability to test four sensors in parallel. We tested one uncoated control sensor and the three coated sensors in parallel. Therefore, at any point during the experiments, all four sensors

were exposed to the same test solution (see SI for schematic). The control sensor served to account for factors that might affect the baseline readings of the sensors, such as changes in the viscosity or density of the solution to which the sensors are exposed.[25,32,33] Measurements were performed with the sensors placed in Q-Sense flow modules. Before each test, the baseline reading of the sensors was monitored for at least 20 min to ensure stability of readings. During tests, sensors were exposed to either air or aqueous solution. For each solution used, data were collected continuously until the sensors reached equilibrium with the solution as defined by a rate of change of areal mass lower than 0.25 $ng.cm^{-2}.min^{-1}$.[25] This equilibrium condition was met within 30 min of contact time for all solutions. Once the QCM reading was stable, the sensor sample was ready to be exposed to a new solution. All tests were performed with a flow rate of 0.1 $mL.min^{-1}$ while system temperature was maintained at 22±0.02 °C using the temperature control feature of the flow module. Frequency change (Δf, Hz) and dissipation change (ΔD, unitless) data gathered during QCM tests indicated that the isolated active layers could be approximated as rigid for QCM data analysis (i.e., minor overtone (n, unitless) dependencies of Δf and ΔD, and $\Delta D/(\Delta f/n) < 4\times10^{-7}$ Hz^{-1}, see SI for details).[34,35] The rigid film approximation is supported by previous work[5,19,25] demonstrating that that when we characterize the physical properties of polyamide active layers isolated on QCM sensors by approximating the isolated active layers as rigid films, we obtain the same results as when we characterize the active layers in intact membranes using other analytical techniques.

2.2.7 Theoretical estimation of partition coefficients

As an additional means of assessing the validity of our findings, we used Donnan theory in concert with Manning counter-ion condensation theory to obtain a theoretical estimate of salt partition coefficients in the active layer of the SWC4+ membrane at pH=5.3. Donnan theory

requires three key values to enable prediction of the salt partition coefficients: fixed charge concentration in the active layer, activity of salts in bulk solution, and salt activity coefficients in the membrane.[36] The fixed charge concentration in the active layer polymer was measured experimentally as C_{FC}= 0.061±0.018 M (see SI), and the activity of salts in solution can be easily calculated based on the salt concentration in solution.[37] Manning theory provides a means of estimating activity coefficients inside charged polymers based on the concentration of fixed charges in the polymer and the average distance between charges.[38] In general, we followed the same treatment of the Donnan-Manning theory used by Kamcev et al.[14,15] for ion partitioning into ion exchange membranes. A detailed explanation of the assumptions and equations used in our calculations is provided in the SI.

2.3 Results and discussion

2.3.1 Measured changes in areal mass of coated QCM sensors during partitioning tests

Figure 2.1 shows representative results for the increase in the areal mass (Δm) of a coated QCM sensor when it was exposed to a sequence of NaCl (Figure 2.1a) and boric acid (Figure 2.1b) test solutions (pH=5.3) with increasing solute concentration. As shown in Figures 2.1a and 2.1b, an increase in the solute concentration in bulk solution always resulted in a corresponding increase in the areal mass of the active layer. Similarly, when the coated sensor was exposed to ultrapure water at the end of the experiment after being exposed to the maximum salt concentration tested (1 M), the areal mass registered by the QCM returned to within 10% of its value at t=0 hr.

We used the measured Δm values to calculate solute partition coefficients (see next section) under the assumption that any potential loss of water mass by the active layer due to osmotic dehydration[39,40] was negligible compared to Δm. This assumption was based on

evidence indicating that neglecting osmotic dehydration would lead to a maximum error in the calculated partition coefficients of less than 14% in all cases, as low as 2-3% for the higher molecular weight salts, and less than 7% for NaCl which is the salt of most relevance in water desalination applications (see SI for details).

2.3.2 Estimation of solute partition coefficients in polyamide

For the estimation of solute partition coefficients in polyamide, the active layer thicknesses (δ, nm) isolated on each of the three sensors used for partitioning tests were needed. These thicknesses were calculated as

$$\delta = \frac{m_{AL}}{\rho_{AL}} \quad , \tag{2.2}$$

where ρ_{AL}=1.24 g.cm^{-3} corresponds to the mass density of the polyamide active layer.[5] The m_{AL} values measured for each of the three sensors were 14303, 13860, and 13701 g.cm^{-2} (average of 13955±255 ng.cm^{-2}) from which corresponding thicknesses of 115, 112, and 111 nm (average of 113±2 nm) were calculated. The calculated thicknesses were used for calculations of molar solute concentration in the active layers as described below.

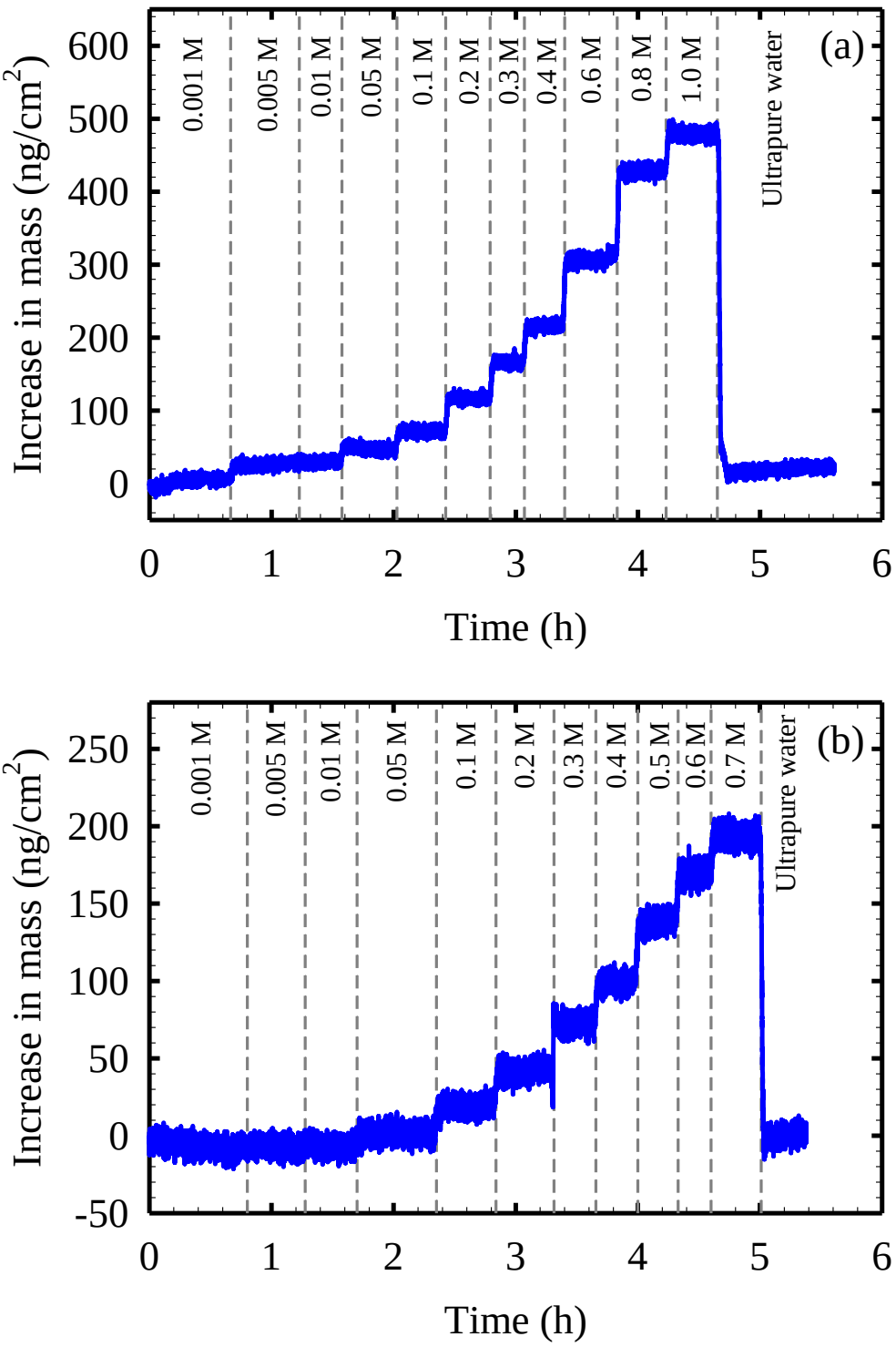

Figure 2.1. Representative results for the increase in the areal mass of a coated QCM sensor when exposed to a sequence of (a) NaCl and (b) boric acid solutions (pH=5.3) with increasing solute concentration. The polyamide active layer coating the sensor was that of the SWC4+ membrane.

For the case of neutral solutes such as boric acid, all solute in the active layer is mobile (i.e., it is available to diffuse through the active layer during solute permeation). Therefore, under the assumption of negligible osmotic dehydration, the measured increase in the areal mass of the active layer when it is exposed to boric acid solution (Δm_B, ng.cm^{-2}) is equal to the mass of mobile boric acid partitioned into the active layer ($m_{B,AL}$, ng.cm^{-2}) as given by

$$\Delta m_B = m_{B,AL} . \tag{2.3}$$

For the case of 1:1 salts such as any alkali metal chloride salt (XCl), some cations (X^+) neutralize the negative fixed charges in the polyamide active layer and therefore do not contribute to the concentration of mobile salt (i.e., they are not available to diffuse through the active layer during solute permeation). Accordingly, the measured increase in the areal mass of the active layer when the active layer is exposed to an XCl solution (Δm_{XCl}, ng.cm^{-2}) is given by

$$\Delta m_{XCl} = m_{X,F} + m_{XCl,AL} \quad , \tag{2.4}$$

where $m_{X,F}$ (ng.cm^{-2}) is the areal mass of cations neutralizing the negative fixed charges, and $m_{XCl,AL}$ (ng.cm^{-2}) is the areal mass of mobile XCl partitioned into the active layer.

In a previous study,[25] we demonstrated that ~95% of negative fixed sites are saturated by cations when the active layer is equilibrated with a (flowing) 1 mM salt solution (i.e., increasing salt concentration three fold to 3 mM increased the measured fixed charge by <5%). It can also be demonstrated (see SI) that the mass increase in the active layer that results from the partitioning of mobile salt from a 1 mM salt solution is under the detection limit of our method. Therefore, it can be safely assumed that

$$m_{X,F} = \Delta m_{XCl,\,1mM} \quad . \tag{2.5}$$

where $\Delta m_{XCl,1\text{mM}}$ is the areal mass increase measured when the active layer is exposed to a 1 mM salt solution. Accordingly, from Equations 4 and 5 we obtain

$$m_{XCl,AL} = \Delta m_{XCl} - \Delta m_{XCl,1\text{mM}} \quad . \tag{2.6}$$

Recent work by Yan et al.,[23] Lin et al.,[19] and Pacheco et al.[41]shows that voids (tens of nanometers in size) exist in the fully-aromatic polyamide active layers of TFC membranes. In our previous study, we reported a thorough characterization of such voids in various membranes, including in the SWC4+ membrane studied here.[19] The results showed that the voids fill up with aqueous solution when the active layers are immersed in it, and that the voids account for a significant volume fraction (f_v) of the active layers (f_v = 0.29±0.01 for the SWC4+ membrane). Therefore, in order to calculate the solute partition coefficient in the polyamide material (as opposed to the net partition coefficient in the whole active layer), the mass change due to solute present in the aqueous solution filling the voids must be accounted for. The measured mass change, Δm, during partitioning tests can be related to the solute concentration in the voids ($C_{s,v}$, M) and polyamide ($C_{s,p}$, M) through

$$\Delta m = \delta\ (C_{S,v} f_v MW_v + C_{S,p}(1 - f_v)MW_p) \tag{2.7}$$

where $C_{s,v}$ is equal to the solute concentration in bulk solution (as the voids fill up with bulk solution during our equilibrium tests), f_v = 0.29±0.01,[19] and MW_v (g.mol^{-1}) and MW_p (g.mol^{-1}) represent the molecular weight of the solute in the voids and in polyamide, respectively.

Once $C_{S,p}$ is calculated using Equation 2.7, the solute partition coefficient (K_p, unitless) between water and polyamide material can be calculated as

$$K_p = \frac{C_{S,p}}{C_{S,bulk}} \quad , \tag{2.8}$$

where $C_{S,bulk}$ (M) is the solute concentration in bulk solution.

For the calculation of $C_{S,p}$ from Equation 2.7, the molecular weights of the solute in polyamide and voids are needed. The molecular weights of solute in the voids (MV_v) and polyamide (MV_p) were calculated as

$$MW_v = MW_{Unhydrated} \quad , \tag{2.9}$$

and

$$MW_p = MW_{Unhydrated} + n_p MW_{Water} \quad , \tag{2.10}$$

respectively, where $MW_{Unhydrated}$ (g.mol^{-1}) is the unhydrated molecular weight of the solute of interest, n_p (unitless) is the hydration number of the solute of interest in polyamide, and MW_{Water}=18.01 g.mol^{-1} is the molecular weight of water. The unhydrated molecular weight of solute is used in Equation 2.9 to account for the presence of solute in the voids because Equation 2.7 requires only the excess mass with respect to the case when no solute is present in the voids; as it is the case for the bulk solution, the excess mass in the system after adding salt is due to the salt added, not to the pre-existing water that hydrates the salt. The hydrated molecular weight of solute is used in Equation 10 to account for the presence of solute in the polymer because, under the framework of solution-diffusion theory,[4] solutes and solvent (water) permeate independently from each other; the excess mass in the polymer due to partitioning of the hydrated solute is independent from the pre-existing mass of partitioned water. Given that the hydration numbers of solutes in polyamide active layers (n_p) are unknown, we assumed the following two extreme cases (Table 2.1): (i) solutes in polyamide are unhydrated (n_p = 0, Scenario A), and (ii) solutes in polyamide have the same hydration number as in bulk solution[42,43] (Scenario B).

For Scenario A (unhydrated solutes), K_p values (Figure 2.2a) were calculated using Equations 3, 6, 7, 8, 9 and 10 and the $MW_{Unhydrated}$ values presented in Table 2.1. We note that the lowest solute concentration in bulk solution ($C_{S,bulk}$) for which K_p values were calculated differs among solutes because, as indicated in the Materials and Methods, only Δm values higher than the limit of quantification (33 ng.cm^{-2}) were used in calculations. Specifically, tests with boric acid, LiCl, NaCl, KCl, RbCl, and CsCl resulted in Δm values above the limit of quantification for $C_{S,bulk} \geq$ 0.1, 0.3, 0.2, 0.05, 0.005, and 0.005 M, respectively (i.e., lower $C_{S,bulk}$ for higher molecular weight solutes, as expected). The K_p results (Figure 2.2a) show that the partition coefficients for each solute were approximately constant at $C_{S,bulk} \geq$ 0.05 M, and decreased with $C_{S,bulk}$ for RbCl and CsCl at the lowest concentrations tested ($C_{S,bulk}$ =0.005-0.05 M). The trend of K_p values with $C_{S,bulk}$ observed in Figure 2a is consistent with that observed by Zhang et al.[13] for the partitioning of cesium into the polyamide active layer of an RO membrane. Zhang et al. reported partition coefficient values that decreased steeply in the $C_{S,bulk}$ range of 0.001-0.050 M, and generally leveled off at higher $C_{S,bulk}$ values.

While the approximately constant partition coefficients obtained at relatively high bulk solution concentrations are consistent with expectations from Donnan theory,[44,45] the decreasing partition coefficients at relatively low bulk solution concentrations are not. For fixed charged films such as polyamide active layers, Donnan theory predicts that salt partition coefficients increase asymptotically with bulk solution concentration as a result of the increased screening of the fixed charges by counter-ions. Specifically, the partition coefficient K_p can be expressed as

$$K_p = K_p^{'} E \quad , \tag{2.11}$$

where E is the Donnan electrostatic exclusion coefficient (see Appendix A for discussion

of E values as a function of $C_{S,bulk}$), and K_p' is the partition coefficient in the absence of Donnan exclusion (i.e., for an equivalent neutral membrane). It can be shown (see Appendix A) that on the basis of Donnan theory, K_p should not vary by more than 10% for $C_{S,bulk} > 0.3$ M for the polyamide active layer studied here ($C_{FC} = 0.061$ M), in agreement with the results in Figure 2.2a. However, at relatively low $C_{S,bulk}$ values, K_p should be significantly lower than at $C_{S,bulk} \geq 0.3$ M (e.g., K_p at $C_{S,bulk} = 0.01$ M should be 82% lower than at $C_{S,bulk} = 0.3$ M). We attribute the unexpectedly high K_p values obtained at $C_{S,bulk} = 0.005$ and 0.01 M to overestimation of the mass of mobile salt partitioned into the active layer at these relatively low salt concentrations. As mentioned above, in our previous study[25] we showed that ~95% (not 100%) of negative fixed charges in polyamide active layers were saturated with cations at $C_{S,bulk} = 1$ mM. Therefore, assuming K_p=1, only at $C_{S,bulk} > C_{FC} = 0.061$ M it is ensured that 95% or more of Δm is due to mobile salt partitioned into the active layer, and not excess cations saturating negative fixed charges. We have indicated this threshold value in Figure 2.2, where partition coefficients to the right of the threshold have a high confidence level (95%), while those to the left of the threshold are expected to correspond to overestimations of the actual partition coefficients, with higher levels of overestimation obtained at lower bulk solution concentrations. The same argument explains the relatively high K_p values reported by Zhang et al.[13] at relatively low bulk solution concentrations.

As mentioned above, on the basis of Donnan theory and in agreement with experimental results, K_p does not vary by more than 10% for $C_{S,bulk} > 0.3$ M. Therefore, for each solute, a representative partition coefficient was calculated as the average of K_p values measured at $C_{S,bulk} > 0.3$ M. The corresponding results (Table 2.1) show that K_p was in the range of 0.22-0.68. For salts, the partition coefficients in the absence of Donnan electrostatic exclusion (K_p') can be

calculated from Equation 11. Given that $E > 0.9$ for $C_{S,bulk} > 0.3$ M, then $K_p < K_p' < K_p/0.9$ in all cases when the representative K_p values reported in Table 2.1 are used in the calculations. For neutral solutes, E=1 so $K_p = K_p'$.

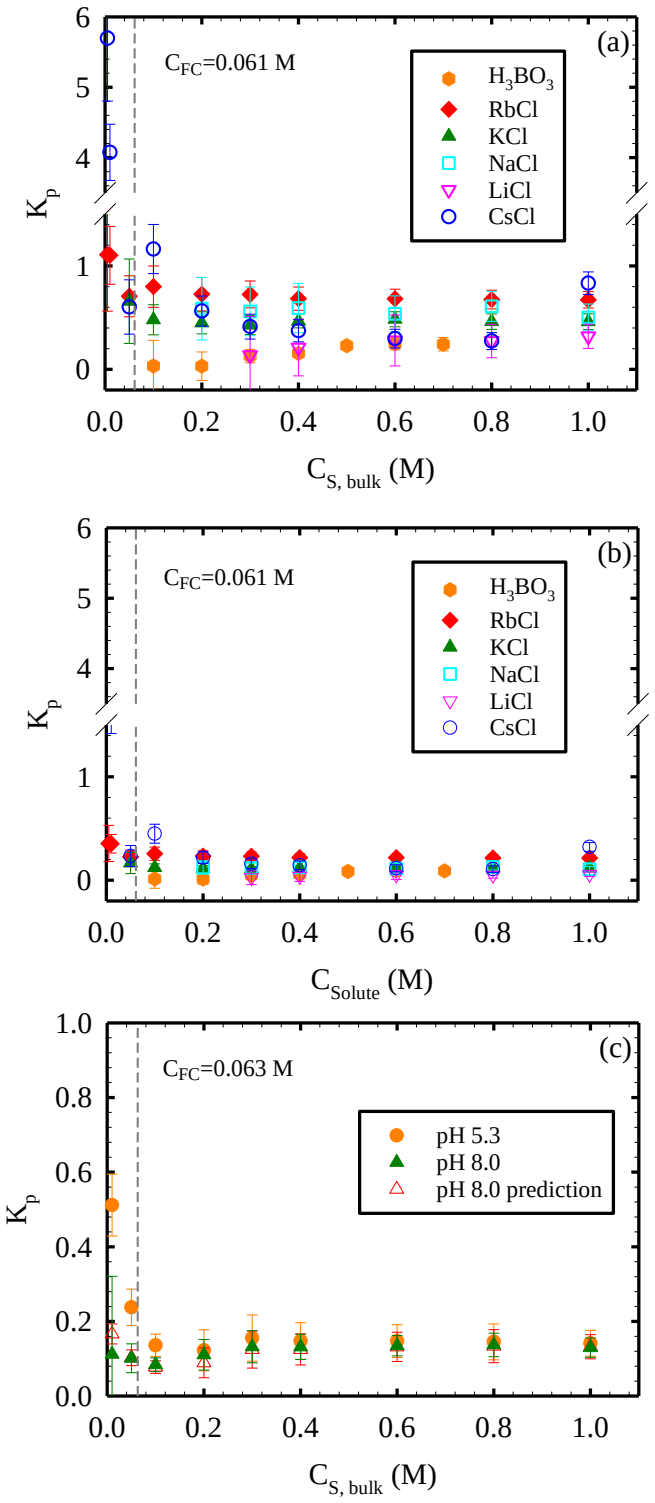

Figure 2.2. Partition coefficient in the polyamide phase of the active layer (K_p) as a function of solute concentration in bulk solution ($C_{S,bulk}$) assuming that solutes in the polyamide active layer (a) are unhydrated (Scenario A) and (b, c) have the same hydration number as in bulk solution (Scenario B). Panels (a) and (b) present results for all solutes at pH=5.3. Panel (c) presents results for NaCl at pH=5.3 and 8.0 obtained during the same experimental run,and includes

predictions of K_p at pH=8.0 (empty symbols) based on the experimental results at pH=5.3 and Donnan exclusion theory. Partition coefficients were calculated based on the areal mass changes (Δm) measured for the coated sensors when exposed to test solutions. Δm values for boric acid, LiCl, NaCl, KCl, RbCl, and CsCl were above the limit of quantification (33 ng.cm^{-2}, see SI) for $C_{S,bulk} \geq$ 0.1, 0.3, 0.2, 0.05, 0.005, and 0.005 M, respectively. At $C_{S,bulk} > C_{FC}$ = 0.061 M it is ensured that 95% or more of any measured Δm is due to mobile salt partitioned into the active layer, and not excess cations saturating negative fixed charges. The relatively high K_p calculated for RbCl and CsCl at $C_{S,bulk}$ = 0.005 and 0.01 M were likely the result of counter-ions neutralizing additional fixed charges in polyamide not neutralized with the reference 1 mM solutions (see main text). Note that the NaCl partitioning results at pH=5.3 in panels (a) and (c) are different by 17% on average. This is likely the result of a 2.5 year storage time of the coated sensors (in the original plastic storage boxes) between the experiments in the two panels.

For Scenario B (hydrated solutes), K_p values were calculated at each $C_{S,bulk}$ condition (Figure 2.2b) using Equations 2.3, 2.6, 2.7, 2.8, 2.9 and 2.10, with n_p values assumed to be equal to the hydration numbers in bulk solution listed in Table 2.1. The n_p values correspond to the average number of hydration molecules in the first hydration shell, which assumes that water molecules beyond the first hydration shell do not move with the ion into the active layer (see SI for basis for this assumption). If ions partitioned into the active layers together with water molecules from beyond the first hydration shell, the partition coefficients would be lower than those reported here. As observed in Figure 2.2b, the trend of K_p values as a function of $C_{S,bulk}$ was similar to that observed for Scenario A in Figure 2a, with overestimation of partition coefficients at $C_{S,bulk} < C_{FC}$, and approximately constant K_p values at relatively high $C_{S,bulk}$ values. For each solute, the representative partition coefficients calculated as the average of K_p values measured for $C_{S,bulk} >$ 0.3 M are presented in Table 2.1 and were found to be in the 0.05-0.22 range. Compared to the partition coefficients obtained from Scenario A (unhydrated solutes), the partition coefficients calculated for Scenario B (hydrated solutes) are 61-82% smaller, but still in the same order of magnitude. In general, the value of the partition coefficient K_p of the alkali metal salts decreased with decreasing atomic weight of the cation, except for CsCl.

2.3.3 Estimation of net solute partition coefficients in active layer

As discussed in the previous section, polyamide active layers contain voids which fill up with bulk solution when immersed in it. Therefore, the net solute partition coefficient in the active layer (K_{net}) differs from the solute partition coefficient in polyamide (K_p) and can be calculated as

$$K_{net} = K_v f_v + K_p (1 - f_v), \tag{2.12}$$

where f_v = 0.29 is the void fraction in the polyamide active layer of the SWC4+ membrane, and K_v represents the solute partition coefficient between the external solution and the solution filling up the voids. Given that the voids are tens of nanometers in size, and in our equilibrium partitioning tests the solution in the voids is in equilibrium with the bulk solution outside the membrane, then K_v =1.

Table 2.1. Summary of partition coefficients (K_p and K_{net}) of CsCl, RbCl, KCl, NaCl, LiCl and boric acid in the polyamide active layer of the SWC4+ membrane at pH=5.3. Scenarios A and B assume unhydrated and hydrated solutes, respectively, in the polyamide phase. Reported values and uncertainties correspond to the average and standard deviation of triplicate samples.

Membrane	Scenario	Hydrated solutes?	Partition coefficient in the polyamide phase (K_p) and net partition coefficient in the active layer (K_{net})					
SWC4+			CsCl	RbCl	KCl	NaCl	LiCl	H_3BO_3
	A	No	0.31±0.05 (0.51±0.04)	0.68±0.05 (0.77±0.03)	0.47±0.04 (0.62±0.03)	0.56±0.09 (0.69±0.06)	0.27±0.10 (0.48±0.07)	0.22±0.03 (0.45±0.02)
	B	Yes	0.12±0.02 (0.38±0.01)	0.22±0.02 (0.44±0.01)	0.12±0.01 (0.37±0.01)	0.12±0.02 (0.37±0.01)	0.05±0.02 (0.32±0.01)	0.08±0.01 (0.35±0.01)
$MW_{Unhydrated}$		g.mol^{-1}	168.36	120.92	78.55	58.44	42.39	61.83
Hydration number = n_p		unitless	15.0[42]	14.4[42]	13.0[42]	12.3[42]	10.9[42]	6.0[a]

[a] Given the similar structure of H_3BO_3 and H_3AsO_3 (i.e., three hydroxyl groups bound to a boron/arsenic atom), the hydration number for H_3BO_3 was assumed to be equal to the number of water molecules (n_p=6) hydrating H_3AsO_3 via hydrogen bonding with the hydroxyl groups.[46,47]

We calculated K_{net} values for each solute for both Scenarios A and B, and the corresponding results are presented in parenthesis in Table 2.1. As expected, the trends for K_{net} across scenarios (A and B) and across solutes are similar to the trends discussed above for K_p. Specifically, K_{net} values were lower for Scenario B than for Scenario A, and generally increased with the molecular weight of the cation, except for CsCl. Importantly, for any given solute, K_{net} values were always higher than K_p values. This is because the solute concentration in the solution inside the voids is higher than in polyamide, as indicated by the finding in the previous section that $K_p < 1$.

Compared to other studies[12,13] where partition coefficients of similar solutes were reported in the range of 3.6-8.1, the partition coefficients reported here (all lower than 1) are much smaller, and in better agreement with intuitive expectations for polyamide active layers as they reject 99+% of salts in solution. We attribute the larger partition coefficients reported in the cited studies to potential artifacts caused by the sample preparation procedures. In the cited studies, membrane samples were dried (i.e., blot-drying, air-drying, freeze-drying) after they had been equilibrated with the aqueous solutions. This was necessary because RBS was used as the analytical technique and RBS operates under vacuum. To try to prevent migration of solutes from the polysulfone support layer to the active layer during the drying procedures, the cited studies centrifuged[14] or freeze-dried[15] the samples, and calculations of partition coefficients were performed under the assumption that such migration had been prevented. By contrast, in our experiments, samples were analyzed by QCM while the membrane samples were in contact with the aqueous solution of interest (and therefore there was no need for drying procedures), and polyamide active layers were isolated from their polysulfone supports

(and therefore the solute sorbed into the supports could not interfere with accurate quantification of solute partitioned into the active layer). Because our experimental procedure avoids the complicating factors of the previously reported procedures, we believe that the results reported here are a significantly closer estimation of the actual partition coefficients of inorganic salts and small acids into the polyamide active layers of RO membranes.

2.3.4 Effect of bulk solution pH on salt partitioning

Figure 2c presents NaCl partitioning results at both pH=5.3 and 8.0, and compares the pH=8.0 data with corresponding predictions made based on the pH=5.3 data and Donnan exclusion theory (see SI for details). The results show that partition coefficients at pH=8.0 were on average only 14% lower than partition coefficients at pH=5.3, and that partitioning at pH=8.0 was successfully predicted within experimental error from pH=5.3 data, confirming the applicability of Donnan theory to RO membranes. We previously reported related work[45] in which we demonstrated that we could successfully predict the rejection of a salt (KI) at pH=8.0 and 10.2 based on rejection data at pH=6.3 and Donnan exclusion theory. Predictions were performed under the assumption that pH affected only the partitioning of ions. Note that pH affects partitioning because it affects membrane charge, which in turns affects the extent to which ions are excluded by the membrane by the (electrostatic) Donnan mechanism. The successful prediction of the effect of pH effect on salt rejection,[45] and salt partitioning (this work), using Donnan theory demonstrates that measurements of partitioning at a single pH and measurements of charge density as a function of pH suffice to predict partitioning at other pH values within experimental error using Donnan exclusion theory.

2.3.5 Comparison of experimental solute partitioning values to values predicted using the Donnan and Manning theories

Figure 2.3 presents comparisons of experimental results of salt partition coefficients into polyamide active layers (K_p) with the theoretical results predicted by the Donnan-Manning theory (i.e., Donnan theory with activity coefficients in the active layer calculated with Manning theory). In Figure 2.3a, the results from Scenario B (hydrated solutes in the active layer) were used as the experimental partition coefficients. While the Donnan-Manning model predicted K_p<1, only the predicted values for NaCl and KCl were consistent with experimental values. The predicted partition coefficients for LiCl were higher than the experimental values, while those for RbCl and CsCl were lower. Similar observations to those made for K_p from Figure 2.3a can be made for the corresponding mobile salt concentrations in polyamide ($C_{S,p}$) presented in Figure S3a in the SI. The fact that the model did not predict partitioning more accurately for salts other than NaCl and KCl could be a result of one of the assumptions of Manning theory breaking down due to the low charge concentration in the SWC4+ membrane, or could be related to hydrophobic or steric interactions not considered by the theory.

As noted above, there is uncertainty in the polyamide-phase hydration numbers for each salt, which may contribute to the poor accuracy of the predictions. To further assess this possibility, for each salt, we evaluated whether there was a polyamide-phase hydration number (n_p) that made the experimental and predicted K_p values agree with each other. While fitting the hydration numbers (see fitted values in legend of Figure 2.3b) resulted in a strong agreement via a 1:1 line between the experimental and predicted mobile salt concentrations in polyamide (R^2=0.96, Figure S3b in Appendix A), the corresponding improvement in the agreement of partition coefficients was less

dramatic (R^2=0.35, Figure 2.3b). The reason that the correlation between the experimental and predicted partition coefficients was not as strong as for mobile salt concentrations is that low $C_{S,bulk}$ values in the denominator of Equation 8 magnified the errors in the predicted mobile salt concentration.

The fitted hydration numbers for NaCl and KCl (12.1 and 13.5, respectively) are close to the values expected in bulk solution (12.3 and 13.0, respectively), while CsCl and RbCl have fitted hydration numbers much higher than those in bulk solution, and LiCl has a fitted hydration number much lower. These implausible hydration numbers may be a result of the limitations of the Donnan-Manning theory, as noted above, and could be magnified by measurement errors in the water absorption capacity of the membrane (see Appendix A).

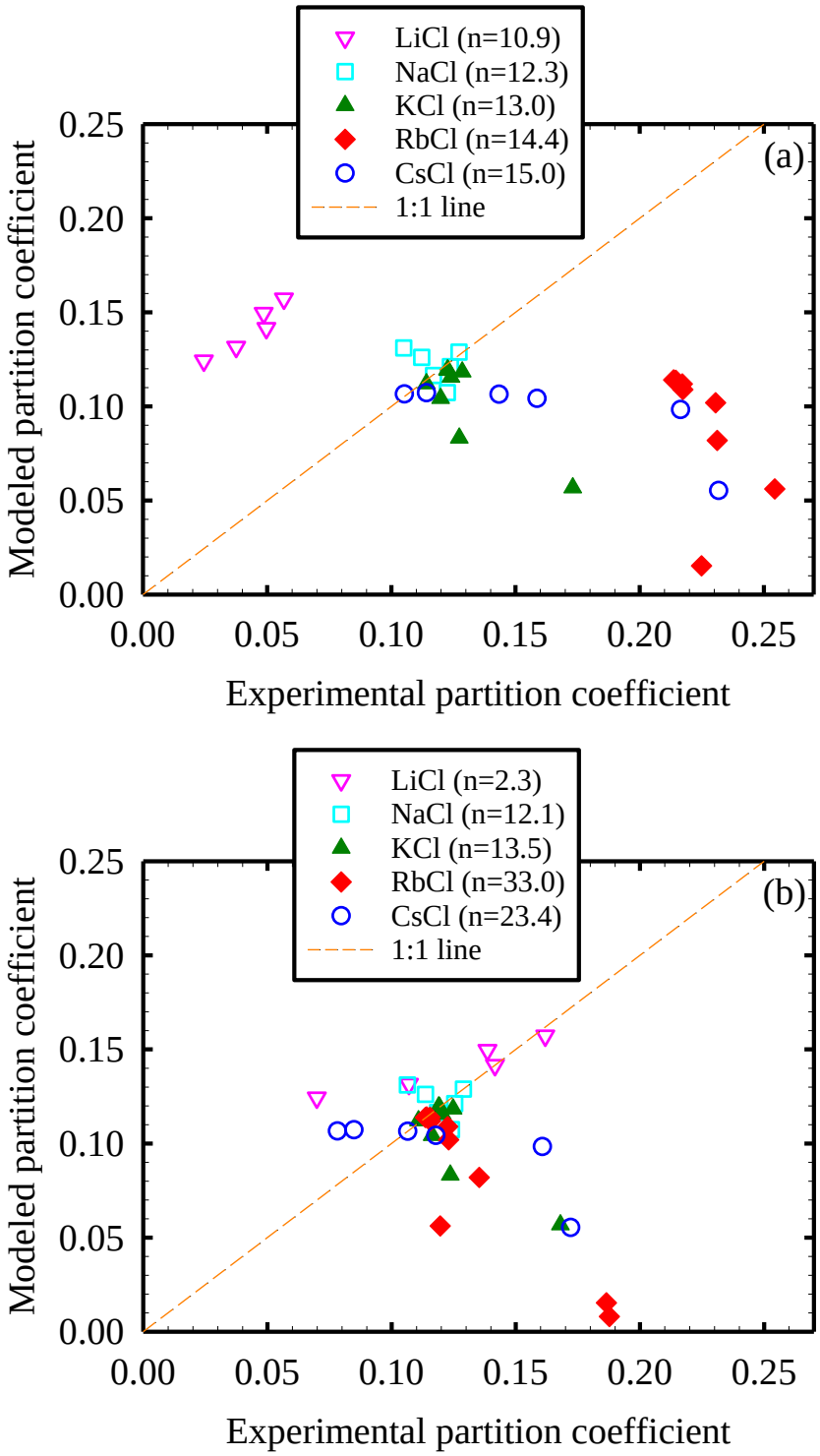

Figure 2.3. Parity plot comparing experimentally-determined salt partition coefficients in the polyamide phase (K_p) of the active layer of the SWC4+ membrane with predictions of Donnan-Manning theory when using (a) ion hydration numbers (n) equal to those in bulk solution (Scenario B), and (b) ion hydration numbers fitted to maximize agreement between experimental results and Donnan-Manning predictions.

2.4 Conclusion

In summary, a bench-top method was developed to determine solute partition coefficients into the polyamide active layers of RO membranes. The method uses a quartz crystal microbalance (QCM) to measure the change in the mass of the active layer caused by the uptake of the partitioned solutes. The method was evaluated using several inorganic salts (alkali metal salts of chloride) and a weak acid of common concern in water desalination (boric acid).

- Overall, the partition coefficients of inorganic salts and small acids obtained experimentally in this study for the polyamide active layer of an RO membrane were lower than 1.
- The range of values of partition coefficients differs from those obtained with other experimental approaches in the literature (3.6-8.1) but is consistent with expectations from Donnan theory (i.e., electrostatic exclusion of ions) and the high salt rejection (99+%) of RO membranes.
- The method developed in this study for the measurement of partition coefficients enables the quantitative characterization of the partition coefficient of salts and small molecules beyond those studied here.
- Measured partition coefficients can be used in future studies to calculate diffusion coefficients based on membrane permeation results and solution-diffusion theory.
- The ability to independently quantify partition coefficients and diffusion coefficients will enhance the fundamental understanding of the mechanisms of contaminant permeation through RO membranes, enable construction of predictive transport

models, and serve as an important tool for guiding membrane modifications to improve performance.

2.5 Acknowledgments

Ryan Kingsbury is gratefully acknowledged for leading the analysis to predict partition coefficients by the Manning theory. Special acknowledgement to Hydranautics for providing the membrane materials. This work was supported by the US National Science Foundation (NSF) (Awards #1264690 and 1336532), and the University of North Carolina Research Opportunities Initiative (ROI) program.

REFERENCES

(1) Nicolaisen, B. Developments in membrane technology for water treatment. *Desalination* **2003**, *153* (1–3), 355–360.

(2) Petersen, R. J. Composite reverse osmosis and nanofiltration membranes. *J. Membr. Sci.* **1993**, *83* (1), 81–150.

(3) Paul, D. R. Reformulation of the solution-diffusion theory of reverse osmosis. *J. Membr. Sci.* **2004**, *241* (2), 371–386.

(4) Wijmans, J. G.; Baker, R. W. The solution-diffusion model: a review. *J. Membr. Sci.* **1995**, *107* (1–2), 1–21.

(5) Lin, L.; Feng, C.; Lopez, R.; Coronell, O. Identifying facile and accurate methods to measure the thickness of the active layers of thin-film composite membranes – a comparison of seven characterization techniques. *J. Membr. Sci.* **2015**, *498*, 167–179.

(6) Bason, S.; Oren, Y.; Freger, V. Characterization of ion transport in thin films using electrochemical impedance spectroscopyII: Examination of the polyamide layer of RO membranes. *J. Membr. Sci.* **2007**, *302* (1–2), 10–19.

(7) Geise, G. M.; Freeman, B. D.; Paul, D. R. Sodium chloride diffusion in sulfonated polymers for membrane applications. *J. Membr. Sci.* **2013**, *427*, 186–196.

(8) Lonsdale, H. K.; Merten, U.; Riley, R. L.; Jay, J. Transport properties of cellulose acetate osmotic membranes. *J. Appl. Polym. Sci.* **1965**, *9*, 1341–1362.

(9) Freger, V.; Ben-David, A. Use of attenuated total reflection infrared spectroscopy for analysis of partitioning of solutes between thin films and solution. *Anal. Chem.* **2005**, *77* (18), 6019–6025.

(10) Ben-David, A.; Oren, Y.; Freger, V. Thermodynamic factors in partitioning and rejection of organic compounds by polyamide composite membranes. *Environ. Sci. Technol.* **2006**, *40* (22), 7023–7028.

(11) Ben-David, A; Bason, S.; Jopp, J.; Oren, Y.; Freger, V. Partitioning of organic solutes between water and polyamide layer of RO and NF membranes: Correlation to rejection. *J. Membr. Sci.* **2006**, *281* (1–2), 480–490.

(12) Mi, B.; Mariñas, B. J.; Cahill, D. G. RBS characterization of arsenic(III) partitioning from aqueous phase into the active layers of thin-film composite NF/RO membranes. *Environ. Sci. Technol.* **2007**, *41* (9), 3290–3295.

(13) Zhang, X.; Cahill, D. G.; Coronell, O.; Mariñas, B. J. Partitioning of salt ions in FT30 reverse osmosis membranes. *Appl. Phys. Lett.* **2007**, *91* (18), 181904.

(14) Kamcev, J.; Paul, D. R.; Freeman, B. D. Ion activity coefficients in ion exchange polymers: Applicability of Manning's counterion condensation theory. *Macromolecules* **2015**, *48* (21), 8011–8024.

(15) Kamcev, J.; Galizia, M.; Benedetti, F. M.; Jang, E.-S.; Paul, D. R.; Freeman, B.; Manning, G. S. Partitioning of mobile ions between ion exchange polymers and aqueous salt solutions: importance of counter-ion condensation. *Phys. Chem. Chem. Phys.* **2016**, *18* (8), 6021-6031.

(16) Manning, G. S. Limiting laws and counterion condensation in polyelectrolyte solutions. III. An analysis based on the Mayer ionic solution theory. *J. Chem. Phys.* **1969**, *51* (8), 3249.

(17) Silberberg, M. S. *Principles of General Chemistry*; McGraw-Hill Higher Education, 2012.

(18) Powell, J.; Luh, J.; Coronell, O. Bulk chlorine uptake by polyamide active layers of thin-film composite membranes upon exposure to free chlorine-kinetics, mechanisms, and modeling. *Environ. Sci. Technol.* **2014**, *48* (5), 2741–2749.

(19) Lin, L.; Lopez, R.; Ramon, G. Z.; Coronell, O. Investigating the void structure of the polyamide active layers of thin-film composite membranes. *J. Membr. Sci.* **2016**, *497*, 365–376.

(20) Freger, V. Swelling and morphology of the skin layer of polyamide composite membranes: An atomic force microscopy study. *Environ. Sci. Technol.* **2004**, *38* (11), 3168–3175.

(21) Lee, J.; Doherty, C. M.; Hill, A. J.; Kentish, S. E. Water vapor sorption and free volume in the aromatic polyamide layer of reverse osmosis membranes. *J. Membr. Sci.* **2013**, *425–426*, 217–226.

(22) Pacheco, F. A.; Pinnau, I.; Reinhard, M.; Leckie, J. O. Characterization of isolated polyamide thin films of RO and NF membranes using novel TEM techniques. *J. Membr. Sci.* **2010**, *358* (1–2), 51–59.

(23) Yan, H.; Miao, X.; Xu, J.; Pan, G.; Zhang, Y.; Shi, Y.; Guo, M.; Liu, Y. The porous structure of the fully-aromatic polyamide film in reverse osmosis membranes. *J. Membr. Sci.* **2015**, *475*, 504–510.

(24) Bason, S.; Oren, Y.; Freger, V. Ion transport in the polyamide layer of RO membranes: Composite membranes and free-standing films. *J. Membr. Sci.* **2011**, *367* (1–2), 119–126.

(25) Perry, L. A.; Coronell, O. Reliable, bench-top measurements of charge density in the active layers of thin-film composite and nanocomposite membranes using quartz crystal microbalance technology. *J. Membr. Sci.* **2013**, *429*, 23–33.

(26) Ripp, J. *Analytical Detection Limit Guidance & Laboratory Guide for Determining Method Detection Limits*; Wisconsin Department of Natural Resources, Laboratory Certificatioin Program, 1996.

(27) Braun, G.; Hater, W.; Kolk, C. zum; Dupoiron, C.; Harrer, T.; Götz, T. Investigations of silica scaling on reverse osmosis membranes. *Desalination* **2010**, *250* (3), 982–984.

(28) Sheikholeslami, R.; Al-Mutaz, I. S.; Koo, T.; Young, A. Pretreatment and the effect of cations and anions on prevention of silica fouling. *Desalination* **2001**, *139* (1–3), 83–95.

(29) Coronell, O.; González, M. I.; Mariñas, B. J.; Cahill, D. G. Ionization behavior, stoichiometry of association, and accessibility of functional groups in the active layers of reverse osmosis and nanofiltration membranes. *Environ. Sci. Technol.* **2010**, *44* (17), 6808–6814.

(30) Powell, J.; Luh, J.; Coronell, O. Amide link scission in the polyamide active layers of thin-film composite membranes upon exposure to free chlorine: kinetics and mechanisms. *Environ. Sci. Technol.* **2015**, *49* (20), 12136–12144.

(31) Koseoglu, H.; Kabay, N.; Yüksel, M.; Sarp, S.; Arar, Ö.; Kitis, M. Boron removal from seawater using high rejection SWRO membranes - impact of pH, feed concentration, pressure, and cross-flow velocity. *Desalination* **2008**, *227* (1–3), 253–263.

(32) O'Sullivan, C. K.; Guilbault, G. G. Commercial quartz crystal microbalances - Theory and applications. *Biosens. Bioelectron.* **1999**, *14* (8–9), 663–670.

(33) Marx, K. A. Quartz crystal microbalance: A useful tool for studying thin polymer films and complex biomolecular systems at the solution-surface interface. *Biomacromolecules* **2003**, *4* (5), 1099–1120.

(34) Reviakine, I.; Johannsmann, D.; Richter, R. P. Hearing what you cannot see and visualizing what you hear: Interpreting quartz crystal microbalance data from solvated interfaces. *Anal. Chem.* **2011**, *83* (23), 8838–8848.

(35) Voinova, M. V.; Rodahl, M.; Jonson, M.; Kasemo, B. Viscoelastic acoustic response of layered polymer films at fluid-solid interfaces : Continuum mechanics approach. *Phys. Scr.* **1999**, *59*, 391–396.

(36) Helfferich, F. *Ion exchange*. McGraw-Hill: New York, 1962.

(37) May, P. M.; Rowland, D.; Hefter, G.; Königsberger, E. A generic and updatable pitzer characterization of aqueous binary electrolyte solutions at 1 bar and 25 °C. *J. Chem. Eng. Data* **2011**, *56* (12), 5066–5077.

(38) Manning, G. S. Limiting laws and counterion condensation in polyelectrolyte solutions II. self-diffusion of the small ions. *J. Chem. Phys.* **1969**, *51* (3), 934–938.

(39) Wang, J.; Mo, Y.; Mahendra, S.; Hoek, E. M. V. Effects of water chemistry on structure and performance of polyamide composite membranes. *J. Membr. Sci.* **2014**, *452*, 415–425.

(40) Geise, G. M.; Paul, D. R.; Freeman, B. D. Fundamental water and salt transport properties of polymeric materials. *Prog. Polym. Sci.* **2014**, *39* (1), 1–24.

(41) Pacheco, F.; Sougrat, R.; Reinhard, M.; Leckie, J. O.; Pinnau, I. 3D visualization of the internal nanostructure of polyamide thin films in RO membranes. *J. Membr. Sci.* **2016**, *501*, 33–44.

(42) Marcus, Y. Effect of ions on the structure of water : Structure making and breaking. *Chem. Rev.* **2009**, *109*, 1346–1370.

(43) Avraham, E.; Noked, M.; Soffer, A.; Aurbach, D. The feasibility of boron removal from water by capacitive deionization. *Electrochim. Acta* **2011**, *56* (18), 6312–6317.

(44) Ohshima, H.; Ohki, S. Donnan potential and surface potential of a charged membrane. *Biophys. J.* **1985**, *47* (5), 673–678.

(45) Coronell, O.; Mi, B.; Mariñas, B. J.; Cahill, D. G. Modeling the effect of charge density in the active layers of reverse osmosis and nanofiltration membranes on the rejection of arsenic(III) and potassium iodide. *Environ. Sci. Technol.* **2013**, *47* (1), 420–428.

(46) Hernández-Cobos, J.; Vargas, M. C.; Ramírez-Solís, A.; Ortega-Blake, I. Aqueous solvation of As $(OH)_3$: A Monte Carlo study with flexible polarizable classical interaction potentials. *J. Chem. Phys.* **2010**, *133* (11), 0–9.

(47) Mähler, J.; Persson, I.; Herbert, R. B. Hydration of arsenic oxyacid species. *Dalton Trans.* **2013**, *42* (5), 1364–1377.

CHAPTER 3 – EFFECT OF FEED WATER PH ON PARTITIONING OF ALKALI METAL SALTS FROM AQUEOUS PHASE INTO THE POLYAMIDE ACTIVE LAYERS OF REVERSE OSMOSIS MEMBRANES

3.1 Introduction

Reverse osmosis (RO) membranes are widely used to meet growing water demands for industrial, agricultural, and domestic applications because they are capable of removing a broad range of dissolved impurities including salt ions and other small molecules.[1–3] Most RO membranes have a three-layer thin-film composite structure comprising a top polyamide active layer (~20-200 nm), an intermediate polysulfone support (20-50 μm), and a polyester backing (50-150 μm).[4] In this composite structure, the polyamide active layer is the main barrier to water and solute transport.

The most widely used mechanistic model describing the transport of water and solutes through RO active layers is the solution-diffusion model.[5] In the solution-diffusion model, solutes permeate through the membrane by partitioning into the active layer, diffusing through the active layer, and then partitioning out of the active layer.[5,6] The permeability of the active layer to solutes (P_S, $m^2.s^{-1}$) can be expressed as

$$P_S = K_S D_S \tag{3.1}$$

where K_S (unitless) is the solute partition coefficient between water and the active layer and D_S ($m^2.s^{-1}$) is the solute diffusion coefficient within the active layer. Thus, solute permeation through RO membranes is largely determined by its partition and diffusion coefficients in polyamide active layers.

While it is relatively easy to obtain P from permeation tests and active layer thickness measurements, it is challenging to independently quantify K_S and D_S. Given that diffusion of solutes through active layer happens in microseconds, there are few experimental methods reported to measure K_S in active layers directly, other than the electrochemical method that only applies for redox couple measurement. In terms of K_S measurement, Wang et al[7] developed a quartz crystal microbalance (QCM) based method to measure inorganic solutes partition coefficient and reported the partition coefficients of all alkali metal chlorides and boric acid between aqueous phase and a type of sweater RO membrane. There is a lack of such data for membranes of different performance level.

The reported impact of feed water pH on membrane salt rejection can be rationalized as the result of the change in salt partitioning (K) caused by the electrostatic Donnan exclusion mechanism: feed water pH affects membrane charge, which affects the electrostatic exclusion of ionic contaminants and thus contaminant rejection. However, while ample evidence exists in the literature that the effect of pH on salt rejection is consistent with Donnan theory,[8–19] very limited information exists on the effect of pH on salt partitioning and its consistency with expectations from Donnan theory.[7] The only relevant study we found was a previous report[7] in which we studied the partitioning of NaCl into a seawater RO membrane at pH 5.3 and 8.0.

Accordingly, given that there is no study available that has investigated the partitioning of multiple salts with multiple membranes covering a broad range of RO performance levels, nor whether the pH effect on salt partitioning is consistent with expectations from Donnan theory, the primary objectives of this study were to: (i) evaluate the partitioning of a group of salts in RO membranes having a broad range of performance levels; (ii) investigate the impact of feed water pH on salt partitioning, and (ii) evaluate whether Donnan theory provides an adequate theoretical

framework to predict the effect of pH on salt partitioning and salt rejection. Solute partition coefficients were measured for chloride salts of alkali metals at several pH conditions of practical interest (pH=5.3, 8.0, and/or 10.5). The partition coefficients measured at pH=8.0 and 10.5 were then compared with those predicted using Donnan theory and the measured partition coefficients at pH=5.3. We present experimental results, model predictions, and discuss the agreement between experimental and predicted values.

3.2 Materials and Methods

3.2.1 Chemicals and solutions

Alkali metals chlorides (CsCl, RbCl, KCl, NaCl, and LiCl) were used as test solutes in partitioning tests. The pH of test solutions was adjusted by addition of hydrochloric acid (HCl) or alkali metal hydroxide (CsOH, RbOH, KOH, NaOH, and LiOH) solutions to target values. All chemicals used to prepare test solutions were ACS grade with 99% or greater purity (Fisher Scientific, Pittsburgh, PA).

3.2.2 Membranes

Five thin-film composite membranes with fully-aromatic polyamide active layers were used in this study including SWC4+ membrane (Hydranautics, Oceanside, CA), XLE (Dow Filmtec, Minneapolis, MN), ESPA3 (Hydranautics, Oceanside, CA), NF90 (Dow Filmtec, Minneapolis, MN), and TFC membranes fabricated in house. These membranes all have uncoated aromatic polyamide active layers, as confirmed by RBS and ATR-FTIR analyses reported elsewhere.[20–22] Membrane coupons (2.5×5.0 cm^2) were cut from flat sheets (provided by the manufacturer for the commercial membranes), thoroughly rinsed with laboratory grade water (>18 MΩ.cm), and stored in laboratory grade water in amber glass bottles until used.

3.2.3 Membrane sample preparation

For each type of membrane, the polyamide active layer of the membrane was separated from the backing layers onto 5Hz QCM sensors so that the measurement of partitioning into the active layer could be performed without interference of the supporting layers. Several studies[23–31] have shown that the characterization results of bulk membrane properties are equivalent for isolated active layers and intact membranes. The detailed active layer isolation procedure was described in our previous work.[27,28] In brief, the polyester layer was manually peeled off first. Then, the polysulfone-polyamide composite was placed against a QCM sensor with polyamide facing the sensor, and dimethylformamide (DMF) was used to dissolve polysulfone, leaving behind a polyamide coated sensor. Next, the active layer coated sensor was air dried, rinsed with laboratory grade water, dried with nitrogen gas, and stored in a plastic box until use. The active layer area isolated on each sensor was 1.54cm^2.

3.2.4 QCM analyses

QCM analyses were used to measure the mass of solute partitioned into the polyamide active layers. We have demonstrated the method for solute partitioning measurement with QCM in our previous work.[7] QCM tests were performed with a Q-Sense E4 quartz crystal microbalance (Biolin Scientific, Lithicum Heights, MD), which is able to test up to four sensors in parallel. QCM analysis was used to measure areal mass change of active layer isolated on QCM sensors (m_{AL}, ng.cm^{-2}) and the change in areal mass (Δm, ng.cm^{-2}) of the active layers when exposed to test solutions during partitioning tests (see next section). Only mass changes greater than the limit of quantification (LOQ=33 ng.cm^{-2}) were used for calculations.[7,32]

For each experimental condition, we tested one uncoated control sensor and two coated sensors in parallel in Q-sense flow modules. Before each test, the baseline reading of the sensors

was monitored for at least 20 min to ensure stability of readings as defined by a rate of change of areal mass lower than 0.25 ng.cm^{-2}.min^{-1}.[27] During tests, sensors were exposed to either air or aqueous solution and data were collected continuously until the sensors reached equilibrium.[27] Once the QCM reading was stable, the sensor was ready to be exposed to a new solution. All tests were performed with a flow rate of 0.1 mL.min^{-1} while system temperature was maintained at 22 ± 0.02 °C using the temperature control feature of the flow module.

For any given alkali metal salt, prior to initiation of a partitioning test, the active layers were hydrated to their fullest extent possible by exposing the coated sensors first to laboratory grade water, and then three times to an alkaline (pH 10.5) solution of the corresponding metal hydroxide and to laboratory grade water.[7,27] This procedure ensures reproducible Δm results.[7,27,33]

3.2.5 Evaluation of Partitioning at pH 5.3

Table 3.1 summarizes the salts and pH conditions for which partitioning was measured for each membrane tested. Partitioning tests were performed at pH 5.3 for all membranes (SWC4+, XLE, ESPA3, NF90, and homemade TFC) and all salts (LiCl, NaCl, KCl, RbCl and CsCl). We chose pH 5.3 as the base pH level at which to evaluate salt partitioning, because aromatic polyamide active layers have been shown[21,34] to have relatively low (<0.1M) charge density at pH values below ~5.5. Thus, the relatively low charge density in active layers enabled us to evaluate salt partitioning with relatively small influence from Donnan (electrostatic) exclusion. Additionally, a pH range of pH≈5-6 is relevant for scaling prevention applications.[35,36] For each salt studied, tests to evaluate partitioning at the base pH of 5.3 were performed by exposing the coated sensors to the following series of solutions: (1) laboratory grade water, (2) a salt solution at pH=5.3 containing the salt of interest at a concentration of 0.001 M, (3) salt solutions at pH=5.3 at increasing salt concentrations of 0.005, 0.01, 0.05, 0.1, 0.2, 0.3, 0.4, 0.6,

0.8 and 1 M, and (4) laboratory grade water. The final exposure of the coated sensor to laboratory grade water served to verify the stability of the baseline reading of the QCM throughout the experiment.

Table 3.1. Summary of salts and pH conditions evaluated for each membrane in partitioning tests.

Membrane	Salts and pH evaluated				
	LiCl	NaCl	KCl	RbCl	CsCl
SWC4+	5.3	5.3, 8.0, 10.5	5.3	5.3	5.3
TFC	5.3	5.3, 8.0, 10.5	5.3	5.3	5.3
XLE	5.3, 10.5	5.3, 8.0, 10.5	5.3, 10.5	5.3, 10.5	5.3, 10.5
ESPA3	5.3	5.3, 8.0, 10.5	5.3	5.3	5.3
NF90	5.3	5.3, 8.0, 10.5	5.3	5.3	5.3

3.2.6 Evaluation of pH effect on salt partitioning

The change in partitioning between pH 5.3 and 8.0, and pH 5.3 and 10.5 was evaluated for NaCl for all membranes (see Table 3.1). Additionally, the change in partitioning between pH 5.3 and 10.5 was evaluated for all chloride salts for the XLE membrane. The coated sensors tested were the same used to evaluate partitioning at pH 5.3. We chose to evaluate pH 8.0 and pH 10.5 because the pH effect on partitioning, measured as the mass change in the coated sensors (Δm, ng.cm^{-2}), is above the detection limit of the QCM at these two pH levels.[7,32] Moreover, these are pH values that are relevant for seawater desalination and boron removal applications.[13,37–39] For each pair of pH values (i.e., pH 5.3 and 8.0, or pH 5.3 and 10.5), tests were performed by exposing the coated sensors to the following series of solutions: (1)

laboratory grade water, (2) a salt solution at pH=5.3 containing the salt of interest at a concentration of 0.001M, (3) a salt solution at pH=8.0 or 10.5 (depending on the pH evaluated) containing the salt of interest at a concentration of 0.001M, (4) repetition of steps 2 and 3 at increasing salt concentrations of 0.005, 0.01, 0.05, 0.1, 0.2, 0.3, 0.4, 0.6, 0.8, and 1 M, and (5) laboratory grade water. The sequential exposure to solutions at pH=5.3 and 8.0, or pH=5.3 and 10.5, at each salt concentration, allowed for direct evaluation of the effect of pH on partitioning.

3.2.7 Calculation of partition coefficients in active layers

At each salt concentration of interest, the salt partition coefficient between the aqueous phase and the polyamide phase (K_p, unitless) was calculated from the areal mass change of the coated sensors caused by exposure to the solution of interest, as described in detail in our previous work.[7] In brief, the salt partition coefficient was calculated as

$$K_p = \frac{C_{S,p}}{C_{S,bulk}} \quad , \tag{3.2}$$

where $C_{S,bulk}$ (M) is the solute concentration in bulk solution and $C_{S,p}$ (M) is the mobile solute concentration in the polyamide phase. $C_{S,p}$ (M) was obtained from the mass of mobile salt in the polyamide active layer ($m_{XCl,AL}$, ng.cm-2) which can be expressed as

$$m_{XCl,AL} = \delta(C_{S,v} f_v MW_v + C_{S,p}(1 - f_v) MW_p) \tag{3.3}$$

where δ (nm) is the active layer thickness, $C_{s,v}$ (M) is the solute concentration in the active layer voids (equal to the solute concentration in bulk solution[7]), f_v (unitless) is the void fraction in the active layer,[28] and MW_v (g.mol^{-1}) and MW_p (g.mol^{-1}) are the molecular weight of the solute in the voids and active layer, respectively. The δ (nm) and f_v values for all active layers

studied were measured and are reported in Table 3.2. The molecular weights of solute in the voids (MW_v) and in the active layer (MW_p) were calculated as

$$MW_v = MW_{Unhydrated} \quad , \tag{3.4a}$$

and

$$MW_p = MW_{Unhydrated} + n_p MW_{Water} \quad , \tag{3.4b}$$

respectively, where $MW_{Unhydrated}$ (g.mol^{-1}) is the unhydrated molecular weight of the solute of interest, n_p (unitless) is the hydration number of the solute of interest in the active layer, and MW_{Water}=18.01 g.mol^{-1} is the molecular weight of water. Note that Equation 3.4a does not mean that solutes are unhydrated in the active layer voids; rather, it means that the added mass to the system is due to the solute, not to the (pre-existing) water molecules that hydrate the solute. Since the hydration numbers of solutes in polyamide active layers (n_p) are unknown, we assumed the following two extreme cases (Table 3.2): (i) solutes in polyamide are unhydrated (n_p = 0, Scenario A), and (ii) solutes in polyamide have the same hydration number as in bulk solution[40,41] (Scenario B).

The mass of mobile salt in the polyamide active layer ($m_{XCl,AL}$, ng.cm^{-2}) was obtained from the measured mass change of the sensor when exposed to the solution of interest in partitioning tests (Δm, ng.cm^{-2}) as

$$m_{XCl,AL} = \Delta m - m_{X,F} - m_w \quad , \tag{3.5}$$

where Δm (ng.cm^{-2}) is the total mass change of the sensor (measured as described in the previous section), $m_{X,F}$ (ng.cm^{-2}) is the change in areal mass of the sensor due to counter-ions neutralizing fixed charges in the active layer, and m_w (ng.cm^{-2}) is the change in areal mass of the

sensor due to water absorption/desorption. Note that since Δm corresponds to the mass change of the sensor with respect to when the sensor is exposed to laboratory grade water (Δm = 0 when the sensor is exposed to laboratory grade water), m_w refers to the additional water absorbed/desorbed as a result of change in water quality, not the total water content in the active layer.

As thoroughly described in our previous work,[7,27] $m_{X,F}$ is measured as the mass change when the coated sensor is exposed to a 1 mM salt solution ($\Delta m_{XCl,1mM}$, ng.cm^{-2}). Accordingly,

$$m_{X,F} = \Delta m_{XCl,1mM} \tag{3.6}$$

and

$$m_{XCl,AL} = \Delta m - \Delta m_{XCl,1mM} - m_w \tag{3.7}$$

In our previous study, m_w (ng.cm^{-2}) was concluded to be negligible in partitioning tests at pH 5.3 in the salt concentration range evaluated ($C_{S,bulk}$ < 1 M).[7] This conclusion was based on experimental results of water absorption/desorption by polyamide active layers as a function of water activity when exposed to water vapor.[42,43] Consistent with this finding, we assumed in the present study that in the partitioning test at pH 5.3, m_w = 0. In the course of this study, we observed that during salt partitioning tests where the effect of pH was evaluated, active layers absorbed additional water at alkaline pH (pH 8.0 and 10.5) that was not released when the pH was returned to the reference pH of 5.3 (Figure 3.1). The sensors released this extra mass when they were air dried which confirmed that the extra mass was accounted for by sorbed water. This extra mass of water (~300 ng.cm^{-2} or less) was negligible compared to the total mass of water in the active layer (~4,000 ng.cm^{-2} or more[28]), but substantial compared to the mass of mobile salt partitioned into the active layer (~500 ng.cm^{-2} or less). Therefore, for each test where the effect

of pH was evaluated, m_w was obtained as the difference between the mass uptake measured at pH 5.3 during the pH effect test (i.e., after exposure to test solution at pH 8.0 or 10.5) and the mass uptake measured at pH 5.3 during the partitioning test at pH 5.3 (see Figure 3.1).

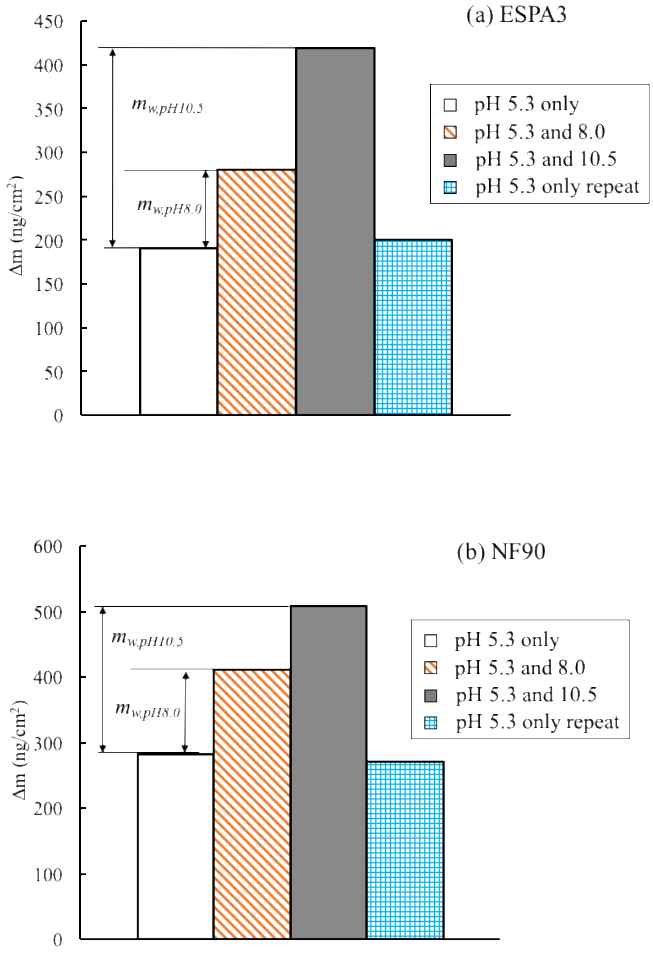

Figure 3.1. Representative $\Delta m_{XCl,AL}$ results for the increase in the areal mass of a coated QCM sensor when exposed to 1 M NaCl solution at pH 5.3. Data shown corresponds to sensors coated with the polyamide active layers of the (a) ESPA3 and (b) NF90 membranes. Each bar in each panel corresponds to independent tests performed with the same set of sensors; the sensors were unmounted from the QCM, rinsed, dried, and remounted on the QCM in between tests. In each panel, from left to right, bars correspond to data obtained when the sensors were exposed to (1) pH=5.3, (2) pH=5.3 after exposure to pH 8.0, (3) pH=5.3 after exposure to pH 10.5, and (4) pH=5.3 after tests (1) through (3).

3.2.8 Prediction of effect of pH on salt partition coefficient in active layers

For thin films with fixed charges like polyamide active layers, the solute partition coefficient is affected by membrane charges as described by Donnan theory.[44,45] Specifically, the partition coefficient K_p can be expressed as

$$K_p = K_p' E \tag{3.8}$$

where K_p' is the partition coefficient in the absence of Donnan exclusion and E is the Donnan electrostatic exclusion coefficient which is given by

$$E = \exp(-\text{arcsinh}\,(\frac{C_{FC}}{2zC_{S,bulk}}))\ , \tag{3.9}$$

where C_{FC} (M), $C_{S,bulk}$ (M), and z (unitless) are the net volume-averaged concentration of fixed charges in the active layer at the pH of interest, the concentration of the symmetrical electrolyte solution, and the charge of the co-ion of interest (-1 for chloride in our case), respectively. The concentrations of fixed charges of all membranes were obtained experimentally with the procedure described in our previous work[27].

As previously reported[44], the partition coefficient of a mobile salt (K, dimensionless) in a polyamide active layer is determined by the partition coefficient of the co-ion as given by

$$K = \frac{\gamma}{\gamma_M} E\ , \tag{3.10}$$

where γ (unitless) and γ_M (unitless) are the activity coefficients of the co-ion in bulk solution and active layer, respectively, and E (unitless) is the Donnan exclusion coefficient as introduced previously. The ratio γ/γ_M in Equation 10 corresponds to K_p' in Equation 3.8. By assuming that γ_M remains approximately constant as a function of pH compared to E, the

partition coefficient at pH=10.5 ($K_{pH10.5}$) can be predicted based on the measured partition coefficient at pH=5.3 ($K_{pH5.3}$) using

$$K_{pH10.5} = K_{pH5.3} \frac{(\gamma E)_{pH10.5}}{(\gamma E)_{pH5.3}} \quad (3.11)$$

Activity coefficients were calculated using the Pitzer model [46,47] and E was calculated as indicated in Equation 3.9. Equation 3.11 was also used to predict partition coefficients at pH 8.0 ($K_{pH8.0}$) using the appropriate charge density in Equation 9 for the calculation of E.

3.2.9 Membrane performance tests

All membrane performance tests were conducted using a cross flow filtration system (see more detailed description in Appendix B). Membrane performance was tested under two pH levels, 5.3 and 10.5. At the start of each experiment, DI water was filtered through the membrane at 22°C at 500 psi for 60 h, which allowed for membrane compaction and other unknown causes of flux decline inherent to bench-scale recirculation systems. After stable flux was achieved, the pure water permeability was determined by measuring the water flux at this pressure (500 psi). Then 1500 ppm NaCl solution was added to the feed tank to start salt rejection test. The system was operated under nine different applied pressures in the range of 125~450 psi at a cross-flow velocity of 25 cm.s^{-1} at the target pH value. At each pressure, after running the system for at least 3 h, both feed and permeate water samples were collected. Salt concentration in the permeate C_p (M) and salt concentration in the feed C_F (M) were determined from feed and permeate conductivity measurements using a conductivity electrode (Accumet 13-620-160, Fisher Scientific, Pittsburgh, PA). Water flux J_v (m.d^{-1}) was determined by measuring the mass of permeate water and filtration time. Observed salt rejection R was calculated as

$$R = 1 - \frac{C_p}{C_F} \quad (3.12)$$

3.2.10 Prediction of effect of pH on salt rejection

The effect of pH on salt rejection can be predicted with similar approach as previously reported.[44] It can be easily demonstrated that, under the framework of the solution-diffusion model for transport of water and solutes through active layers,[5] the salt rejection *R* under negligible concentration polarization is given by

$$R = \frac{1}{1+\frac{B}{J_V}} \quad (3.13)$$

where *B* (m.d^{-1}) is the solute diffusive permeation coefficient given by

$$B = \frac{P}{\delta} = \frac{K_S D_S}{\delta} \quad , \quad (3.14)$$

where (m) is the active layer thickness.[5]

In order to predict the change in salt rejection as a function of pH, we made the assumption that and D_S are approximately constant as a function of pH and remains constant as a function of pH compared to Donnan exclusion coefficien *E*.[48] From Equation 10 and 14, *B* values at two pH conditions can be related by

$$B_{pH10.5} = B_{pH5.3} \frac{(\gamma E)_{pH10.5}}{(\gamma E)_{pH5.3}} \quad (3.15)$$

So the steps to predict the rejection of NaCl are: (i) $B_{pH5.3}$ was obtained with Equation 14 and data from performance tests with NaCl at pH=5.3; (ii) $B_{pH10.5}$ was calculated with Equation 15, membrane charge density, and $B_{pH5.3}$; and (iii) NaCl rejection at pH 10.5 was predicted with Equation 13 and $B_{pH10.5}$.

3.3 Results and Discussion

3.3.1 Partitioning at pH 5.3

Partition coefficient results at pH 5.3 for all alkali metal chlorides (i.e., LiCl, NaCl, KCl, RbCl and CsCl) in the polyamide active layers of the SWC4+, XLE, ESPA3, NF90, and TFC membranes are presented in Table 3.2. The partition coefficients reported in Table 3.2 correspond to the average of K_p values measured at $C_{S,bulk}$ = 0.6 M, which is relevant to seawater NaCl concentration. At this concentration at pH 5.3, the Donnan exclusion coefficient approximates unity (E > 0.976), thus making K_p approximately constant.

Table 3.2. Summary of partition coefficients [a] of CsCl, RbCl, KCl, NaCl and LiCl in the polyamide active layer of SWC4+, XLE, ESPA3, NF90, and TFC membranes at pH 5.3. Scenarios A and B assume unhydrated and hydrated solutes in the polyamide phase, respectively.

		partition coefficient in the polyamide phase (K_p)				
membrane	hydrated solutes?	CsCl	RbCl	KCl	NaCl	LiCl
SWC4+	No	0.20±0.00	0.25±0.06	0.11±0.04	0.14±0.01	0.11±0.03
	Yes	0.08±0.01	0.08±0.02	0.03±0.01	0.03±0.00	0.02±0.01
XLE	No	0.32±0.05	0.30±0.05	0.06±0.00	0.28±0.04	0.05±0.02
	Yes	0.12±0.02	0.09±0.02	0.01±0.00	0.06±0.01	0.01±0.00
ESPA3	No	0.33±0.06	0.22±0.03	0.11±0.00	0.17±0.03	0.10±0.03
	Yes	0.13±0.02	0.07±0.01	0.03±0.00	0.04±0.01	0.02±0.01
NF90	No	0.45±0.07	0.35±0.04	0.36±0.07	0.28±0.07	0.46±0.12
	Yes	0.17±0.03	0.11±0.01	0.09±0.02	0.06±0.01	0.08±0.02
TFC	No	0.35±0.01	0.22±0.01	0.25±0.01	0.14±0.02	0.06±0.03
	Yes	0.13±0.00	0.07±0.00	0.06±0.00	0.03±0.00	0.01±0.01
$MW_{unhydrated}$	$g.mol^{-1}$	168.36	120.92	78.55	58.44	42.39
hydration number=n_p	unitless	15.0[49]	14.4[49]	13.0[49]	12.3[49]	10.9[49]

[a] Reported values and uncertainties correspond to the average and standard deviation of duplicate samples.

Consistent with our previous findings for the SWC4+ membrane,[7] the partition coefficients for all membranes were lower than 1 for all solutes studied. Specifically, partition

coefficients for unhydrated (hydrated) alkali chlorides were in the 0.05-0.45 (0.01-0.17) range. The partition coefficients obtained in this and our previous study[7] were significantly lower (K_p < 1) compared to those reported for various inorganic salts (KI, KBr, CsCl, or Na_2WO_4) and arsenious acid in studies[50,51] (K_p > 3.6) where other experimental procedures were used for partitioning measurements. Our partitioning results (i.e., K_p < 1) are in better agreement with intuitive expectations as polyamide active layers exhibit NaCl rejection levels of 97+% (i.e., 99.7%, 99.0%, 98.5%, 97.0% and 97.5%, for the SWC4+, XLE, ESPA3, NF90, and TFC membranes, respectively),[52–55] and therefore would be expected to exclude salts (i.e., K_p < 1) as opposed have a higher affinity for them than water (i.e., K_p > 1). Further, electrostatic exclusion of ions by the Donnan mechanism also predicts partition coefficients lower than 1.[7,45] We believe that the larger partition coefficients reported in the cited studies are the result of the drying steps to which the membrane samples were subjected between exposure to the solution of interest and sample analysis[50,51]; in our experimental procedure, partitioning is measured while the sample is exposed to the solution of interest, and therefore, no drying step is required.

For each membrane, partition coefficients were relatively similar across alkali chlorides, except for LiCl which generally had the lowest partition coefficient under either of the assumptions (i.e., hydrated or unhydrated ions). Given that lithium has a significantly larger hydrated ionic radius (3.8 Å)[56] compared to the other cations tested (3.6 Å for Na^+ and ~3.3 Å for K^+, Rb^+ and Cs^+)[56], the results suggest that ions partition in a (at least partially) hydrated state, steric effects play a role in the differences in partitioning observed among salts, and partition coefficient calculations assuming hydrated ions are more accurate than those assuming unhydrated ions. Atomistic modeling studies[57–63] of ions in crosslinked aromatic polyamide also support that ions are hydrated within polyamide active layers. For example, Hughes et al[60]

reported 6.0 water molecules of hydration for Na^+, which is similar to 5.6 water molecules of hydration in bulk solution.

We were unable to further evaluate from a theoretical perspective the observed differences in partitioning among chloride salts. This is because no theoretical model has proven to describe well differences in salt partitioning on the basis of salt idendity, when salts have the same charge and similar size (e.g., NaCl vs KCl). Specifically, Donnan theory only takes into account ion charge,[45] and Manning theory[64–66]–which takes into account ion identity- was proven to not work well for an aromatic polyamide active layer.[7]

Comparing membranes, the membrane with the lowest salt rejection (NF90, 97.0% nominal NaCl rejection[55]) generally had the highest partition coefficient for all solutes. By contrast, the membrane with the highest salt rejection (SWC4+, 99.7% nominal NaCl rejection[52]) always had the lowest or second lowest partition coefficients. For NaCl specifically, NF90 had the highest partition coefficient ($K_{p,hyd}$ = 0.06±0.01) and SWC4+ had the lowest one ($K_{p,hyd}$ = 0.03±0.00, hydrated). Given that when comparing any two membranes, the membrane with higher NaCl rejection did not necessarily have the lower partition coefficient (e.g., NF90 and XLE have 97.0% and 99.0% nominal NaCl rejection, respectively[53,55], but the same NaCl partition coefficient $K_{p,hyd}$ = 0.06±0.01), the partitioning results indicate that salt diffusion coefficients play an important role in salt rejection differences among aromatic polyamide membranes.

3.3.2 Effect of pH on NaCl partitioning

As discussed above, assuming that ions have a hydration number equal to that in bulk solution (Scenario B) is likely more representative of the hydration state of partitioned ions than

assuming ions are unhydrated (Scenario A). Therefore, in the remainder of this manuscript we only discuss partition coefficients results obtained under the assumption of hydrated ions and present representative results for unhydrated ions in the Appendix B.

We initially focus our attention on the effect that changing the bulk solution pH from 5.3 to 10.5 had on the partitioning of NaCl (Figure 3.2). The corresponding results presented in Figure 3.2 show that, for all membranes, NaCl partitioning was lower at pH 10.5 than at pH 5.3. Partition coefficients for NaCl at pH 10.5 and at a bulk salt concentration of $C_{s,bulk}$ = 0.6 M (i.e., representative of seawater) were in the 0.028-0.072 range with NF90 and SWC4+ having the highest (0.072±0.009) and lowest (0.028±0.003) NaCl partition coefficients, respectively. In general, for each membrane, greater differences in partitioning were observed at lower salt concentration in bulk solution, consistent with expectations from Donnan theory.[45] At greater salt concentration in bulk solution, the additional sites in the membrane active layers that ionize when the pH is increased from 5.3 to 10.5 are screened to a larger extent resulting in smaller increases in ion exclusion.[10,45]

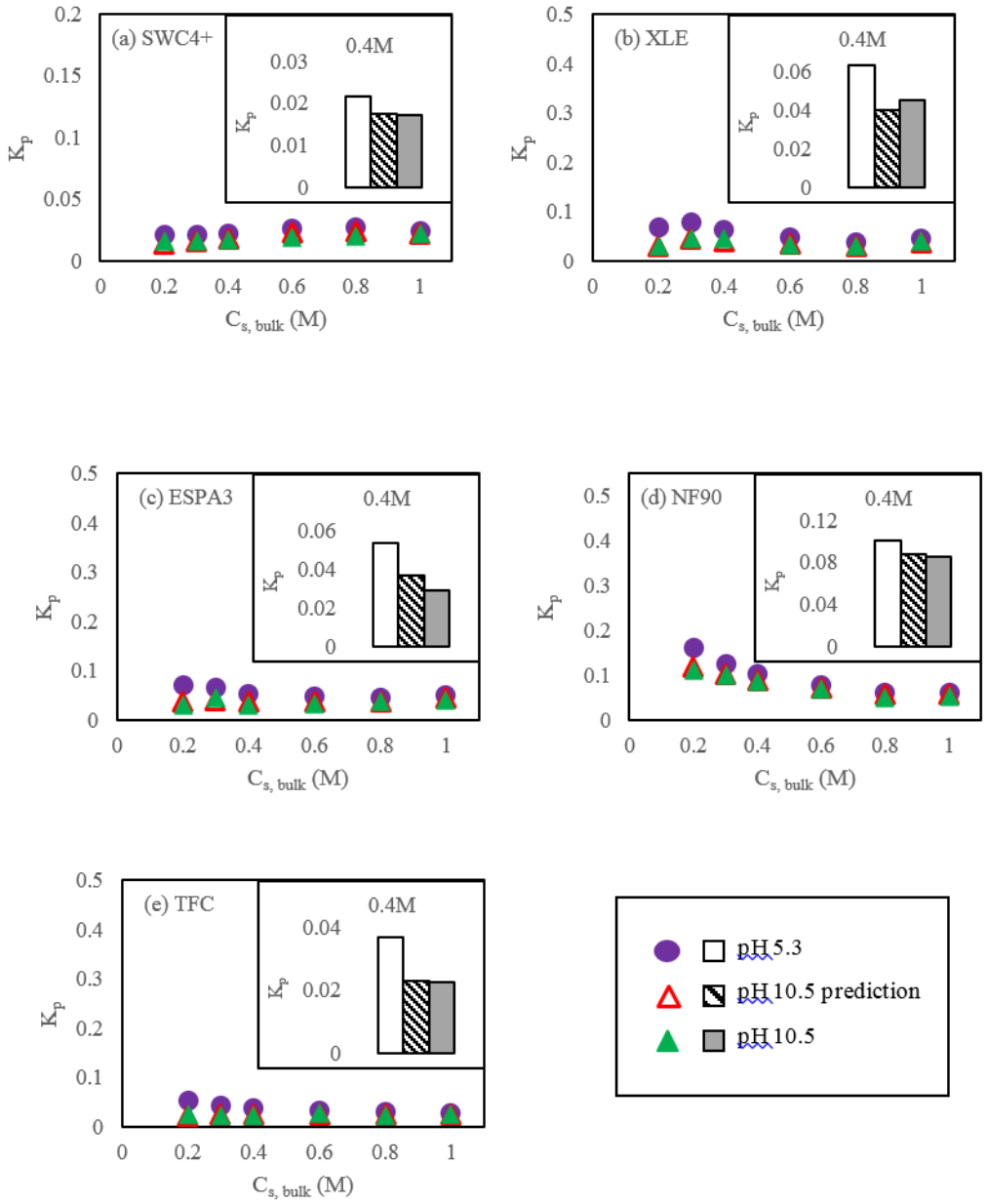

Figure 3.2. Partition coefficient of NaCl in the polyamide phase (K_p) of representative active layer samples from (a) SWC4+ (b) XLE (c) ESPA3 (d) NF90 and (e) TFC membranes as a function of solute concentration in bulk solution ($C_{S,bulk}$) assuming that solutes in polyamide have the same hydration number as in bulk solution (Scenario B). All panels present results at pH 5.3 and 10.5 (solid symbols) obtained during the same experimental run, and include predictions of K_p at pH 10.5 (empty symbols) based on the experimental results at pH 5.3 and Donnan theory (Equation 11). Only mass changes greater than the limit of quantification (LOQ = 33 ng.cm^{-2}) from QCM tests were used for calculations, which correspond to $C_{S,bulk} > 0.1$M in this set of experiments.[7,32]

We compared the experimental and predicted differences in NaCl partitioning between pH 5.3 and pH 10.5 (Figure 3.2). Predictions were obtained as described in the Materials and Methods section based on an extended solution-diffusion model including Donnan theory (Equations 3.9-3.11) and membrane charge density measurements (Table 3.3). The corresponding results show that experiment and prediction were in close agreement for all membranes across the entire range of salt concentration in bulk solution ($C_{s,bulk} \leq 1$ M). Experimental and predicted values were typically within 22.1% of each other, and were more than 10% different only in 24 out of 60 conditions tested (i.e., duplicates of 5 membranes x 6 concentrations). Thus, the results indicate that Donnan theory provides an adequate theoretical framework to predict the effect of pH on NaCl partitioning in polyamide RO membranes of a broad range of performance properties.

Table 3.3. Measured layer thicknesses, charge densities and void fractions for membrane active layers. Reported values and uncertainties correspond to the average and standard deviation of duplicate samples.

Membrane properties		SWC4+	XLE	ESPA3	NF90	TFC
Active layer thickness (nm)		87±6	113±9	111±7	139±1	77±19
Charge Density (M)	pH=5.3	0.031±0.000	0.023±0.009	0.011±0.002	0.015±0.001	0.014±0.002
	pH=8.0	0.134±0.016	0.164±0.050	0.072±0.007	0.144±0.005	0.172±0.049
	pH=10.5	0.207±0.000	0.300±0.053	0.146±0.029	0.310±0.011	0.351±0.086
Void fraction (unitless)		0.07±0.01	0.31±0.02	0.28±0.14	0.15±0.02	0.15±0.03

We also evaluated NaCl partitioning in all membranes at pH 8.0 (Figure 3.3). Consistent with expectations from Donnan theory[45], the NaCl partition coefficients at pH 8.0 were intermediate between those obtained at pH 5.3 and 10.5. At $C_{s,bulk}$ = 0.6 M, NaCl partition coefficients at pH 8.0 were in the 0.024-0.059 range with NF90 and SWC4+ having the highest

(0.059±0.008) and lowest (0.024±0.002) values, respectively. A comparison of experimental and predicted (Equations 3.9-3.11) differences in NaCl partitioning between pH 5.3 and pH 8.0 (Figure 3.3) shows that as for the pH 5.3 vs pH 10.5 case (Figure 3.2), experiment and prediction were in close agreement for all membranes. Experimental and predicted values were typically within 20.5% of each other and were more than 10% different only in 28 out of 60 conditions tested (i.e., duplicates of 5 membranes x 6 concentrations). Thus, the results reinforce the observation that Donnan theory provides an adequate theoretical framework to predict the effect of pH on NaCl partitioning in polyamide RO membranes.

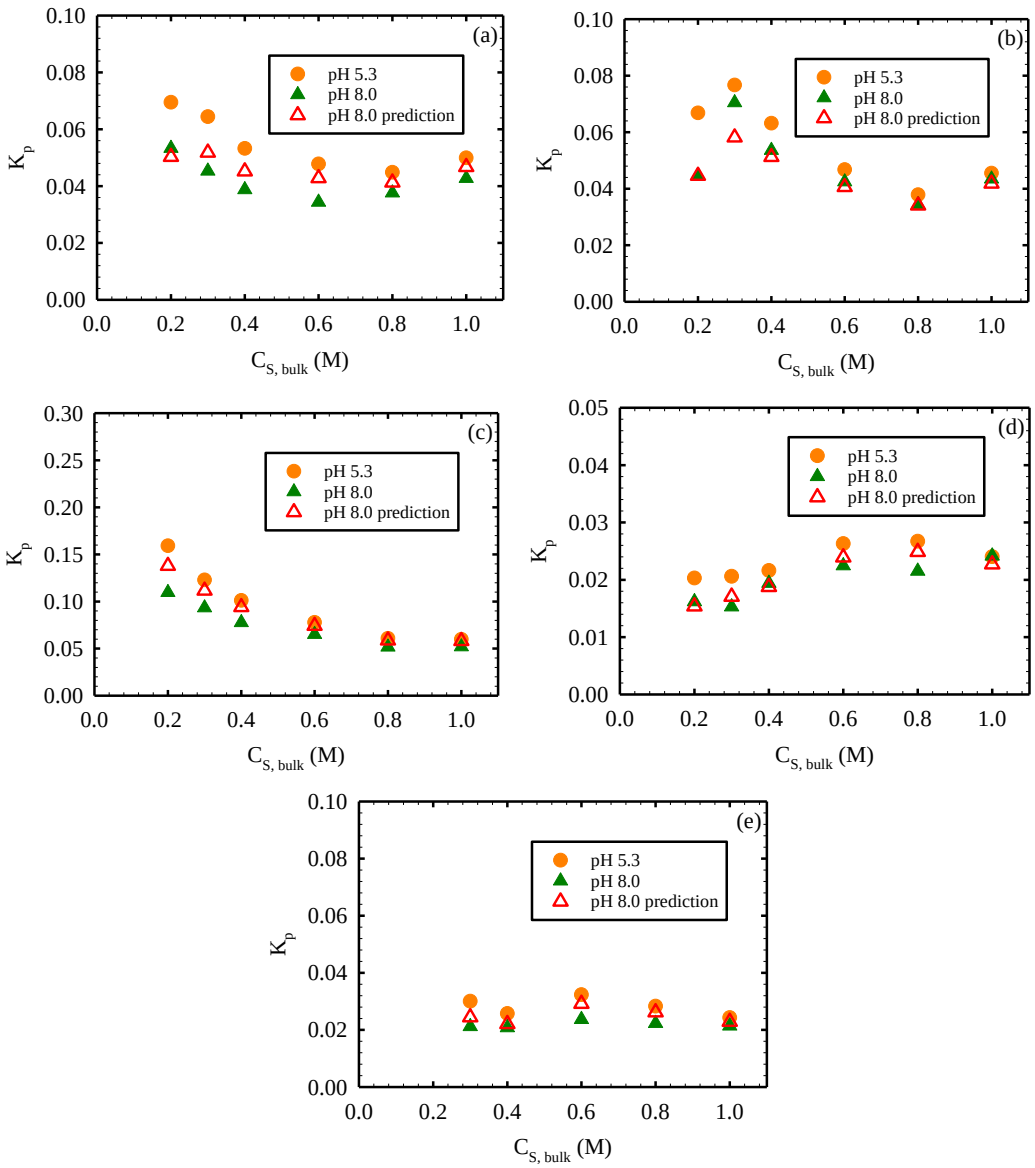

Figure 3.3. Partition coefficient of NaCl in polyamide phase of representative active layer samples (K_p) from (a) XLE (b) ESPA3 (c) NF90 (d) SWC4+ and (e) TFC membranes as a function of solute concentration in bulk solution ($C_{S,bulk}$) assuming that solutes in the polyamide layer have the same hydration number as in bulk solution (Scenario B). All panels present results at pH 5.3 and 8.0 (solid symbols) obtained during the same experimental run, and include predictions of K_p at pH 8.0 (empty symbols) based on the experimental results at pH 5.3 and Donnan exclusion theory.

3.3.3 Effect of pH on the partitioning of other chloride salts of alkali metals

Similarly as for NaCl, we evaluated the effect that pH had on the partitioning of LiCl, KCl, RbCl and CsCl in polyamide membranes (Figure 3.4). The XLE membrane was used as the test membrane and experiments were performed at pH 5.3 and 10.5. Consistent with the results

obtained for NaCl (Figure 3.2) and expectations from Donnan theory, partition coefficients for LiCl, KCl, RbCl and CsCl at pH 10.5 were always lower than at pH 5.3. Also as for NaCl, partition coefficients at pH 10.5 for LiCl, KCl, RbCl and CsCl were in the 0.029-0.144 range for ionic strengths representative of that of seawater ($C_{s,bulk}$ = 0.6 M); among the five chloride salts, RbCl (K_p = 0.144±0.031) and KCl (K_p = 0.029±0.003) had the highest and lowest partition coefficients, respectively.

For each LiCl, KCl, RbCl and CsCl, we compared the experimental and predicted (Equations 9-11) differences in partitioning between pH 5.3 and pH 10.5 (Figure 3.4). The corresponding results show that, as for NaCl partitioning (Figures 3.2 and 3.3), experiment and prediction were in close agreement for all salts across the range of salt concentration in bulk solution tested. Experimental and predicted values were typically within 20.2% of each other and were more than 10% different only in 26 out of 60 conditions tested (i.e., duplicates of 1 membranes x 6 concentrations x 5 salts including NaCl). Thus, the results indicate that Donnan theory provides an adequate theoretical framework to predict the effect of pH on the partitioning of not just NaCl, but of all chloride salts of alkali metals, in polyamide RO membranes.

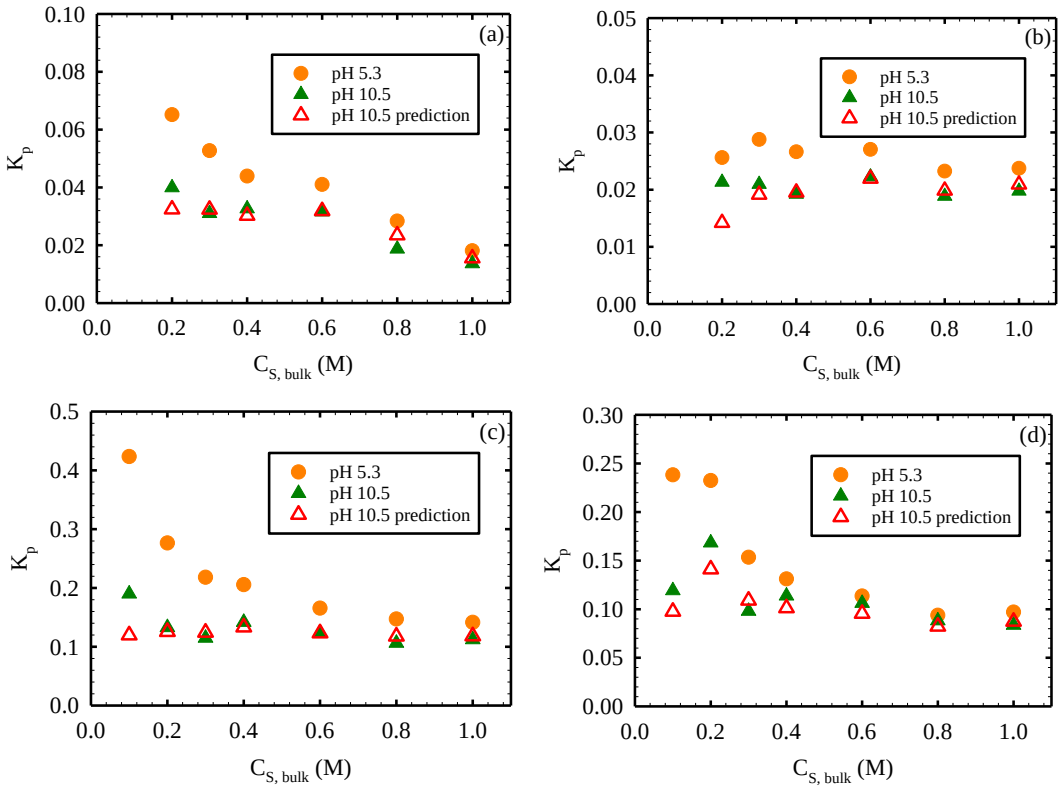

Figure 3.4. Partition coefficient in the polyamide phase (K_p) of XLE membrane as a function of solute concentration in bulk solution ($C_{S,bulk}$) assuming that solutes in the polyamide layer have the same hydration number as in bulk solution (Scenario B). Panels (a), (b), (c) and (d) present results for LiCl, KCl, RbCl, and CsCl, respectively. All panels present results at pH 5.3 and 10.5 obtained during the same experimental run, and include predictions of K_p at pH 10.5 (empty symbols) based on the experimental results at pH 5.3 and Donnan exclusion theory. Partition coefficients were calculated based on the areal mass changes ($\Delta m_{XCl,AL}$) measured for the coated sensors when exposed to test solutions.

3.3.4 Donnan theory prediction of the effect of pH on salt rejection

Figure 3.5 presents NaCl rejection results at pH 5.3 (circles) and pH 10.5 (diamonds), as well as the solution-diffusion model fit to the pH 5.3 data (solid lines) and prediction of rejection at pH 10.5 (dashed lines) using Donnan theory. Fitted and predicted model parameters are summarized in Table 3.4. As observed in Figure 3.5, for all membranes, Donnan theory successfully predicted the change in NaCl rejection caused by the change in feed solution pH. For example, at a transmembrane pressure of 250 psi, the difference between the measured and predicted rejections were 0.03, 0.14, 0.01, 0.08, and 0.16 percentages points for the SWC4+,

XLE, ESPA3, NF90 and TFC membranes, respectively. Consistent with these results, Coronell et al[10] reported that the same modeling approach used here successfully predicted the change in rejection of potassium iodide (KI) caused by a change in feed solution pH from pH 5.3 to pH 8.0 and 10.5.

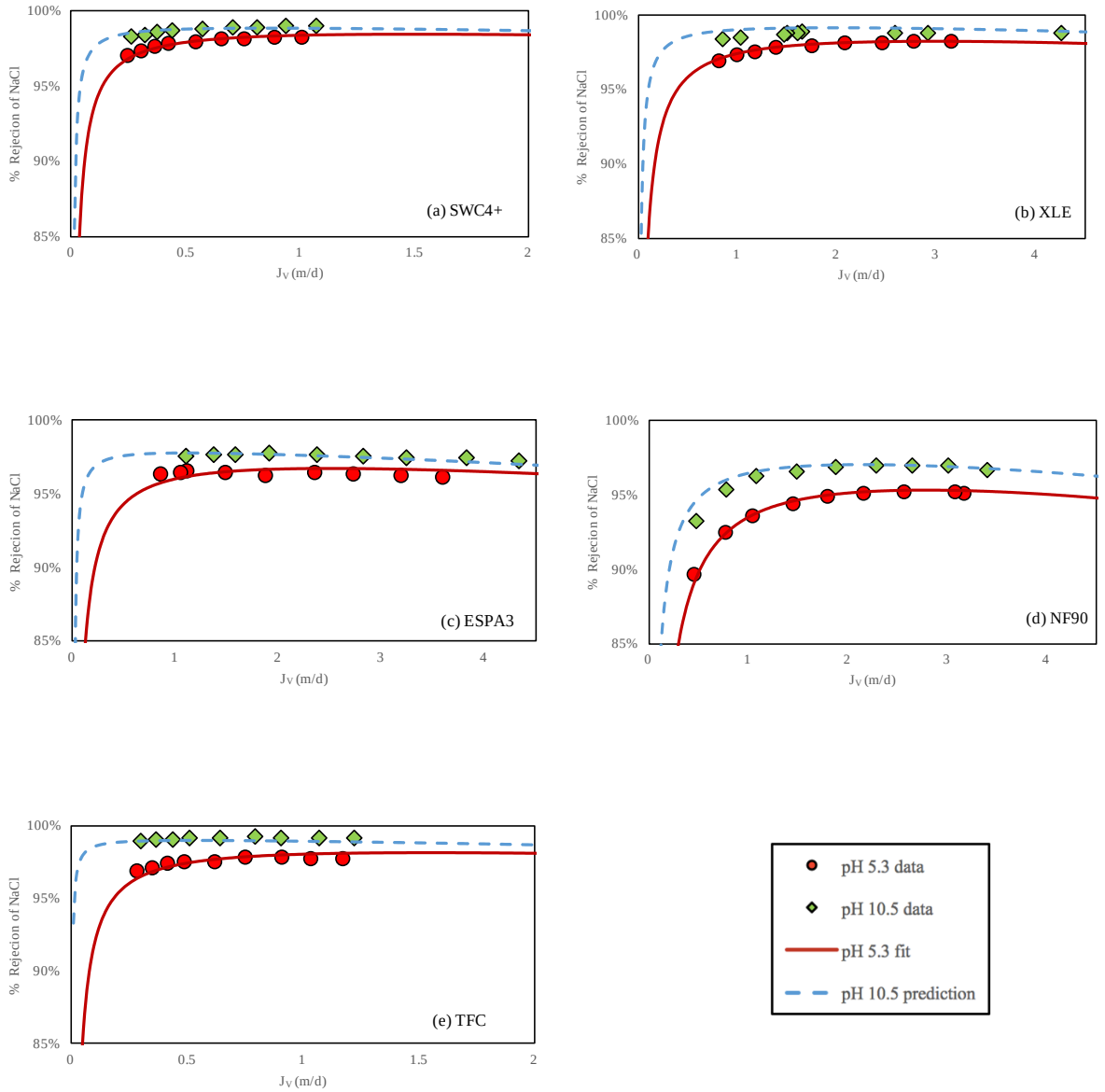

Figure 3.5. Rejection of sodium chloride (NaCl) as a function of pH by the (a) SWC4+, (b) XLE, (c) ESPA3, (d) NF90 and (e) TFC membranes. Red and green indicate pH values of 5.3

and 10.5, respectively. Continuous lines correspond to model fitting results, and dashed lines correspond to model predictions. A summary of fitted and predicted model parameters is presented in Table 3.4.

Table 3.4. Summary of parameters related to the prediction of the rejection of sodium chloride (NaCl) by the SWC4+, XLE, ESPA3, NF90, and TFC membranes at pH values in the 5.3−10.5 range based on rejection results at pH = 5.3.

Membrane		SWC4+	XLE	ESPA3	NF90	TFC
B (m/d)	pH 5.3 fit	0.0059	0.0240	0.0197	0.0447	0.0076
	pH 10.5 fit	0.0021	0.0056	0.0043	0.0232	0.0006
	pH 10.5 prediction	0.0016	0.0065	0.0030	0.0195	0.0006

The successful prediction by Donnan theory of the effect of pH on salt partitioning (i.e., chloride salts of alkali metals in Figures 3.2 and 3.3) and salt rejection (i.e., NaCl in Figure 3.5 and KI in ref 10) serves as evidence that changes in salt rejection with pH are mostly attributable to corresponding changes in salt partitioning, not salt diffusion (i.e., salt diffusion coefficients do not significantly change with feed solution pH). This conclusion is reached on the basis that the predictions assume that changes in salt rejection with pH are caused entirely by corresponding changes in salt partition coefficient. Our results also show that measurements of salt partitioning at a single pH and measurements of charge density as a function of pH can serve as data inputs in predictive models of the performance of RO membranes. The results also support that the solution-diffusion model and Donnan theory could serve as theoretical framework for such predictive models.

3.4 Conclusion

In summary, I performed a comprehensive characterization of the partitioning of chloride salts of alkali metals (LiCl, NaCl, KCl, RbCl and CsCl) from aqueous phase into the polyamide active layers of five polyamide TFC membranes, including one prepared in-house and four commercial membranes (SWC4+. XLE, ESPA3 and NF90). I also evaluated the pH effect on the

partitioning of alkali metal salts, and whether the pH dependence of salt partitioning and rejection are consistent with predictions from Donnan exclusion theory. The conclusions from this chapter are:

- For all membranes, the partition coefficients of all salts were lower than 1 and did not differ much among different RO membranes.
- The results and analysis also showed that, for all membranes tested, Donnan theory provided an appropriate theoretical framework to predict the effect of pH on salt partitioning (evaluated for all chloride salts of alkali metals) and salt rejection (evaluated for NaCl).
- Changes in salt rejection with feed solution pH are primarily driven by changes in salt partitioning with likely minimal (or absent) changes in salt diffusion.

3.5 Acknowledgements

We acknowledge Hydranautics for providing the membrane materials. This work was supported by the US National Science Foundation (NSF) (Award Nos. 1264690 and 1336532), and Dissertation Completion Fellowship from UNC Graduate School.

REFERENCES

(1) Nicolaisen, B. Developments in Membrane Technology for Water Treatment. *Desalination* **2003**, *153* (1–3), 355–360.

(2) Shannon, M.; Bohn, P. W.; Elimelech, M.; Georgiadis, J. G.; Mariñas, B. J.; Mayes, A. M. Science and Technology for Water Purification in the Coming Decades. *Nature* **2008**, *452* (March), 301–310.

(3) Elimelech, M.; Phillip, W. A. The Future of Seawater and the Environment. *Science (80-.).* **2011**, *333* (August), 712–718.

(4) Petersen, R. J. Composite Reverse Osmosis and Nanofiltration Membranes. *J. Memb. Sci.* **1993**, *83* (1), 81–150.

(5) Wijmans, J. G.; Baker, R. W. The Solution-Diffusion Model: A Review. *J. Memb. Sci.* **1995**, *107* (1–2), 1–21.

(6) Paul, D. R. Reformulation of the Solution-Diffusion Theory of Reverse Osmosis. *J. Memb. Sci.* **2004**, *241* (2), 371–386.

(7) Wang, J.; Kingsbury, R. S.; Perry, L. A.; Coronell, O. Partitioning of Alkali Metal Salts and Boric Acid from Aqueous Phase into the Polyamide Active Layers of Reverse Osmosis Membranes. *Environ. Sci. Technol.* **2017**, *51* (4), 2295–2303.

(8) Wagner, E. M. Van; Sagle, A. C.; Sharma, M. M.; Freeman, B. D. Effect of Crossflow Testing Conditions , Including Feed PH and Continuous Feed Filtration , on Commercial Reverse Osmosis Membrane Performance. **2009**, *345*, 97–109.

(9) Xu, Y.; Lebrun, R. E. Investigation of the Solute Separation by Charged Nanofiltration Membrane: Effect of PH, Ionic Strength and Solute Type. *J. Memb. Sci.* **1999**, *158* (1–2), 93–104.

(10) Coronell, O.; Mi, B. Modeling the Effect of Charge Density in the Active Layers of Reverse Osmosis and Nanofiltration Membranes on the Rejection of Arsenic (III) and Potassium Iodide. *Environ. Sci. …* **2012**, *47* (Iii), 420–428.

(11) Lipp, P.; Gimbel, R.; Frimmel, F. H. Parameters Influencing the Rejection Properties of FT30 Membranes. *J. Memb. Sci.* **1994**.

(12) Wang, X.; Wangb, W.; Wang, D. Experimental Investigation on Separation Performance of Nanofiltration Membranes for Inorganic Electrolyte Solutions. **2002**, *145*, 115–122.

(13) Desalination, E.; Rheinisch-westfi, I. W. W.; Universiti, G.; Mehta, R.; Brahmbhatt, H.; Mukherjee, M.; Bhattacharya, A.; Hagmeyer, G.; Gimbel, R.; Hyung, H.; et al. Boron Removal from Seawater Using High Rejection SWRO Membranes - Impact of PH, Feed Concentration, Pressure, and Cross-Flow Velocity. *Desalination* **2008**, *227* (1–3), 253–263.

(14) Bandini, S.; Drei, J.; Vezzani, D. The Role of PH and Concentration on the Ion Rejection in Polyamide Nanofiltration Membranes. **2005**, *264*, 65–74.

(15) Hoang, T.; Stevens, G.; Kentish, S. The Effect of Feed PH on the Performance of a Reverse Osmosis Membrane. *DES* **2010**, *261* (1–2), 99–103.

(16) Mazzoni, C.; Bruni, L.; Bandini, S. Nanofiltration : Role of the Electrolyte and PH on Desal DK Performances †. **2007**, 2254–2262.

(17) Dalwani, M.; Benes, N. E.; Bargeman, G.; Stamatialis, D.; Wessling, M. Effect of PH on the Performance of Polyamide / Polyacrylonitrile Based Thin Film Composite Membranes. *J. Memb. Sci.* **2011**, *372* (1–2), 228–238.

(18) Hurwitz, G.; Guillen, G. R.; Hoek, E. M. V. Probing Polyamide Membrane Surface Charge , Zeta Potential , Wettability , and Hydrophilicity with Contact Angle Measurements. **2010**, *349*, 349–357.

(19) Childress, A. E.; Elimelech, M. Relating Nanofiltration Membrane Performance to Membrane Charge (Electrokinetic) Characteristics. *Environ. Sci. Technol.* **2000**, *34* (17), 3710–3716.

(20) Tang, C. Y.; Kwon, Y. N.; Leckie, J. O. Effect of Membrane Chemistry and Coating Layer on Physiochemical Properties of Thin Film Composite Polyamide RO and NF Membranes. II. Membrane Physiochemical Properties and Their Dependence on Polyamide and Coating Layers. *Desalination* **2009**, *242* (1–3), 168–182.

(21) Coronell, O.; González, M. I.; Mariñas, B. J.; Cahill, D. G. Ionization Behavior, Stoichiometry of Association, and Accessibility of Functional Groups in the Active Layers of Reverse Osmosis and Nanofiltration Membranes. *Environ. Sci. Technol.* **2010**, *44* (17), 6808–6814.

(22) Coronell, O.; Mariñas, B. J.; Cahill, D. G. Depth Heterogeneity of Fully Aromatic Polyamide Active Layers in Reverse Osmosis and Nanofiltration Membranes. *Environ. Sci. Technol.* **2011**, *45* (10), 4513–4520.

(23) Freger, V. Swelling and Morphology of the Skin Layer of Polyamide Composite Membranes: An Atomic Force Microscopy Study. *Environ. Sci. Technol.* **2004**, *38* (11), 3168–3175.

(24) Lee, J.; Doherty, C. M.; Hill, A. J.; Kentish, S. E. Water Vapor Sorption and Free Volume in the Aromatic Polyamide Layer of Reverse Osmosis Membranes. *J. Memb. Sci.* **2013**, *425–426*, 217–226.

(25) Pacheco, F. A.; Pinnau, I.; Reinhard, M.; Leckie, J. O. Characterization of Isolated Polyamide Thin Films of RO and NF Membranes Using Novel TEM Techniques. *J. Memb. Sci.* **2010**, *358* (1–2), 51–59.

(26) Yan, H.; Miao, X.; Xu, J.; Pan, G.; Zhang, Y.; Shi, Y.; Guo, M.; Liu, Y. The Porous Structure of the Fully-Aromatic Polyamide Film in Reverse Osmosis Membranes. *J. Memb. Sci.* **2015**, *475*, 504–510.

(27) Perry, L. A.; Coronell, O. Reliable, Bench-Top Measurements of Charge Density in the Active Layers of Thin-Film Composite and Nanocomposite Membranes Using Quartz Crystal Microbalance Technology. *J. Memb. Sci.* **2013**, *429*, 23–33.

(28) Lin, L.; Lopez, R.; Ramon, G. Z.; Coronell, O. Investigating the Void Structure of the Polyamide Active Layers of Thin-Film Composite Membranes. *J. Memb. Sci.* **2016**, *497*, 365–376.

(29) Lin, L.; Feng, C.; Lopez, R.; Coronell, O. Identifying Facile and Accurate Methods to Measure the Thickness of the Active Layers of Thin-Film Composite Membranes – a Comparison of Seven Characterization Techniques. *J. Memb. Sci.* **2015**, *498*, 167–179.

(30) Bason, S.; Oren, Y.; Freger, V. Characterization of Ion Transport in Thin Films Using Electrochemical Impedance SpectroscopyII: Examination of the Polyamide Layer of RO Membranes. *J. Memb. Sci.* **2007**, *302* (1–2), 10–19.

(31) Bason, S.; Oren, Y.; Freger, V. Ion Transport in the Polyamide Layer of RO Membranes: Composite Membranes and Free-Standing Films. *J. Memb. Sci.* **2011**, *367* (1–2), 119–126.

(32) Wisconsin Department of Natural Resources. *Analytical Detection Limit Guidance & Laboratory Guide for Determining Method Detection Limits*; 1996.

(33) Lin, L.; Lopez, R.; Ramon, G. Z.; Coronell, O. Investigating the Void Structure of the Polyamide Active Layers of Thin-Film Composite Membranes. *J. Memb. Sci.* **2016**, *497*, 365–376.

(34) Powell, J.; Luh, J.; Coronell, O. Amide Link Scission in the Polyamide Active Layers of Thin-Film Composite Membranes upon Exposure to Free Chlorine: Kinetics and Mechanisms. *Environ. Sci. Technol.* **2015**, *49* (20), 12136–12144.

(35) Braun, G.; Hater, W.; Kolk, C. zum; Dupoiron, C.; Harrer, T.; Götz, T. Investigations of Silica Scaling on Reverse Osmosis Membranes. *Desalination* **2010**, *250* (3), 982–984.

(36) Sheikholeslami, R.; Al-Mutaz, I. S.; Koo, T.; Young, A. Pretreatment and the Effect of Cations and Anions on Prevention of Silica Fouling. *Desalination* **2001**, *139* (1–3), 83–95.

(37) Sagiv, A.; Semiat, R. Analysis of Parameters Affecting Boron Permeation through Reverse Osmosis Membranes. *J. Memb. Sci.* **2004**, *243* (1–2), 79–87.

(38) Hyung, H.; Kim, J. A Mechanistic Study on Boron Rejection by Sea Water Reverse Osmosis Membranes. **2006**, *286*, 269–278.

(39) Richards, L. A.; Vuachère, M.; Schäfer, A. I. Impact of PH on the Removal of Fluoride , Nitrate and Boron by Nanofiltration / Reverse Osmosis. *DES* **2010**, *261* (3), 331–337.

(40) Marcus, Y. Effect of Ions on the Structure of Water : Structure Making and Breaking. *Chem. Rev.* **2009**, *109*, 1346–1370.

(41) Avraham, E.; Noked, M.; Soffer, A.; Aurbach, D. The Feasibility of Boron Removal from Water by Capacitive Deionization. *Electrochim. Acta* **2011**, *56* (18), 6312–6317.

(42) Wang, J.; Mo, Y.; Mahendra, S.; Hoek, E. M. V. Effects of Water Chemistry on Structure and Performance of Polyamide Composite Membranes. *J. Memb. Sci.* **2014**, *452*, 415–425.

(43) Geise, G. M.; Paul, D. R.; Freeman, B. D. Fundamental Water and Salt Transport Properties of Polymeric Materials. *Prog. Polym. Sci.* **2014**, *39* (1), 1–24.

(44) Coronell, O.; Mi, B.; Mariñas, B. J.; Cahill, D. G. Modeling the Effect of Charge Density in the Active Layers of Reverse Osmosis and Nanofiltration Membranes on the Rejection of Arsenic(III) and Potassium Iodide. *Environ. Sci. Technol.* **2013**, *47* (1), 420–428.

(45) Ohshima, H.; Ohki, S. Donnan Potential and Surface Potential of a Charged Membrane. *Biophys. J.* **1985**, *47* (5), 673–678.

(46) Pitzer, K. S.; Mayorga, G. Thermodynamics of Electrolytes II. Activity and Osmotic Coefficients for Strong Electrolytes with One or Both Ions Univalent. *J. Chem. Inf. Model.* **1973**, *77* (19), 2300–2308.

(47) Pitzer, K. S. *Activity Coefficients in Electrolyte Solutions*, 2nd ed.; CRC Press: Boston, 1991.

(48) Coronell, O.; Mi, B.; Cahill, D. G. Modeling the Effect of Charge Density in the Active Layers of Reverse Osmosis and Nano Fi Ltration Membranes on the Rejection of Arsenic(III) and Potassium Iodide. *Environ. Sci. Technol.* **2013**, *47* (Iii), 420–428.

(49) Marcus, Y. Effect of Ions on the Structure of Water : Structure Making and Breaking Effect of Ions on the Structure of Water : Structure Making and Breaking. *Chem. Rev.* **2009**, *109* (February), 1346–1370.

(50) Mi, B.; Mariñas, B. J.; Cahill, D. G. RBS Characterization of Arsenic(III) Partitioning from Aqueous Phase into the Active Layers of Thin-Film Composite NF/RO Membranes. *Environ. Sci. Technol.* **2007**, *41* (9), 3290–3295.

(51) Zhang, X.; Cahill, D. G.; Coronell, O.; Mariñas, B. J. Partitioning of Salt Ions in FT30 Reverse Osmosis Membranes. *Appl. Phys. Lett.* **2007**, *91* (18), 181904.

(52) Hydranautics. SWC4+ 8040 seawater reverse osmosis element datasheet. http://www.lenntech.com/Data-sheets/Hydranautics-SWC4+8040.pdf (accessed Aug 20, 2016).

(53) Information, P.; Specifications, P. Dow Filmtec. XLE-440 extra low energy RO element datasheet, Form No. 609-00245- 0606. http://www.lenntech.com/Data-sheets/Dow-Filmtec-XLE-440.pdf (accessed Aug 20, 2016).

(54) Hydranautics. ESPA3-4040 brackish water reverse osmosis membrane element datasheet. http://www.lenntech.com/Data-sheets/Hydranautics-ESPA3-4040.pdf (accessed Aug 20, 2016).

(55) Dow Filmtec. NF90-400 nanofiltration element datasheet, Form No. 609-00345-0312 http://www.lenntech.com/Data-sheets/Dow-Filmtec-NF90-400.pdf (accessed Aug 20, 2016).

(56) Dove, P. M.; Nix, C. J. The Influence of the Alkaline Earth Cations, Magnesium, Calcium, and Barium on the Dissolution Kinetics of Quartz. *Geochim. Cosmochim. Acta* **1997**, *61* (16), 3329–3340.

(57) Harder, E.; Walters, D. E.; Bodnar, Y. D.; Faibish, R. S.; Roux, B. Molecular Dynamics Study of a Polymeric Reverse Osmosis Membrane. *J. Phys. Chem. B* **2009**, *113* (30), 10177–10182.

(58) Shen, M.; Keten, S.; Lueptow, R. M. Dynamics of Water and Solute Transport in Polymeric Reverse Osmosis Membranes via Molecular Dynamics Simulations. *J. Memb. Sci.* **2016**, *506*, 95–108.

(59) Kolev, V.; Freger, V. Molecular Dynamics Investigation of Ion Sorption and Permeation in Desalination Membranes. *J. Phys. Chem. B* **2015**, *119* (44), 14168–14179.

(60) Hughes, Z. E.; Gale, J. D. A Computational Investigation of the Properties of a Reverse Osmosis Membrane. *J. Mater. Chem.* **2010**, *20* (36), 7788.

(61) Ridgway, H. F.; Orbell, J.; Gray, S. Molecular Simulations of Polyamide Membrane Materials Used in Desalination and Water Reuse Applications: Recent Developments and Future Prospects. *J. Memb. Sci.* **2017**, *524* (October 2016), 436–448.

(62) Gai, J.; Gong, X.; Zhang, X.; Kang, W.; Wang, W. Key Role of Hydrates in Determining Ion Rejection by Polyamide Membrane. *Polym. Eng. Sci.* **2015**, *55* (2), 466–473.

(63) Ding, M.; Szymczyk, A.; Aziz, G. On the Structure and Rejection of Ions by a Polyamide Membrane in Pressure-Driven Molecular Dynamics Simulations. *Desalination* **2015**, 76–80.

(64) Kamcev, J.; Paul, D. R.; Freeman, B. D. Ion Activity Coefficients in Ion Exchange Polymers: Applicability of Manning's Counterion Condensation Theory. *Macromolecules* **2015**, *48* (21), 8011–8024.

(65) Kamcev, J.; Galizia, M.; Benedetti, F. M.; Jang, E.-S.; Paul, D. R.; Freeman, B.; Manning, G. S. Partitioning of Mobile Ions Between Ion Exchange Polymers and Aqueous Salt Solutions: Importance of Counter-Ion Condensation. *Phys. Chem. Chem. Phys.* **2016**, No. 1.

(66) Manning, G. S. Limiting Laws and Counterion Condensation in Polyelectrolyte Solutions. III. An Analysis Based on the Mayer Ionic Solution Theory. *J. Chem. Phys.* **1969**, *51* (8), 3249.

CHAPTER 4 – RELATIVE IMPORTANCE OF GEOMETRICAL AND INTRINSIC SALT TRANSPORT PROPERTIES OF ACTIVE LAYERS IN THE SALT REJECTION BY POLYAMIDE THIN-FILM COMPOSITE MEMBRANES

4.1 Introduction

Nowadays, membrane processes are the primary separation technology used in desalination and wastewater reclamation.[1–3] Polyamide thin-film composite membranes (TFC) play a key role in providing clean water to satisfy agricultural, industrial and municipal needs.[4] A typical TFC membrane comprises three layers: a polyamide top active layer (~20-200 nm), a polysulfone intermediate layer (~20-50 μm) and a polyester backing layer (~50-150 μm).[5] The active layer is the main barrier to water and salt transport through the membrane so its structure and properties dramatically affect membrane performance.[5–7]

TFCs have shown to be effective desalination technologies (salt rejection in the range of 97.0%-99.9)[8–13] but there is a continued need to improve their capabilities. Effective tailoring of materials requires a fundamental understanding of the transport mechanisms of water and salt during membrane separation. Transport models that relate membrane properties and performance are the tools used to understand membrane transport, and the solution-diffusion model is the most widely used one.[14,15] In the solution-diffusion model, salt transport through the membrane is described as a three-step process: (1) salt molecules partition into the active layer from the feed water side, (2) salt molecules diffuse through the active layer, and (3) salt molecules partition out of the

active layer to the permeate side. The ease with which salts permeate the membrane is quantified through the solute permeation coefficient B ($m \cdot s^{-1}$), as given by[14]

$$B = \frac{P_S}{\delta} \tag{4.1}$$

where P_S (unitless) is the salt permeability of the active layer salt and δ (m) is the active layer thickness. The salt permeability can be expressed as

$$P_S = K_S D_S \tag{4.2}$$

where K_S (unitless) is the salt partition coefficient between water and the active layer and D_S ($m \cdot s^{-1}$) is the salt diffusion coefficient within the active layer.

Equation 4.1 and 4.2 indicate that B is determined by the geometrical properties (δ) and intrinsic salt transport properties (K_S and D_S) of the active layer. So far, there are no studies found in the literature that have evaluated the relative importance of geometrical and intrinsic transport properties in the differences observed in salt permeability for polyamide TFC membranes.

In order to investigate the correlation of δ, P_S, K_S and D_S to B in polyamide active layers, each of these properties needs to be characterized. While B can be easily obtained from permeation tests, it has been proved challenging to individually quantify K_S and D_S due to the extreme thinness of the polyamide active layer (~20-200 nm). Given that the time scale of salt diffusion through active layers is short (within 10^{-2} seconds), limited experimental studies exist that measured D_S in the active layer experimentally. In fact, we could only find one such study[16]; this study used an electrochemical method that only applies to redox couples but not contaminants of common interest in water treatment. Recent advances in the characterizations of membrane active layer properties, including

active layer thickness[17], charge density[18] and salt partitioning[19,20], enables the independent measurement of salt partition coefficient and thus, the calculation of salt diffusion coefficients within the active layer using Equation 4.2.

Accordingly, the primary objective of this study was to evaluate the relative importance of active layer properties to explain the differences observed in salt rejection among TFC membranes having the same membrane chemistry. To accomplish this goal, we tested salt permeability for a group of polyamide membranes having the crosslinked aromatic polyamide chemistry, and quantified geometrical and salt transport properties. With this information, we were able to investigate the leading order causes of differences in observed salt rejection among crosslinked aromatic polyamide TFCs.

4.2 Materials and Methods

4.2.1 Salts and feed waters

All chemicals used were ACS grade with 99% or greater purity (Fisher Scientific, Pittsburgh, PA). Sodium chloride (NaCl) was used as the representative strong electrolyte in permeation tests. Characteristics of feed solutions included a target NaCl concentration of 1500 $mg.L^{-1}$, pH of 5.3, and temperature of 22°C. The pH of test solutions was adjusted by addition of hydrochloric acid (HCl) or sodium hydroxide (NaOH) solutions. Feed solutions containing chloride salts of other alkali metal ions (Li^+, K^+, Rb^+ and Cs^+) and boric acid were also tested. Corresponding water characteristics and results are presented in Appendix C.

4.2.2 Membranes and membrane sample preparation

Five thin-film composite membranes with fully-aromatic polyamide active layers[21] were used in this study including SWC4+ membrane[22] (Hydranautics, Oceanside,

CA), XLE membrane[23] (Dow Filmtec, Minneapolis, MN), ESPA3 membrane[24] (Hydranautics, Oceanside, CA), NF90[25] (Dow Filmtec, Minneapolis, MN) and TFC membranes fabricated in house. The commercial membranes were received from the manufactures as flat sheets. TFC membranes were fabricated through interfacial polymerization of meta-phenylene diamine (MPD, 3.5 wt% in aqueous solution) and trimesoyl chloride (TMC, 0.15 wt% in Isopar G^{TM} solution) on polysulfone supports (PS20 ultrafiltration membrane cut into 17.8 × 25.4 cm^2 pieces, Nanostone Water, Inc., Oceanside, CA). The detailed fabrication procedure can be found in Appendix C[26] Membranes were cut into 2.5 × 5.0 cm^2 coupons for characterization of physico-chemical properties and salt partitioning, and 11.0 × 8.0 cm^2 coupons for permeation experiments. The coupons were then thoroughly rinsed with ultrapure water (>18 MΩ.cm), and stored in ultrapure water in plastic bottles for at least 24 h until used. For determination of active layer thickness, void fractions and salt partition coefficients active layers were isolated on quartz crystal microbalance (QCM) sensors. The full active layer isolation procedure is reported elsewhere.[19] In brief, the polyester backing layer was manually peeled off, leaving the dual layers of polysulfone and polyamide, which was placed against the QCM sensors with the active layer facing to the sensor. Then dimethylformamide (DMF) was applied to dissolve the polysulfone, leaving the thin active layer attached to the sensor.

4.2.3 Salt permeation tests

Salt permeance was evaluated in a cross-flow filtration system as shown in Figure 4.1. Triplicates samples of each type of membrane were tested. For each experiment, 10 L of feed solution were prepared in a glass reservoir with 25 L capacity. The temperature of the feed solution was controlled using a cooling coil. The pH of the feed solution was

controlled using an automatic pH controller delivering concentrated HCl and NaOH solutions. A Hydra-Cell pump (Wanner Engineering, Minneapolis, MN) was used to circulate the feed solution through four, flat-sheet RO cells in-series (effective membrane area of 35.6 cm^2), where the membranes were placed, and back to the feed reservoir. The feed solution was pumped at a crossflow velocity of 25 $cm.s^{-1}$ (flow rate of 22.5 $L.h^{-1}$) and applied pressures in the range of 0.86-3.10 MPa (125-450 psi). The flow rate and hydraulic pressure were adjusted by changing the pump speed and/or adjusting the metering valves (Swagelok, Wake Forest, NC). The flow rate was monitored with a flowmeter (King, Garden Grove, CA) at the end of the fourth cell and the pressures were monitored with pressure transducers (Omega Engineering, Swedesboro, NJ) located immediately downstream of the pump, immediately upstream of each of the four cells and immediately downstream of the fourth cell. Feed spacers and permeate carriers cut from spiral-wound elements were used in the feed and permeate channels, respectively. During the first 60 h of operation, the system was operated continuously at 3.45 MPa (500 psi) with ultrapure water (pH 10.5 and 22°C). This initial phase was designed to allow for membrane compaction before the actual permeation tests. At the end of this initial 60-hour compaction period, the feed solution was replaced for the test salt solution. During the subsequent 30 h, the system was operated under nine different applied pressures (i.e., decreasing from 3.10 MPa to 0.86 MPa, 450 to 150 psi), where each pressure was used for at least 3 h. At each pressure, both feed and permeate water samples were collected. The water volume sampled per membrane per experiment was below 200 mL to minimize the change in salt concentration in the feed. Salt concentration in feed C_F (M) and permeate C_p (M) samples were determined by

measuring the conductivity of the corresponding water sample and converting the conductivity to concentration using standard curves. Water flux J_v (m.d^{-1}) was obtained from measurements of mass of water permeated, permeation time, and membrane effective area (35.6 cm^2). For each membrane, the solute permeation coefficient B was obtained by fitting C_p, C_F, and J_v data to[27]

$$\mathrm{R} = 1 - \frac{C_P}{C_F} = \frac{(1-\bar{\alpha})J_V}{(B+\bar{\alpha}J_V)\exp\left(\frac{J_V}{k}\right)+(1-\bar{\alpha})J_V} \tag{4.3}$$

where R (unitless) is the salt rejection of the membrane, (unitless) is the advective transport coefficient, and k (m.d^{-1}) is the salt mass transfer coefficient in the concentration polarization layer. The values of B, and k were fitted using the curve fitting tool from Matlab (The MathWorks, Inc., Natick, MA, USA).

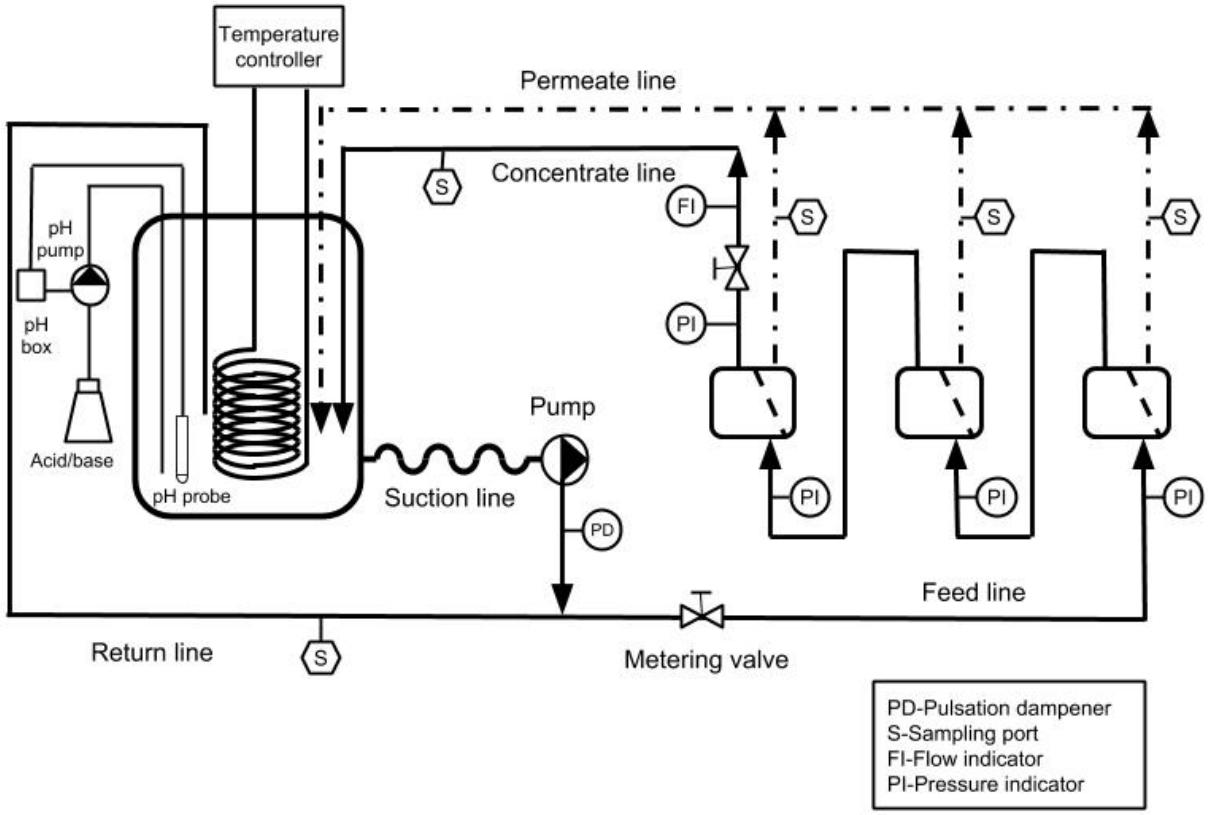

Figure 4.1. Schematic of cross-flow membrane filtration system used in permeation tests. Solid lines, dot-dashed lines, and dashed lines represent feed water lines, permeate lines and membranes, respectively.

4.2.4 Transmission electron microscopy analyses

Transmission electron microscopy (TEM) was used to image the cross sections of membrane samples as described by Lin et al[17,20]. The membrane samples were dehydrated with 100% ethanol, infiltrated and embedded with LR white resin (London Resin Co., Reading, UK) diluted in ethanol, cured at 48℃ for three days, and cut into thin slices (~90-100 nm) with a Sorvall MT 6000 Ultramicrotome (RMC Co., Tucson, AR). Three images were taken for each type of membrane with a JEOL 100CX II TEM (JEOL USA, Peabody, MA) at magnification of 72,000 ×.

4.2.5 Atomic force microscopy analyses

Atomic force microscopy (AFM) analyses were performed to measure surface roughness of membrane samples. For each type of membrane, triplicate samples were tested. A projected surface area of 10 × 10 μm^2 was analyzed on each sample using an Asylum Research MFP-3D AFM (Santa Barbara, CA) equipped with Tap300Al tips (BudgetSensors, Bulgaria). The surface roughness was calculated as mean deviation roughness from the AFM surface profiles as described elsewhere.[28]

4.2.6 Quartz crystal microbalance analyses

QCM analyses were used to obtain areal mass of active layer isolated on QCM sensors (m_{AL}, $ng.cm^{-2}$), the areal mass of water uptake by the active layer when exposed to liquid water (m_l, $ng.cm^{-2}$), areal mass of water uptake by the active layer when exposed to humidified nitrogen gas at 96% relative humidity (m_v, $ng.cm^{-2}$), and the uptake of salt by the active layer (m_s, $ng.cm^{-2}$) when exposed to solutions. Tests were performed with a

Q-Sense E4 quartz crystal microbalance (Biolin Scientific, Lithicum Heights, MD) which has a mass sensitivity on the order of a few ng.cm^{-2}. We tested in parallel two coated sensors and one uncoated control sensor which was used to account for changes of QCM reading resulted from difference in the density and viscosity of the testing fluid. All tests were performed with a flow rate of 0.1 mL.min^{-1} while system temperature was maintained at 22 ± 0.02 °C using the temperature control feature of the flow modules. Measured m_{AL} values were used to obtain active layer thicknesses, m_{AL}, m_l, and m_v values were used to calculate active layer void fractions, and m_{AL} and m_s values were used to estimate salt partition coefficients (see next section). This guaranteed that all experimentally measured physico-chemical properties of any given active layer were obtained from the same set of duplicate samples.

4.2.7 Calculation of void fractions of active layers

The void fraction (f, unitless) of each type of membrane was calculated with m_{AL}, m_l, and m_v values obtained from QCM measurements as[20]

$$f = \frac{(m_l - m_v)\rho_{AL}}{\rho_w m_{AL}} \quad (4.2)$$

where ρ_w =1.0 g.cm^{-3} is the density of water and ρ_{AL} =1.24 g.cm^{-3} is the average mass density of the polyamide active layer. Void fraction results reported correspond to the average and standard deviation for duplicate samples of 1.54 cm^2 in area.

4.2.8 Calculation of active layer thickness

Studies have shown that pores exist inside of active layers and there is evidence of some level of interconnectivity among pores in active layers[20,29,30]. However, it remains

unclear how extensive the interconnectivity is among pores. In order to take into account the pore structure when estimating the active layer thickness that presents resistance to salt transport, we took a two-scenario approach by assuming: (i) there is no interconnectivity among pores, and (ii) complete interconnectivity among pores. For the scenario of no interconnectivity among pores, the total active layer thickness (δ_{AL}, nm) presents resistance to salt transport.[31] Thus, the obtained m_{AL} value from QCM analyses was used to calculate active layer thickness with the equation below

$$\delta_{AL} = \frac{m_{AL}}{\rho_{AL}} \tag{4.3}$$

where ρ_{AL} =1.24 g.cm^{-3} is the dry mass density of polyamide active layer [17,32,33].

For the scenario of complete interconnectivity among pores, the pores do not connect the feed and permeate sides because there is a dense top film where pores are absent[20,29,34] (see Figure 4.2) at the feed side of the active layer. The relevant thickness that presents resistance to salt transport is the thickness of the dense top film (δ_{TF}, nm), which corresponds to the average thickness of the region between membrane surface and the first set of pores from the surface. The dense film thickness was calculated using the method reported by Lin et al[31]. In brief, the thickness was calculated by taking the ratio of the area (indicated in Figure 4.2) and the length of the top film area. Thickness values reported for both scenarios correspond to the average and standard deviation of duplicate samples.

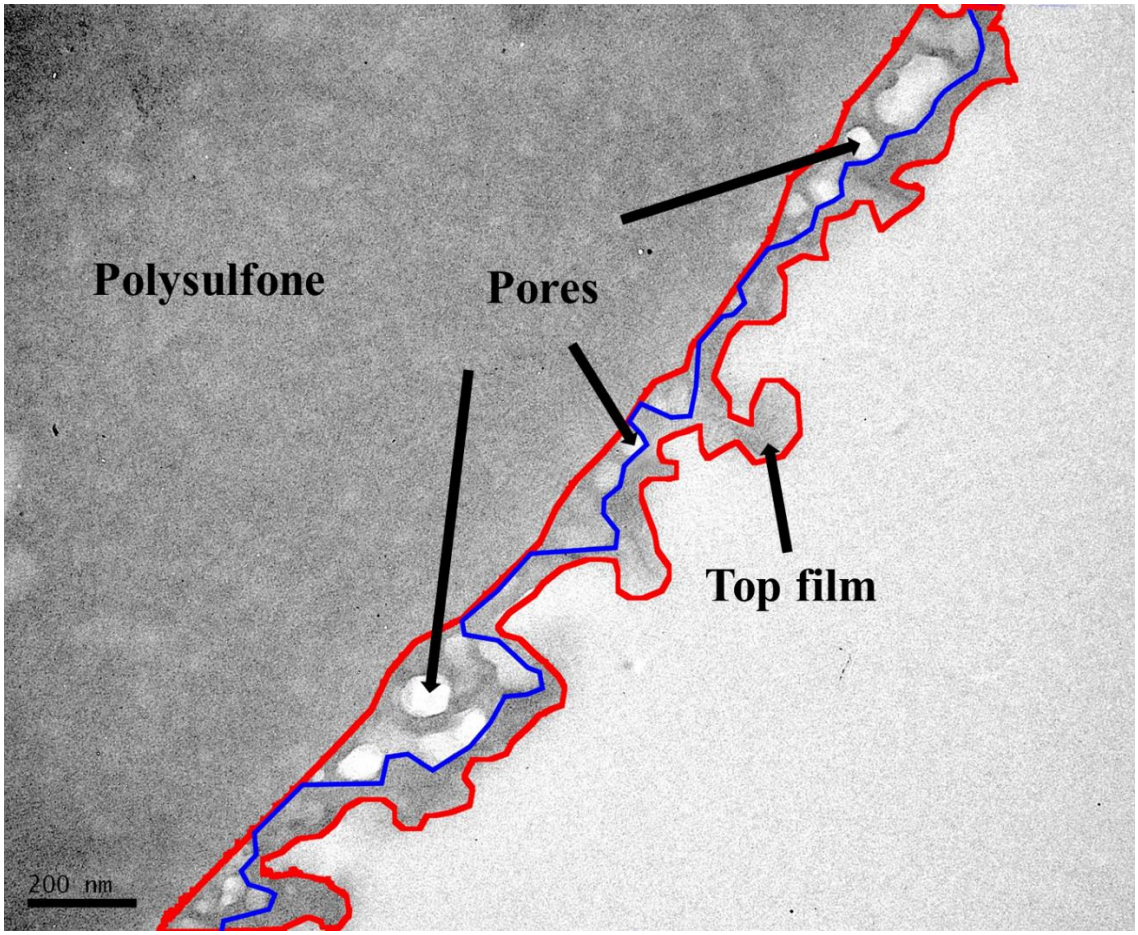

Figure 4.2. Representative cross-sectional TEM image of a polyamide thin-film composite membrane. The image shown corresponds to that of a sample of the homemade TFC membrane. The red lines outline the perimeter of the active layer. The dense top film is delimited by the membrane surface (top red line) and the first set of pores from the surface (blue line).

4.2.9 Pore diameter measurements

The diameter of pores inside of the active layer was measured from TEM images using ImageJ. For each type of membrane, we calculated the mean pore diameter as the average of all pore diameters measured in triplicate TEM images as described elsewhere.[31]

4.2.10 Calculation of salt partition coefficients

Salt partition coefficients in the active layer were determined using the method

reported by Wang et al.[19] The method is based on QCM measurements of the mass of salt partitioned into active layers isolated onto QCM sensors; the details of the method and corresponding calculation procedures can be found in Ref [19] and Appendix C. We obtained both the salt partition coefficients in the polymer phase (K_p) of the active layer and the net partition coefficient (K_{AL}) in the entire active layer (which includes the contribution of salts in the active layer pores). For both K_p and K_{AL} cases, we calculated values assuming that ions partitioned in an unhydrated state into the polymer phase ($K_{p,unhyd}$ and $K_{AL,unhyd}$) as well as in a hydrated state ($K_{p,hyd}$ and $K_{AL,hyd}$). This is because atomistic modeling studies[35–41] of ions in crosslinked aromatic polyamide indicate that ions are hydrated within polyamide active layers but the accurate hydration number in the polyamide active layer remains unknow. Salt partition coefficients for the commercial membranes studied are reproduced for this study from our previous work[19].

4.2.11 Statistical correlation analyses

To evaluate the statistical correlation between any two variables, we performed Pearson product moment correlation and least-square linear regression analyses using SigmaPlot v13.0 (Systat Software, Inc., San Jose, CA, USA). We provide *p* values for the Pearson product moment correlation when appropriate. The correlation analyses between two membrane properties are limited by the natural variability among replicate samples of the same type of membrane. The reported *p*-values serve as general indicators of the strength of the correlations between any two properties analyzed. Note that the weak correlations between any two variables do not indicated they are not interrelated. On the contrary, a correlation, even if a weak one, indicates that the dependent variable is also impacted by the independent variable.

4.3 Results and discussion

4.3.1 Correlation between solute permeation coefficient and geometrical properties of active layer.

Results for all membrane properties discussed in this study are summarized in Table 4.1. We started by evaluating the statistical correlation between the solute permeation coefficient (B) and active layer thickness. Figure 4.3a presents the values of B as a function of total active layer thickness (δ_{AL}) and top film thickness (δ_{TF}). The results showed that while the difference between the salt permeance of the membranes with lowest salt rejection ($B = 5.00 \times 10^{8}$ m.s^{-1} for NF90) and highest salt rejection ($B = 0.69 \times 10^{8}$ m.s^{-1} for SWC4+) was approximately 7-fold, the difference in active layer thickness between the thickest and thinnest membranes was about 2-fold, which is lower but on the same order of magnitude. Specifically, the total active layer thickness ranged from 71 ± 17 nm (TFC) to 139 ± 1 (NF90), and top film thickness ranged from 29 ± 12 nm (ESPA3) to 40 ± 8 (NF90). Note that the membranes with smaller active layer thickness have higher solute permeation coefficient. In other words, the thinner membranes seem to present larger resistance for salt transport, which means these membranes are denser and have better performance in terms of salt rejection. According to Equation 1, there is a theoretical linear relationship between the log scale of solute permeation coefficient and log scale of thickness so we performed linear regression of log (B) with log (δ_{AL}), and log (B) with log (δ_{TF}). Statistical analyses showed that there was a relatively strong correlation between B and δ_{AL} (p=0.024), but weak correlation between B and δ_{TF} (p=0.60). The results indicate that whole active layer thickness highly correlates with salt permeance, however, it counteracts the prediction from the solution-diffusion model (Equation 4.1) that the increase in thickness should decrease the salt permeance. Note that the solution-diffusion

model assumes the active layer to be a uniform layer. A polyamide membrane active layer with voids does not represent a uniform polyamide layer. Thus, the observed correlation does not necessarily indicate causality. The dense top layer of the membrane is a relatively good representative for a uniform polyamide layer that presents the resistance of salt transport through the membrane but no strong statistical correlation was found between top film thickness and salt permeance. So the results indicate that thickness was not the principal factor that determines the differences in salt permeance.

Table 4.1. Geometric and solute transport properties of membrane active layers: total thickness (δ_{AL}), top film thickness (δ_{TF}), pore volume fraction (f), mean pore diameter (d), surface roughness (σ), solute permeation coefficient (B), salt partition coefficient in the active layer polymer (K_p), salt diffusion coefficient in the active layer polymer assuming complete interconnectivity among pores ($D_{p,CI}$), salt partition coefficient in the active layer (K_{AL}), salt diffusion coefficient in the active layer (D_{AL}) and water permeability coefficient (A). All the salt properties correspond to NaCl properties unless otherwise specified. Uncertainties represent standard deviations between duplicate or triplicate samples. The values of geometric properties of XLE, ESPA3, and NF90 have been reproduced from reference 31 since the membranes were the same used in that study.[31]

Property	Scenario	Units	SWC4+	XLE	ESPA3	NF90	TFC
δ_{AL}	-	nm	86 ± 5	113 ± 9	111 ± 7	139 ± 1	71 ± 17
δ_{TF}	-	nm	40 ± 6	34 ± 8	29 ± 12	40 ± 8	40 ± 5
f	-	-	0.11± 0.01	0.31 ± 0.02	0.28 ± 0.14	0.15 ± 0.02	0.15 ± 0.04
d	-	nm	41 ± 24	29 ± 20	26 ± 13	29 ± 23	55 ± 27
σ	-	nm	98 ± 2	49 ± 8	81 ± 4	81 ± 30	72 ± 6
$B\times10^{8}$	-	m/s	0.69 ± 0.04	1.88 ± 0.02	2.56 ± 0.66	5.00 ± 0.34	0.83 ± 0.05
K_p	unhydrated[x]	M/M	0.16 ± 0.06	0.38 ± 0.09	0.33 ± 0.08	0.67 ± 0.13	0.18 ± 0.10
	hydrated[y]		0.03 ± 0.01	0.08 ± 0.02	0.07 ± 0.03	0.14 ± 0.03	0.04 ± 0.02
$D_p\times10^{13}$	i	m^2/s	1.03 ± 0.21	0.56 ± 0.14	0.85 ± 0.30	0.37 ± 0.13	0.32 ± 0.19
	ii		4.94 ± 0.99	2.65 ± 0.65	4.09 ± 0.18	1.75 ± 0.62	1.53 ± 0.90
K_{AL}	i	M/M	0.20 ± 0.05	0.56 ± 0.06	0.52 ± 0.05	0.72 ± 0.11	0.31 ± 0.08
	ii		0.08 ± 0.03	0.35 ± 0.01	0.33 ± 0.02	0.25 ± 0.02	0.18 ± 0.02
$D_{AL}\times10^{13}$	i	m^2/s	0.29 ± 0.07	0.38 ± 0.05	0.55 ± 0.15	0.97 ± 0.16	0.19 ± 0.07
	ii		0.72 ± 0.30	0.61 ± 0.05	0.86 ± 0.23	2.75 ± 0.31	0.32 ± 0.09
$A\times10^{11}$	-	m/s/Pa	0.42 ± 0.00	1.29 ± 0.04	1.59 ± 0.06	1.31 ± 0.05	0.47 ± 0.05

[x] indicates analyses performed assuming unhydrated ions in polyamide. [y] indicates analyses performed assuming ions in polyamide have the same hydration number as in bulk solution.

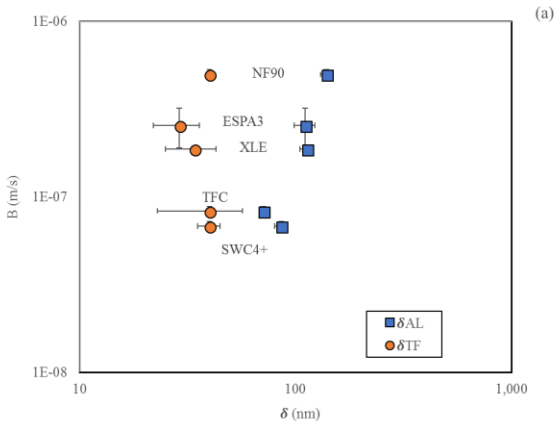
(a)
1E-06
1E-07
1E-08
B (m/s)
NF90
ESPA3
XLE
TFC
SWC4+
δAL
δTF
10
100
1,000
δ (nm)

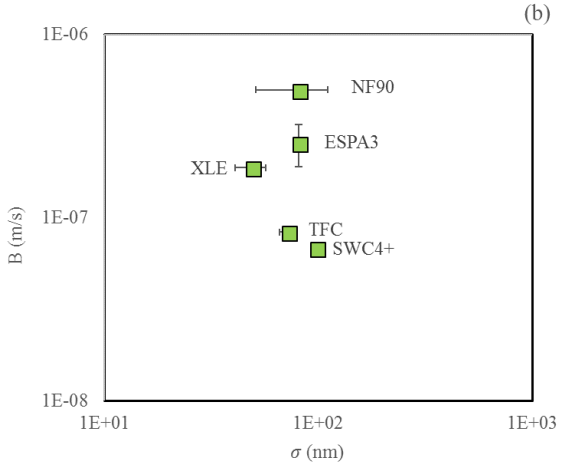
(b)
1E-06
1E-07
1E-08
B (m/s)
NF90
ESPA3
XLE
TFC
SWC4+
1E+01
1E+02
1E+03
σ (nm)

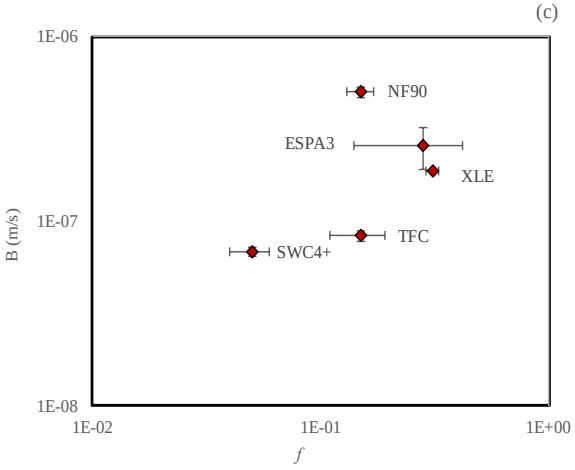
(c)
1E-06
1E-07
1E-08
B (m/s)
NF90
ESPA3
XLE
TFC
SWC4+
1E-02
1E-01
1E+00
f

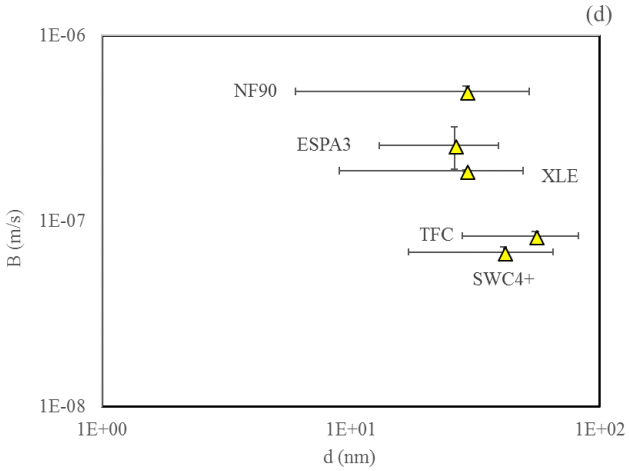

Figure 4.3. Solute permeation coefficient of NaCl (*B*) as a function of geometrical properties of the active layer including (a) thickness, (b) surface roughness, (c) pore fraction and (d) pore diameter In panel (a), results for total thickness (δ_{AL}) and top film thickness (δ_{TF}) are presented. Values and error bars for δ represent average and standard deviation of duplicate samples, respectively. Values and error bars for *B*, σ, *f*, and *d* represent average and standard deviation of triplicate samples, respectively.

We also evaluated the correlation between the solute permeation coefficient and other three geometrical properties of the active layer, including membrane surface roughness (σ) (Figure 4.3b), pore volume fraction (*f*) (Figure 4.3c) and pore diameter (*d*) (Figure 4.3d). The difference between the highest (σ = 98 ± 2 nm for SWC4+) and lowest (σ = 49 ± 8 nm for XLE) surface roughness was 2-fold. Likewise, the difference between the highest (*d* = 41 ± 24 nm for SWC4+) and lowest (*d* = 26 ± 13 nm for ESPA3) pore diameter was approximately 2-fold. In a similar manner, the difference between highest (*f* = 0.31 ± 0.02 for XLE) and lowest (*f* = 0.11 ± 0.01 for SWC4+) pore fraction was 6-fold but with most of the membranes falling in the narrow *f* range of 0.15-0.31. Statistical analyses showed that there was not a strong correlation between *B* and σ (p=0.802), *B* and *d* (p=0.24), or *B* and *f* (p=0.748). The weak correlations observed between solute permeation coefficient and surface roughness, pore fraction, and pore diameter indicate

that none of these three properties of the active layer were a principal factor determining the differences in salt permeance observed among the five polyamide membranes tested.

Overall, the results in Figure 4.3 indicate that the studied geometric properties (i.e., thickness, surface roughness, pore fraction, pore diameter,) of active layers are not principal factors in determining the differences in salt permeance observed among crosslinked aromatic polyamide membranes.

4.3.2 Correlation between solute permeation coefficient and salt permeability

As indicated by Equation 1, the solute permeation coefficient (B) scales linearly with the ratio between the solute permeability (P_S) and active layer thickness. Since in the last section differences in active layer thickness were not found to explain the differences in B values observed among membranes, P_S should be a focus. Figure 4.4 presents the values for B as a function of P_S. The results showed that the variance in B was on the same order of magnitude as the variance in P_S. Specifically, while the difference between the salt permeance of the membranes with lowest salt rejection ($B = 5.00 \times 10^8$ m.s^{-1} for NF90) and highest salt rejection ($B = 0.69 \times 10^8$ m.s^{-1} for SWC4+) was approximately 7-fold, the difference in salt permeability between the most (5.87×10^{15} m.s^{-2} for NF90) and least (6.95×10^{14} m.s^{-2} for SWC4+) permeable membranes was about 12-fold. As indicated by Equation 1, B scales linearly with the ratio between P_S and active layer thickness. Thus, there is a theoretical linear relationship between the log scale of B and log scale of P_S. Statistical analyses showed that there was a very strong linear correlation between B and P_S ($p < 0.01$, $R^2 > 0.99$, see Figure 4.4), indicating that P_S is an important factor determining the differences in B among membranes.

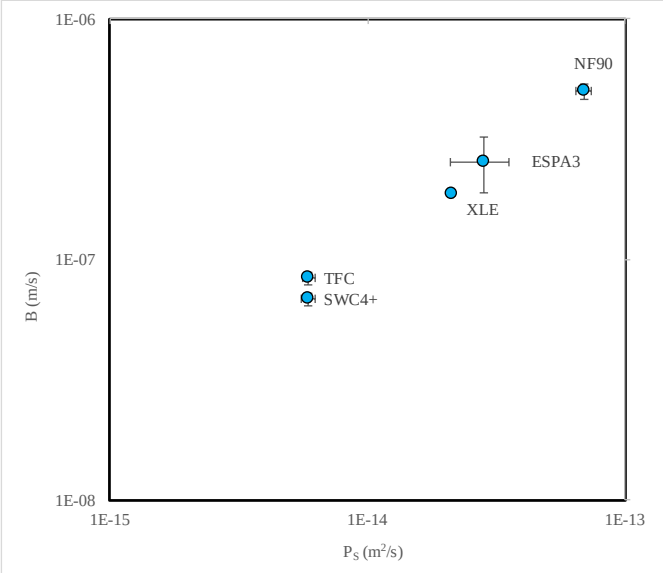

Figure 4.4. Salt diffusive permeation coefficient of NaCl (B) as a function of salt permeability (P_S). Values and error bars for B and P_S represent average and standard deviation of triplicate samples, respectively. Values and error bars represent average and standard deviation, respectively, for triplicate samples.

In summary, the results in Figure 4.3 and 4.4 indicate that differences in salt permeance (P_S), and not differences in geometrical properties, are the principal factor determining the differences in solute permeation coefficient (B) observed among crosslinked aromatic polyamide membranes. Note that while the absolute values of B are directly and indirectly proportional to Ps and thickness, respectively (Equation 1), active layers with a greater B have a higher P_S, but not necessarily a lower thickness. Other parameters of importance not taken into account in the analytical model (Equation 1) include higher order geometrical properties such pore spatial distributions.

4.3.3 Salt partition and diffusion coefficients in the active layer

As noted the previous sections, salt permeability (P_S) showed a relatively strong correlation with salt permeance (B). As indicated by Equation 4.1, the salt permeability scales linearly with the salt partition coefficient (K_S) and salt diffusion coefficient (D_S). We

obtain K_S and D_S for the analysis of their relative contribution to the salt permeability through active layers in the two limiting cases of no interconnectivity and complete interconnectivity among pores. We then evaluated the statistical correlations between P_S and K_S, and P_S and D_S values.

The calculated $K_{p,unhydrated}$ and $K_{p,hydrated}$ values (see Table 4.1) show that seawater RO membranes (SWC4+ and TFC) had the lowest partition coefficient and diffusion coefficient, brackish water membranes (XLE and ESPA3) had intermediate K_p and D_p values, and the NF membrane (NF90) had the highest partition and diffusion coefficients. Specifically, these values were in the 0.16-0.67 and 0.03-0.14 range and are on the same order of magnitude with 0.2, the partition coefficient of NaCl obtained by Frommer at al[42] from experiment with thick (~0.4 mm) aromatic polyamide films. The calculated $K_{AL,unhydrated}$ and $K_{AL,hydrated}$ values were in the 0.20-0.72 and 0.08-0.35 range, respectively (see Table 4.1). While the salt partition coefficients calculated assuming that ions were unhydrated in the polymer phase were larger than those calculated assuming hydrated ions, all calculated partition coefficients were lower than 1. This indicates that the mobile salt is in lower concentration in the active layer than in bulk solution, consistent with the ability of the membranes to reject salts.

Due to the microsecond time-scale of salt diffusion in the polyamide membranes, there are currently no experimental methods to measure salt diffusion coefficients in polyamide active layers.[20,33,43] Therefore, we used experimental values for other relevant parameters as inputs to the solution-diffusion model (Equation 4.1 and 4.2) to estimate the salt diffusion coefficient in the polyamide active layer. In the case of complete pore interconnectivity, salt diffusion coefficient in the polyamide phase can be calculated using

the salt partition coefficient in the polyamide phase (K_p) and top film thickness (δ_{TF}). The calculated $D_{p,unhydrated}$ and $D_{p,hydrated}$ values were in the $0.32 \times 10^{13} - 1.03 \times 10^{13}$ m.s^{-2} and $1.53 \times 10^{13} - 4.94 \times 10^{13}$ m.s^{-2} range, respectively. These values are in the same order of magnitude with the NaCl diffusion coefficients reported by Frommer et al ($0.8 \times 10^{13} - 1.5 \times 10^{13}$ m.s^{-2}) measured with an aromatic polyamide film with a thickness of ~0.4 mm.[42] When estimating the net salt diffusion coefficient in the whole active layer, it was assumed that there is no interconnectivity among pores. The whole active layer thickness (δ_{AL}) and net partition coefficients of the whole active layer, $K_{AL,unhydrated}$ and $K_{AL,hydrated}$, were used in the equation and the corresponding salt diffusion coefficient under the two assumptions were denoted as $D_{AL,unhydrated}$ and $D_{AL,hydrated}$, respectively. The range of estimated $D_{AL,unhydrated}$ and $D_{AL,hydrated}$ values were $0.19 \times 10^{13} - 0.97 \times 10^{13}$ m.s^{-2} and $0.32 \times 10^{13} - 2.75 \times 10^{13}$ m.s^{-2}. When taking into account the pore structure, seawater RO membranes (SWC4+ and TFC) still have the lowest partition coefficient, but the NF membrane (NF90) no longer has the highest K_p values. Instead, brackish water membranes (XLE and ESPA3) tend to have the highest partition coefficient of the whole active layer.

4.3.4 Correlation between salt permeability and salt partition and diffusion coefficients.

Figure 4.4 presents the value for P_S as a function of K_p (Figure 4.5a) and D_p (Figure 4.5b). The results in Figure 4.4a show that along with the approximately 12-fold difference observed between the highest and lowest P_S values, there was a 4-fold difference between the highest and lowest K_p value. The difference between the highest and lowest D_p value was also around 4-fold, indicating partitioning and diffusion might both contribute to the variance in salt permeability. Statistical analyses showed that there was a very strong linear

correlation between P_S and K_p ($p < 0.004$, $R^2 > 0.95$ for both $K_{p,unhydrated}$ and $K_{p,hydrated}$). Similarly, there was a very strong linear correlation between P_S and D_p ($p < 0.006$, $R^2 > 0.94$ for both $D_{p,unhydrated}$ $D_{p,hydrated}$). Thus, the results indicate that both salt partition and diffusion play important roles in, and have similar contributions to, the differences in salt permeability observed among membranes.

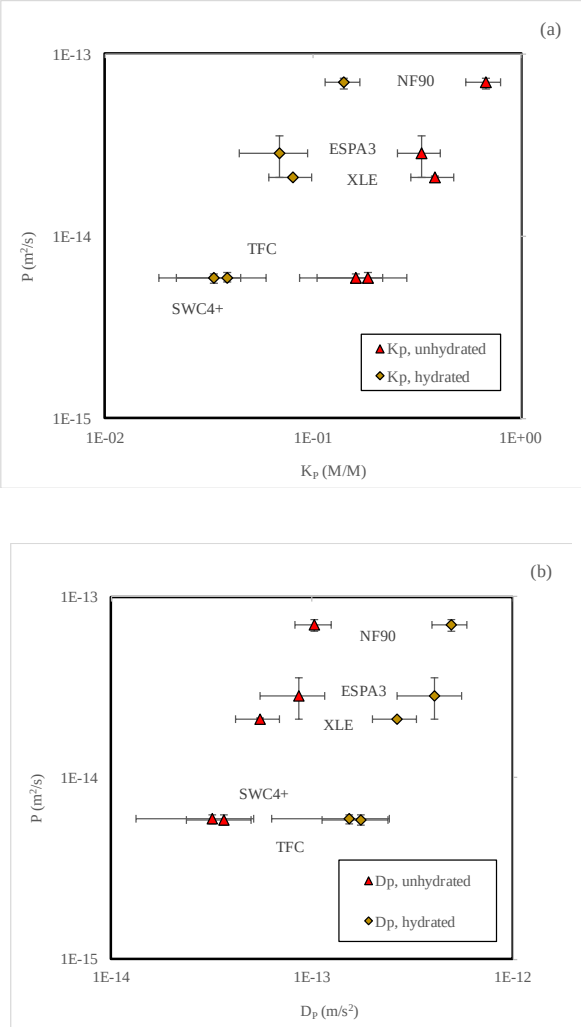

Figure 4.5. Salt permeability of NaCl (P_S) as a function of (a) salt partition coefficient in the active layer polymer assuming salt was not hydrated during partitioning ($K_{p,\ unhydrated}$) and assuming salt was fully hydrated during partitioning ($K_{p,\ hydrated}$), and (b) salt diffusion coefficient calculated with unhydrated partition coefficient ($D_{p,\ unhydrated}$) and salt diffusion coefficient calculated with hydrated partition coefficient ($D_{p,\ hydrated}$). Values and error bars represent average and standard deviation, respectively, for triplicate samples.

Considering significant pore fractions in the active layer, we also evaluated whether net salt partition coefficient ($K_{AL,unhydrated}$) and net diffusion coefficient ($D_{AL,unhydrated}$) of the whole active layer were correlated to salt permeability (see Figure 4.6). Statistical analyses results also showed that there was a strong correlation between both P_S and $K_{AL,unhydrated}$ ($p < 0.02$, $R^2 > 0.91$), and P_S and $D_{AL,unhydrated}$ ($p < 0.02$, $R^2 > 0.86$). By contrast, there was only a weak linear correlation between P_S and $K_{AL,hydrated}$ ($p = 0.19$, $R^2 = 0.48$), and P_S and $D_{AL,hydrated}$ ($p = 0.08$, $R^2 = 0.70$). The net values may not have as good correlations as the polymer values above because the net values do not take into account the structure of pores. Given that this analysis shows that taking the pore structure is important in discerning the importance of the different parameters for salt transport, and the approach above is crude in that it uses a one-dimensional model to take into account pores existing in a 3D structure, there is a need to obtain D values from 2D or 3D microscale modeling. However, the current analysis (in this paper) clearly indicates that both K and D are important contributors to the differences in P among membranes, and the values reported here serve as good approximations in the absence of the 2D/3D microscale modeling.

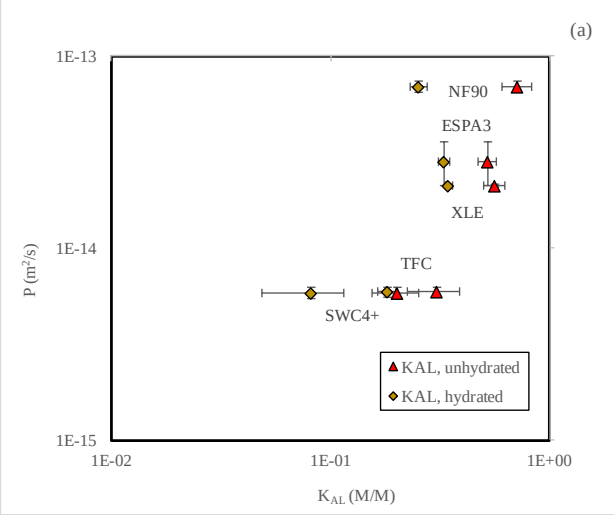

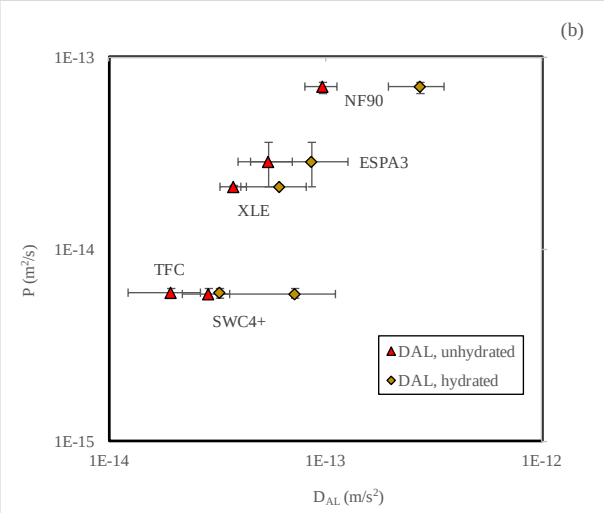

Figure 4.6. Salt permeability of NaCl (P_S) as a function of (a) salt partition coefficient in the whole active layer assuming salt was not hydrated during partitioning ($K_{AL,\ unhydrated}$) and assuming salt was fully hydrated during partitioning ($K_{AL,\ hydrated}$), and (b) salt diffusion coefficient calculated with unhydrated partition coefficient ($D_{AL,\ unhydrated}$) and salt diffusion coefficient calculated with hydrated partition coefficient ($D_{AL,\ hydrated}$). Values and error bars represent average and standard deviation, respectively, for triplicate samples.

4.3.5 Correlation between solute permeation coefficient and water permeance in the active layer

Statistical analysis of solute and water permeance was performed and the results showed that the relationship between *B* and *A* of NF90 does not fall in the trend of the other membranes (see Figure 4.7). Among the four types of RO membranes, *B* and *A* have a strong linear correlation ($p=0.005$, $R^2 > 0.98$). Compared to RO membrane, the NF membrane tends to have higher solute permeation coefficient *B* at the same water permeance *A*. This is consistent with the expectation from membrane performance that an NF membrane has lower salt rejection rate compared to an RO membrane.

Lin et al thoroughly investigated and reported the relative importance of geometrical properties, including active layer thickness δ, pore fraction *f*, surface

roughness σ and pore dimension *d*, and intrinsic water transport properties (water partition coefficient *K* and water diffusion coefficient *D*) of active layers in the water permeability of polyamide membranes. They concluded that water diffusion coefficient is the main contributor to the large difference in water permeability observed among membranes. Geometrical properties of active layers and water partition coefficients in active layers play a role in water permeation but they do not account for the large difference in water permeability observed among membranes. In this study of solute permeability coefficient, we concluded that solute diffusion and partition coefficients are the main contributors to the differences in solute permeation coefficient among membranes; by contrast, geometrical properties were not principal factors determining these differences.

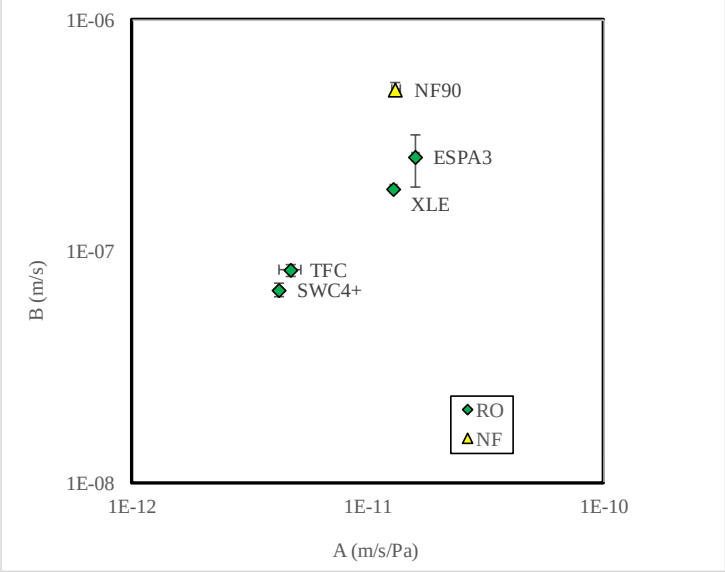

Figure 4.7. Solute permeation coefficient of NaCl (*B*) as a function of water permeability coefficient (*A*). Values and error bars represent average and standard deviation, respectively, for triplicate samples.

4.4 Conclusion

In summary, I have evaluated which among geometrical and salt transport

properties of the active layers of polyamide thin-film composite membranes account for the difference in salt rejection observed among a group of five crosslinked aromatic polyamide membranes. The active layer thickness, surface roughness, pore fraction, salt permeability of NaCl, NaCl partition coefficient of the active layers were evaluated experimentally. The NaCl diffusion coefficient in the active layer were calculated with solution-diffusion model.

- NaCl diffusion coefficient in the polyamide phase of all the five tested membrane active layers were found to be in the range of $0.32 \pm 0.19 \times 10^{13}$ - $4.94 \pm 0.99 \times 10^{13}$ $m^2.s^{-1}$.
- Net diffusion coefficient might not serve as a representative parameter for solute transport analysis due to the lack of 2D/3D modeling of membrane active layer that can take into account the pore structures.
- The experimental and statistical results indicate that while geometrical properties of active layers (thickness, pore volume fraction, roughness) play a role in salt permeation, they do not account for the differences in salt permeability observed among membranes.
- The differences in salt permeability observed among membranes are mainly due to the differences in salt partition and diffusion coefficients in active layers. This conclusion was reached for the two limiting cases of no interconnectivity among pores and complete interconnectivity among pores, and therefore is expected to be valid for intermediate interconnectivity.

4.5 Acknowledgment

The author thanks Wallace Ambrose and Dr. Carrie Donley at the Chapel Hill

Analytical and Nanofabrication Laboratory (CHANL) in Chapel Hill, NC, for assistance in TEM and AFM. This work was supported by the US National Science Foundation (NSF) (Award Nos. 1264690 and 1336532), and Dissertation Completion Fellowship from UNC Graduate School.

REFERENCES

(1) Geise, G. M.; Park, H. B.; Sagle, A. C.; Freeman, B. D.; McGrath, J. E. Water Permeability and Water/Salt Selectivity Tradeoff in Polymers for Desalination. *J. Memb. Sci.* **2011**, *369* (1–2), 130–138.

(2) Werber, J. R.; Deshmukh, A.; Elimelech, M. The Critical Need for Increased Selectivity, Not Increased Water Permeability, for Desalination Membranes. *Environmental Science and Technology Letters*. 2016.

(3) Werber, J. R.; Bull, S. K.; Elimelech, M. Acyl-Chloride Quenching Following Interfacial Polymerization to Modulate the Water Permeability, Selectivity, and Surface Charge of Desalination Membranes. *J. Memb. Sci.* **2017**, *535*, 357–364.

(4) Nicolaisen, B. Developments in Membrane Technology for Water Treatment. *Desalination* **2003**, *153* (1–3), 355–360.

(5) Petersen, R. J. Composite Reverse Osmosis and Nanofiltration Membranes. *J. Memb. Sci.* **1993**, *83* (1), 81–150.

(6) Bellona, C.; Drewes, J. E.; Xu, P.; Amy, G. Factors Affecting the Rejection of Organic Solutes during NF/RO Treatment - A Literature Review. *Water Res.* **2004**, *38* (12), 2795–2809.

(7) Ramon, G. Z.; Hoek, E. M. V. Transport through Composite Membranes, Part 2: Impacts of Roughness on Permeability and Fouling. *J. Memb. Sci.* **2013**, *425–426*, 141–148.

(8) Xie, W.; Geise, G. M.; Freeman, B. D.; Lee, H.-S.; Byun, G.; McGrath, J. E. Polyamide Interfacial Composite Membranes Prepared from M-Phenylene Diamine, Trimesoyl Chloride and a New Disulfonated Diamine. *J. Memb. Sci.* **2012**, *403–404*, 152–161.

(9) Ghosh, A. K.; Hoek, E. M. V. Impacts of Support Membrane Structure and Chemistry on Polyamide–polysulfone Interfacial Composite Membranes. *J. Memb. Sci.* **2009**, *336* (1–2), 140–148.

(10) Kong, C.; Kanezashi, M.; Yamomoto, T.; Shintani, T.; Tsuru, T. Controlled Synthesis of High Performance Polyamide Membrane with Thin Dense Layer for Water Desalination. *J. Memb. Sci.* **2010**, *362* (1–2), 76–80.

(11) Song, Y.; Sun, P.; Henry, L.; Sun, B. Mechanisms of Structure and Performance Controlled Thin Film Composite Membrane Formation via Interfacial Polymerization Process. *J. Memb. Sci.* **2005**, *251* (1–2), 67–79.

(12) Kadhom, M.; Deng, B. Synthesis of High-Performance Thin Film Composite (TFC) Membranes by Controlling the Preparation Conditions: Technical Notes. *J. Water Process Eng.* **2018**, No. November, 1–8.

(13) Park, S. J.; Kwon, S. J.; Kwon, H. E.; Shin, M. G.; Park, S. H.; Park, H.; Park, Y. I.; Nam, S. E.; Lee, J. H. Aromatic Solvent-Assisted Interfacial Polymerization to Prepare High Performance Thin Film Composite Reverse Osmosis Membranes Based on Hydrophilic Supports. *Polym. (United Kingdom)* **2018**, *144*, 159–167.

(14) Wijmans, J. G.; Baker, R. W. The Solution-Diffusion Model: A Review. *J. Memb. Sci.* **1995**, *107* (1–2), 1–21.

(15) Paul, D. R. Reformulation of the Solution-Diffusion Theory of Reverse Osmosis. *J. Memb. Sci.* **2004**, *241* (2), 371–386.

(16) Bason, S.; Oren, Y.; Freger, V. Characterization of Ion Transport in Thin Films Using Electrochemical Impedance SpectroscopyII: Examination of the Polyamide Layer of RO Membranes. *J. Memb. Sci.* **2007**, *302* (1–2), 10–19.

(17) Lin, L.; Feng, C.; Lopez, R.; Coronell, O. Identifying Facile and Accurate Methods to Measure the Thickness of the Active Layers of Thin-Film Composite Membranes – a Comparison of Seven Characterization Techniques. *J. Memb. Sci.* **2015**, *498*, 167–179.

(18) Perry, L. A.; Coronell, O. Reliable, Bench-Top Measurements of Charge Density in the Active Layers of Thin-Film Composite and Nanocomposite Membranes Using Quartz Crystal Microbalance Technology. *J. Memb. Sci.* **2013**, *429*, 23–33.

(19) Wang, J.; Kingsbury, R. S.; Perry, L. A.; Coronell, O. Partitioning of Alkali Metal Salts and Boric Acid from Aqueous Phase into the Polyamide Active Layers of Reverse Osmosis Membranes. *Environ. Sci. Technol.* **2017**, *51* (4), 2295–2303.

(20) Lin, L.; Lopez, R.; Ramon, G. Z.; Coronell, O. Investigating the Void Structure of the Polyamide Active Layers of Thin-Film Composite Membranes. *J. Memb. Sci.* **2016**, *497*, 365–376.

(21) Powell, J.; Luh, J.; Coronell, O. Bulk Chlorine Uptake by Polyamide Active Layers of Thin-Film Composite Membranes upon Exposure to Free Chlorine-Kinetics, Mechanisms, and Modeling. *Environ. Sci. Technol.* **2014**, *48* (5), 2741–2749.

(22) Hydranautics. SWC4+ 8040 seawater reverse osmosis element datasheet. http://www.lenntech.com/Data-sheets/Hydranautics-SWC4+8040.pdf (accessed Aug 20, 2016).

(23) Information, P.; Specifications, P. Dow Filmtec. XLE-440 extra low energy RO element datasheet, Form No. 609-00245- 0606. http://www.lenntech.com/Data-sheets/Dow-Filmtec-XLE-440.pdf (accessed Aug 20, 2016).

(24) Hydranautics. ESPA3-4040 brackish water reverse osmosis membrane element datasheet. http://www.lenntech.com/Data-sheets/Hydranautics-ESPA3-4040.pdf (accessed Aug 20, 2016).

(25) Dow Filmtec. NF90-400 nanofiltration element datasheet, Form No. 609-00345-0312 http://www.lenntech.com/Data-sheets/Dow-Filmtec-NF90-400.pdf (accessed Aug 20, 2016).

(26) Lind, M. L.; Suk, D. E.; Nguyen, T. V.; Hoek, E. M. V. Tailoring the Structure of Thin Film Nanocomposite Membranes to Achieve Seawater RO Membrane Performance. *Environ. Sci. Technol.* **2010**, *44* (21), 8230–8235.

(27) Coronell, O.; Mi, B.; Cahill, D. G. Modeling the Effect of Charge Density in the Active Layers of Reverse Osmosis and Nano Fi Ltration Membranes on the Rejection of Arsenic(III) and Potassium Iodide. *Environ. Sci. Technol.* **2013**, *47* (Iii), 420–428.

(28) Kwak, S. Y.; Jung, S. G.; Yoon, Y. S.; Ihm, D. W. Details of Surface Features in Aromatic Polyamide Reverse Osmosis Membranes Characterized by Scanning Electron and Atomic Force Microscopy. *J. Polym. Sci. Part B Polym. Phys.* **1999**, *37* (13), 1429–1440.

(29) Yan, H.; Miao, X.; Xu, J.; Pan, G.; Zhang, Y.; Shi, Y.; Guo, M.; Liu, Y. The Porous Structure of the Fully-Aromatic Polyamide Film in Reverse Osmosis Membranes. *J. Memb. Sci.* **2015**, *475*, 504–510.

(30) Karan, S.; Jiang, Z.; Livingston, A. G. Sub-10 Nm Polyamide Nanofilms with Ultrafast Solvent Transport for Molecular Separation. *Science (80-.).* **2015**, *348* (6241), 1347–1351.

(31) Lin, L.; Weigand, T. M.; Farthing, M. W.; Jutaporn, P.; Miller, C. T.; Coronell, O. Relative Importance of Geometrical and Intrinsic Water Transport Properties of Active Layers in the Water Permeability of Polyamide Thin-Film Composite Membranes. *Rev.* **2018**, 1–36.

(32) Kolev, V.; Freger, V. Hydration, Porosity and Water Dynamics in the Polyamide Layer of Reverse Osmosis Membranes: A Molecular Dynamics Study. *Polymer (Guildf).* **2014**, *55* (6), 1420–1426.

(33) Zhang, X.; Cahill, D. G.; Coronell, O.; Mariñas, B. J. Absorption of Water in the Active Layer of Reverse Osmosis Membranes. *J. Memb. Sci.* **2009**, *331* (1–2), 143–151.

(34) Kłosowski, M. M.; McGilvery, C. M.; Li, Y.; Abellan, P.; Ramasse, Q.; Cabral, J. T.; Livingston, A. G.; Porter, A. E. Micro-to Nano-Scale Characterisation of Polyamide Structures of the SW30HR RO Membrane Using Advanced Electron Microscopy and Stain Tracers. *J. Memb. Sci.* **2016**, *520*, 465–476.

(35) Harder, E.; Walters, D. E.; Bodnar, Y. D.; Faibish, R. S.; Roux, B. Molecular Dynamics Study of a Polymeric Reverse Osmosis Membrane. *J. Phys. Chem. B* **2009**, *113* (30), 10177–10182.

(36) Shen, M.; Keten, S.; Lueptow, R. M. Dynamics of Water and Solute Transport in Polymeric Reverse Osmosis Membranes via Molecular Dynamics Simulations. *J. Memb. Sci.* **2016**, *506*, 95–108.

(37) Kolev, V.; Freger, V. Molecular Dynamics Investigation of Ion Sorption and Permeation in Desalination Membranes. *J. Phys. Chem. B* **2015**, *119* (44), 14168–14179.

(38) Hughes, Z. E.; Gale, J. D. A Computational Investigation of the Properties of a Reverse Osmosis Membrane. *J. Mater. Chem.* **2010**, *20* (36), 7788.

(39) Ridgway, H. F.; Orbell, J.; Gray, S. Molecular Simulations of Polyamide Membrane Materials Used in Desalination and Water Reuse Applications: Recent Developments and Future Prospects. *J. Memb. Sci.* **2017**, *524* (October 2016), 436–448.

(40) Gai, J.; Gong, X.; Zhang, X.; Kang, W.; Wang, W. Key Role of Hydrates in Determining Ion Rejection by Polyamide Membrane. *Polym. Eng. Sci.* **2015**, *55* (2), 466–473.

(41) Ding, M.; Szymczyk, A.; Aziz, G. On the Structure and Rejection of Ions by a Polyamide Membrane in Pressure-Driven Molecular Dynamics Simulations. *Desalination* **2015**, 76–80.

(42) Frommer, M. A.; Murday, J. S.; Messalem, R. M. Solubility and Diffusivity of Water and of Salts in an Aromatic Polyamide Film. *Eur. Polym. J.* **1973**, *9* (4), 367–373.

(43) Lee, J.; Doherty, C. M.; Hill, A. J.; Kentish, S. E. Water Vapor Sorption and Free Volume in the Aromatic Polyamide Layer of Reverse Osmosis Membranes. *J. Memb. Sci.* **2013**, *425–426*, 217–226.

CHAPTER 5 - CONCLUSIONS

This dissertation focused on evaluating whether solute partitioning, solute diffusion, and/or active layer thickness account for the variance in solute permeability among polyamide active layers of thin film composite membranes. To accomplish the overall goal of this project, my research plan focused on: (1) developing a method to measure solute partition coefficient from aqueous solution into polyamide active layer of TFC membranes; (2) quantifying the solute partition and diffusion coefficient inside polyamide active layers of TFC membranes with a broad range of performance levels; and (3) determining which parameter among solute partition coefficient, solute diffusion coefficient and active layer thickness accounts for the most difference in solute permeation among TFC membranes with a broad range of performance levels.

A quartz crystal microbalance (QCM) based bench-top method was developed to determine solute partition coefficients into the polyamide active layers of RO membranes. Partition coefficients of solutes including all alkali metal chlorides (LiCl, NaCl, KCl, RbCl, CsCl) and boric acid into five types of TFC membranes (SWC4+, XLE, ESPA3, NF90, and homemade TFC) were measured. The salt diffusion coefficients in membrane active layers were calculated from measured salt partition coefficients, salt permeation coefficients measured through permeation tests, and active layer thicknesses. The pH effect on the partitioning of alkali metal salts, and whether the pH dependence of salt partitioning and rejection are consistent with predictions from Donnan exclusion theory were also studied. The active layer thickness, surface roughness, pore fraction, salt permeability of NaCl, NaCl partition coefficient of the active layers

were evaluated experimentally to evaluate which among geometrical and salt transport properties of the active layers of polyamide thin-film composite membranes account for the difference in salt rejection observed among a group of five crosslinked aromatic polyamide membranes. Key findings form this work are as follows:

(1) For all membranes, the partition coefficients of all inorganic salts and small acids obtained experimentally in this dissertation were lower than 1.

(2) The range of values of partition coefficients differs from those obtained with other experimental approaches in the literature (3.6-8.1) but is consistent with expectations from Donnan theory (i.e., electrostatic exclusion of ions) and the high salt rejection of TFC membranes.

(3) All the partition coefficients fall into the range of 0.01 ± 0.00 - 0.46 ± 0.12 and the partition coefficient did not differ much among different TFC membranes.

(4) For all membranes tested, Donnan theory provided an appropriate theoretical framework to predict the effect of pH on salt partitioning (evaluated for all chloride salts of alkali metals) and salt rejection (evaluated for NaCl).

(5) Changes in salt rejection with feed solution pH are primarily driven by changes in salt partitioning with likely minimal (or absent) changes in salt diffusion.

(6) The NaCl diffusion coefficient in the active layer were calculated with solution-diffusion model and were found to be in the range of $0.32 \pm 0.19 \times 10^{13}$ - $4.94 \pm 0.99 \times 10^{13}$ $m^2.s^{-1}$ for all the membrane tested.

(7) Net diffusion coefficient of the whole active layer might not serve as a representative parameter for solute transport analysis due to the lack of 2D/3D modeling of membrane active layer that can take into account of the pore structures.

(8) While geometrical properties of active layers (thickness, pore volume fraction, roughness) in active layers play a role in salt permeation, they do not account for the differences in salt permeability observed among membranes.

(9) The differences in salt permeability observed among membranes are mainly due to the differences in both salt partition and diffusion coefficients in active layers.

(10) The methods provided here help to independently quantify partition coefficients and diffusion coefficients, which will enhance the fundamental understanding of the mechanisms of contaminant permeation through RO membranes, enable construction of predictive transport models, and serve as an important tool for guiding membrane modifications to improve performance.

(11) The method developed in this dissertation for the measurement of partition coefficients enables the quantitative characterization of the partition coefficient of salts and small molecules beyond those studied here.

CHAPTER 6 - FUTURE WORK

While exploring the solute transport properties in the polyamide active layer of TFC membranes, this dissertation has provided useful tools and raised questions that open avenues for future research. The research topics that can be developed which are relevant to this dissertation work are:

(1) What are the other possible ways to quantify solute partition coefficient in the membrane active layer? As discussed in Chapter 2, there are only a few studies that have measured solute partition coefficient in the polyamide membrane active layers. Other than measuring the mass of solute uptake from the active layer mentioned in this work, there could be other approaches. The QCM-based method provided a good range of solute partition coefficients but it will be good to compare with results from other methods. Currently the solute diffusion coefficient can only be calculated from solute partition coefficient thus the more accurate measurements of partition coefficients could help to better quantify diffusion coefficients.

(2) With QCM analysis presented in this work, an assumption had to made because another important question remains unknown: what are the hydration numbers of solutes in the polyamide active layer? A better understanding of the chemistry in a hydrated membrane would greatly enhance the knowledge of solute-water-membrane interaction, thus provide efficient guidance on membrane modification for better performance.

(3) How to better model membrane active layer structure to take into account the pores' effect on solute transport through membrane active layers? As shown throughout chapters 2-4, the existence of pores in the active layer has significant effects on the solute transport properties of membrane active layers. This study has only considered pore diameter, which is a limited study of the pore structure. With 2D/3D modeling, more parameters like average size, size distribution, and spatial resolution can be accounted for and the result would be more accurate and lead to new insights.

(4) Are transport properties of other solutes in the polyamide active layers similar to the ones studies here? Mostly NaCl (sometimes other alkali metal chlorides) and boric acid were used as example solutes in this work. Are the findings still applicable to other solutes (i.e., other contaminants of interest in water treatment)? Or will the change in solute significantly change the interaction between solute and active layers? Besides, it will be good to investigate how solution chemistry, other than pH studies here, affect solute transport properties in membrane active layers, which may provide new insight for membrane development process operation.

APPENDIX A: SUPPORTING INFORMATION FOR CHAPTER 2

Section S1. Measurement of concentration of negative fixed charges in active layer.

The concentration of negative fixed charges at pH=5.3 and 8.0 in the active layer of the SWC4+ membrane was measured using the QCM-based procedure described in detail in our previous work.[1] The coated sensors used to measure the negative fixed charge were the same three coated sensors used in the partitioning tests. In brief, with the coated sensors placed in the QCM, the negative fixed charges were saturated with cesium ions (Cs^+) by exposing the coated sensors to a 0.001 M cesium chloride (CsCl) solution at pH=5.3 or 8.0. The corresponding mass of Cs^+ (Δm_{Cs}, $ng.cm^{-2}$) neutralizing the fixed charges in each sensor was measured with the QCM. Given that Cs^+ has on average less than one water molecule of hydration,[2] and there is a 1:1 correspondence between carboxylate groups and Cs^+ ions, the molar concentration of fixed charges was calculated as

$$C_{FC} = \frac{\Delta m_{Cs}}{(1 - f_v) MW_{Cs} \delta}, \tag{A1}$$

where MW_{Cs} = 132.91 $g.mol^{-1}$ is the molecular weight of cesium, f_v (unitless) is the void fraction of the active layer, and δ (cm) is the active layer thickness. The active layer thickness was calculated for each coated sensor as

$$\delta = \frac{m_{AL}}{\rho_{AL}}, \tag{A2}$$

where ρ_{AL}=1.24 $g.cm^{-3}$ corresponds to the mass density of the active layer.[3] Using this procedure, we estimated C_{FC} = 0.061±0.018 M at pH=5.3 for the triplicate QCM sensors tested for partitioning tests at pH=5.3 with all solutes. We also estimated C_{FC} = 0.063±0.003 M and

0.198±0.051 M at pH=5.3 and 8.0, respectively, for the NaCl partitioning tests evaluating pH effect on salt partitioning.

Due to different ion activities at different ionic strengths, C_{FC} values measured at $C_{S,bulk}$ = 0.001 M may be slightly different from those at other $C_{S,bulk}$ conditions. However, there is no experimental method available to measure C_{FC} at non-dilute conditions, nor a theoretical approach to calculate accurately how C_{FC} changes with $C_{S,bulk}$. This is because there are no means to accurately estimate activity coefficients ($\gamma\pm$) in the active layer. Nevertheless, we can make a conservative estimate of the error introduced when assuming that C_{FC} is the same at all $C_{S,bulk}$ values. Assuming that activity coefficients in the active layer change as those in bulk solution, the greatest error occurs at $C_{S,bulk}$ ~0.5-1.0 M at which activity coefficients reach their lowest value (i.e., γ=0.65-0.75 for HCl and NaCl solutions[4]). Using pK_a=5.3 for carboxylate groups in the polyamide active layer (estimated from previous work[5]), it can be shown using acid-base chemistry[6] that the fractions (α_1) of carboxylic groups that are ionized at ionic strengths of 0.001 M ($\gamma\pm$=0.97) and 0.5-1.0 M ($\gamma\pm$=0.65) are α_1 = 0.51 and α_1 = 0.61, respectively. Therefore, the results indicate that the error in C_{FC} is not greater than 20% throughout the range of $C_{S,bulk}$ conditions tested. Given that we measured C_{FC} = 0.06 M at an ionic strength of 0.001 M, and this C_{FC} value corresponds to an areal mass of Na^+ of 16 ng.cm^{-2}, then the error would be no greater than 16 ng.cm^{-2}×20% = 3 ng.cm^{-2}. As observed in Figure 2.1, this areal mass uncertainty is negligible compared to the mass changes measured during partitioning tests.

Section S2. Determination of method detection limit and limit of quantification on *Δm* measurements.

Even though the QCM instrument has a detection limit of a few ng.cm^{-2},[24] we carefully examined the reliability of our *Δm* measurements as follows. Separate tests were performed in

which the sensors were exposed to 7 cycles of ultrapure water (30 min) and 1 mM KCl solution (30 min) with a final exposure to ultrapure water to evaluate the method detection limit (MDL) and limit of quantification (LOQ) on Δm measurements.

The MDL is defined as the lowest quantity of a substance that can be distinguished from the absence of that substance (a blank value) within a stated confidence limit.[23] The MDL is calculated as

$$MDL = t_{(n-1,1-\alpha=99)} \times S \quad , \qquad \text{(A3)}$$

where $t_{(n-1,1-\alpha=99)} = 3.143$ is the students' t value appropriate for a 99% confidence level and a standard deviation estimate with 6 degrees of freedom, and S = 3.266 ng.cm^{-2} is the standard deviation calculated from the mass changes measured in 7 replicate cycles of sample exposure to ultrapure water and 1 mM KCl solution.

The LOQ corresponds to the value above which quantitative results may be reasonably measured and is computed as

$$LOQ = 10 \times S \quad . \qquad \text{(A4)}$$

Thus, the MDL and LOQ of this partition experiment were 11 and 33 ng.cm^{-2}, respectively.

Section S3. Schematic of experimental setup for QCM tests with four sensors in parallel.

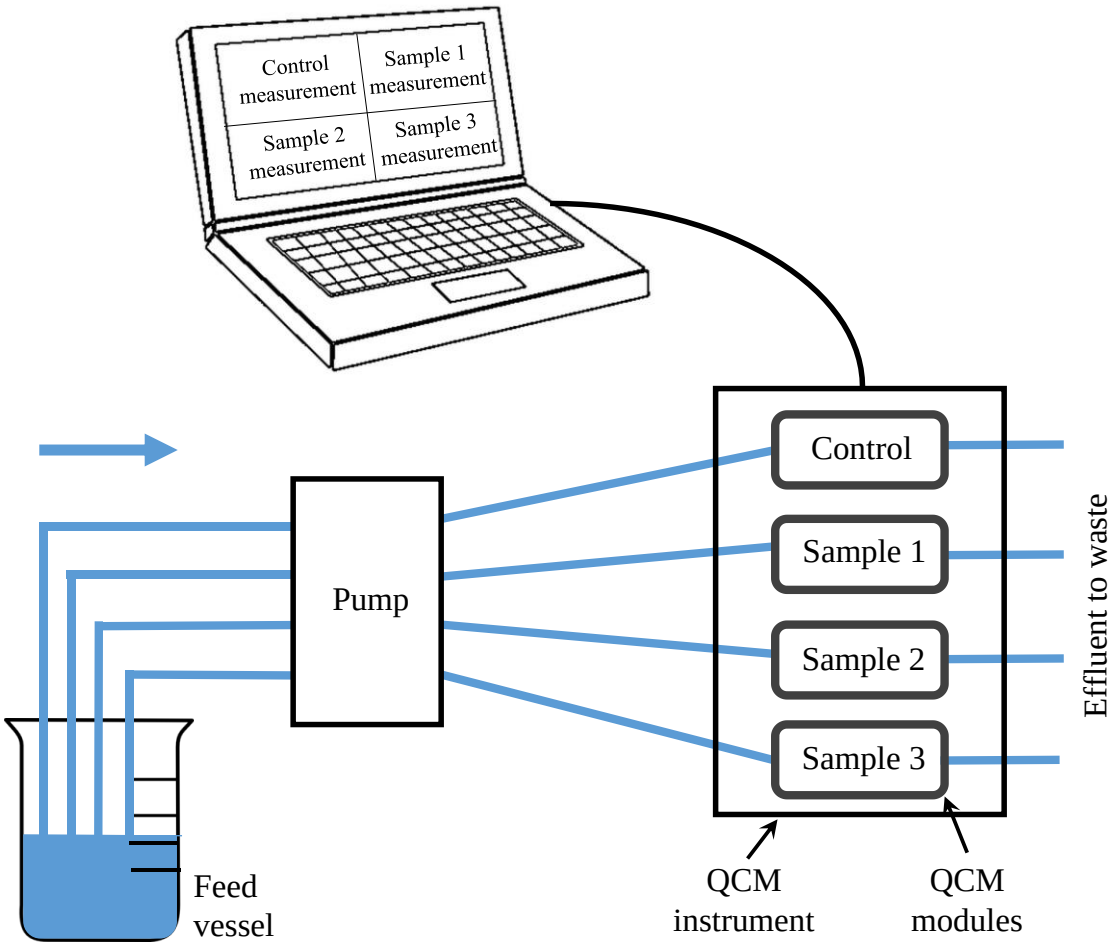

Figure S1. Schematic of experimental setup for QCM tests. The QCM instruments holds four flow modules, each of which holds one QCM sensor. One module holds an uncoated control sensor, and each of the other three modules holds a sensor coated with the crosslinked aromatic polyamide active layer of the SWC4+ membrane. The pump withdraws test solution from the feed vessel, sending the solution to the four flow modules simultaneously. In this manner, at any point during a QCM experiment, the four sensors are exposed to the same test solution.

Section S4. Evidence that isolated aromatic polyamide active layers can be approximated as rigid films for QCM data analysis.

Here we provide evidence that crosslinked aromatic polyamide films can be approximated as rigid films for QCM data modeling. All experiments were performed with a QCM-D, which monitors changes in frequency (Δf, Hz) and dissipation (ΔD, unitless) simultaneously. The viscoelastic nature of a film on a sensor can be identified by overtone (n, unitless) dependencies of the measured Δf and ΔD responses and large dissipation values. For a perfectly rigid and homogeneous film (for which the Sauerbrey equation can be used), the Δf and ΔD responses for various overtones overlap at all overtones.[7,8] On the contrary, for a viscoelastic film, the Δf and ΔD responses at different overtones would not match. In our experiments, we collected and compared Δf and ΔD data at overtones n = 3, 5, 7 and 9. The results (see illustrative data in Figure S2) show that Δf and ΔD from different overtones overlap fairly closely with each other, which indicates that the films can be approximated as rigid (note that the small overtone dependencies of Δf and ΔD are likely in part the result of the intrinsic inhomogeneity of polyamide active layers). Another criterion to decide whether the film can be approximated as rigid is the $\Delta D/(\Delta f/n)$ ratio (Hz^{-1}). Reviakine et al.[7] suggested that a film can be considered rigid when the $\Delta D/(\Delta f/n)$ ratio is less than 4×10^{-7} Hz^{-1} for 5 MHz sensors, such as those used in our study. In our partitioning experiments, all the $\Delta D/(\Delta f/n)$ values are less than 4×10^{-7} Hz^{-1}. While the above guidelines support the validity of approximating the isolated crosslinked aromatic polyamide active layers as rigid films, the strongest evidence for the validity of the rigid film approximation is the experimental evidence in previous studies. Specifically, we have previously shown that when we characterize the physical properties of polyamide active layers isolated on QCM sensors (i.e., concentration of fixed charges,[1] void fraction,[9] and thickness[3]) by approximating the isolated active layers as rigid films (i.e., by using the Sauerbrey equation to analyze the QCM data), we obtain the same results

as when we characterize the (non-isolated) active layers in intact membranes using other analytical techniques.

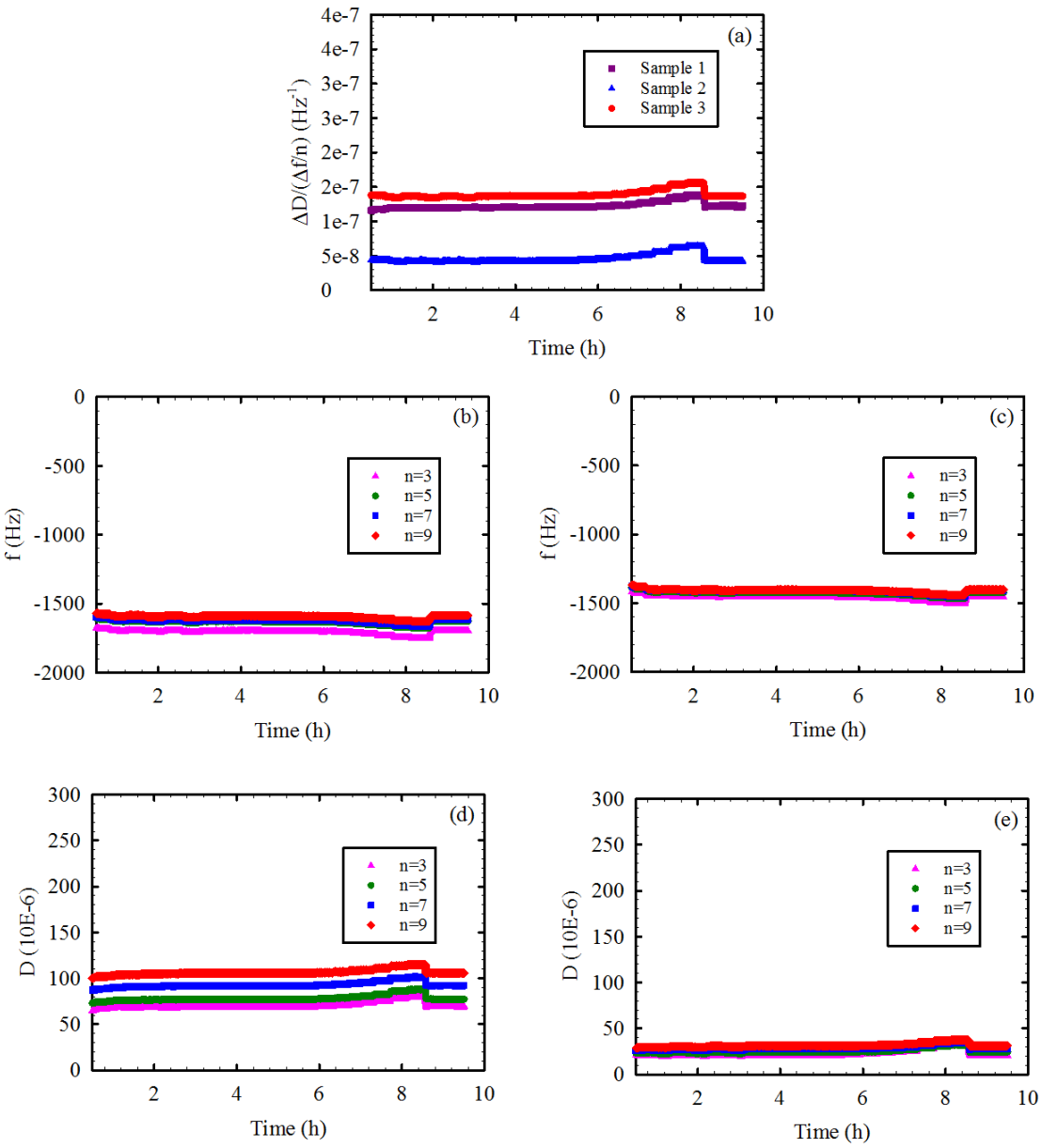

Figure S2. Representative data for (a) $\Delta D/(\Delta f/n)$ ratio, (b,c) frequency change (Δf), and (d,e) dissipation change (ΔD) for sensors coated with the crosslinked aromatic polyamide active layer of the SWC4+ membrane. Panel (a) shows results for the three sensors. Sample 1 and sample 3 behaved similarly, while Sample 2 had a lower $\Delta D/(\Delta f/n)$ ratio. Panels (b) and (d) present Δf and ΔD data, respectively, for Sample 1 as representative of Samples 1 and 3. Panels (c) and (e) present Δf and ΔD data, respectively, for Sample 2.

Section S5. Application of Manning ion condensation theory to the calculation of salt partition coefficients in polyamide active layers.

Background and assumptions. Manning's counter-ion condensation theory, originally developed for linear polyelectrolytes in salt solution, was recently demonstrated to successfully predict the partitioning of co-ions into charged polymer ion-exchange membranes.[10,11] When applied to membranes, this theory provides a way to predict ion activity coefficients in the membrane phase. Its apparent success in ion exchange membranes and underlying development based on electrostatic interactions suggest that it could provide a useful complement to conventional Donnan theory for RO/NF membranes, as Donnan theory normally requires assumptions about the membrane-phase activity coefficients.[10] However, to our knowledge, Manning theory has not yet been applied to RO/NF membranes, which carry a significantly lower fixed charge concentration than ion exchange membranes.

The development of the Manning theory contains several assumptions that may limit its applicability to RO/NF membranes. First, it assumes that fixed charge groups in the membrane are close enough together that they can be approximated by a uniform line charge.[12] This assumption may break down due to the relatively low charge of RO/NF membranes (e.g., 0.061 M for the SWC4+ membrane at pH=5.3). The theory also assumes that adjacent fixed charge groups do not interact with one another (i.e., they are screened by ions and solvent dielectric effects).[12] Like Donnan theory, Manning theory considers only electrostatic interactions between ions and fixed charges. Therefore, steric effects and hydrophobic interactions are not accounted for. Finally, it should be noted that Manning theory was developed as a "limiting law" most appropriate near zero salt concentration.[13] Nevertheless, its success in predicting sorption for external salt concentrations of up to 1 M in ion exchange membranes[10] suggests that this limitation may not be of practical significance.

Calculation of the Manning parameter (ξ). Central to the development of the Manning theory is the "Manning parameter" (ξ, unitless). Briefly, if the fixed charge groups are closer together than a certain critical distance characterized by ξ, then counter-ions in solution "condense" or become permanently associated with the charged groups.[11,12] Ions that condense are effectively removed from the adjacent solution and reduce the apparent membrane charge density acting on the ions remaining in solution.

The Manning parameter is defined as the ratio between the Bjerrum length (λ_b, m) of the solution in contact with the polymer (in the case discussed here, the membrane-phase solution) and the average distance (b, m) between fixed charge sites on the polymer chain. ξ is calculated by[10]

$$\xi = \frac{\lambda_b}{b} = \frac{e^2}{4\pi\varepsilon_o\varepsilon_r kTb} \quad , \qquad \text{(A5)}$$

where e (C) is the fundamental charge, ε_o (F.m^{-1}) is the vacuum permittivity, ε_r (unitless) is the relative permittivity (dielectric constant) inside the membrane, k (J.K^{-1}) is the Boltzmann constant, and T (K) is the temperature.

To estimate ξ for the polyamide active layer of the SWC4+ membrane it is therefore necessary to determine the relative permittivity inside the membrane and the distance between fixed charges. More specifically, since Donnan-Manning theory assumes a homogeneous charged domain, these parameters must be determined for the polyamide phase itself. As noted in the main text, polyamide active layers contain voids in addition to polymer. Therefore, the presence of these voids must be accounted for when calculating ξ.

The relative permittivity of the hydrated polyamide phase was calculated following the

approach of Kamcev et al.[11] via a volume-fraction-weighted average of the permittivity of pure water (80.1)[14] and of polyamide in the active layer. The permittivity of dry polyamide was estimated as 3.4 by Bason et al. based on structure-property correlations,[15] and this value is consistent with the typical range of 3-6 reported by others for polymers typically used in NF membranes.[16]

To determine the volume fraction of water in the hydrated polyamide phase, the observed water uptake was first corrected for the presence of voids by subtracting the mass of water in the voids from the total mass of water absorbed. The mass of water absorbed by the active layer (Δm_w, ng.cm^{-2}) is given by

$$\Delta m_w = m_L - m_{AL} \quad , \qquad \text{(A6)}$$

where m_L (ng.cm^{-2}) is the measured mass of the (wet) coated QCM sensor when the sensor is exposed to ultrapure water, and m_{AL} is the measured mass of the (dry) coated sensor when it is exposed to air. The mass of water absorbed by the voids ($m_{w,v}$) is calculated as

$$m_{w,v} = f_v \delta \rho_w \quad , \qquad \text{(A7)}$$

where ρ_w = 0.998 g.cm^{-3} is the density of pure water. Any water absorbed by the active layer that is not inside the voids must be absorbed the polyamide itself. Therefore, the mass of water in the hydrated polyamide phase ($m_{w,p}$) is given by

$$m_{w,p} = \Delta m_w - m_{w,v} \, , \qquad \text{(A8)}$$

and the volume of water absorbed by polyamide per unit area of active layer ($V_{w,p}$, cm^3.cm^{-2} active layer), is given by

$$V_{w,p} = \Delta m_{w,p} / \rho_w \quad . \qquad \text{(A9)}$$

The active layer thickness δ, calculated from measured mass (see main text) can be interpreted as the volume of active layer (including voids) per unit area of active layer ($cm^3.cm^{-2}$). Therefore, the volume of polyamide per unit area of active layer (V_p, $cm^3.cm^{-2}$ active layer) is

$$V_p = (1 - f_v)\delta \quad , \tag{A10}$$

and the volume fraction of water in the hydrated polyamide phase (ϕ, unitless), is given by

$$\phi = \frac{V_{w,p}}{V_p} = \frac{V_{w,p}}{(1 - f_v)\delta} \quad , \tag{A11}$$

where δ and $V_{w,p}$ are expressed in consistent units (e.g., $cm^3.cm^{-2}$). In calculating the volume fraction, we ignore the possibility of osmotic (de)swelling of the active layer (see main text). After calculating the volume fraction (22%) of water in the polyamide phase, we estimated the relative permittivity of the hydrated polymer as 20.0.

In the original development of the Manning theory, the distance between fixed charge groups was calculated based on the (linear) polymer structure. In this work, however, we lack precise information about the polymer structure of the SWC4+ membrane, and the geometry of interest is a 3-dimensional region rather than a linear polymer in solution. As such, we assume that the fixed charges are uniformly distributed throughout the active layer and use the lattice distance, based on the measured concentration of fixed charge groups in polyamide after accounting for the presence of voids in the active layer ($\overline{C}_{FC}$, M), to determine b (m) according to

$$b = (1000\overline{C}_{FC}N_A)^{-\frac{1}{3}} \quad , \tag{A12}$$

where N_A is Avogadro's number and the overbar on $\overline{C}_{FC}$ indicates that the concentration

is expressed in moles of charge per liter of water sorbed by the polymer.

This approach to estimate *b* differs from that used by Kamcev et al.[11] for analysis of ion exchange membranes. Kamcev et al. also assumed that charged groups were uniformly distributed throughout the membrane, but they used knowledge about the polymer structure to estimate the linear distance between groups along the polymer chain. We believe that the lattice distance approach is equally consistent with the assumption of uniform charge distribution, while being more convenient to apply when details of the membrane structure are unknown. Using the above procedure, we estimated b = 2.9 nm and ξ = 0.96 for the polyamide active layer of the SWC4+ membrane.

Calculation of the mobile sorbed salt concentration when ξ < 1. As noted above, the value of the Manning parameter, ξ, determines whether or not ion condensation occurs.[12] Different equations must be used depending on whether ξ is greater or less than a critical value (1 in the case of monovalent co-ions and monovalent fixed charge groups). When the Manning expression for membrane-phase activity coefficients for $\xi > 1$ is combined with Donnan theory, the mobile sorbed salt concentration in the membrane can be determined from[10]

$$(\overline{C}_{FC} + \overline{C}_M)\overline{C}_M \left(\frac{\overline{C}_{FC}}{\xi \overline{C}_M} + 1 \right) \left(\frac{\overline{C}_{FC}}{\overline{C}_M} + 1 \right)^{-1} \exp\left[- \frac{\frac{\overline{C}_{FC}}{\overline{C}_M}}{\frac{\overline{C}_{FC}}{\overline{C}_M} + 2\xi} \right] = C^2 \gamma^2 \quad , \qquad \text{(A13)}$$

where $\overline{C}_M$ (M) is the concentration of mobile salt in the polyamide phase, γ is the mean activity coefficient of the salt in bulk solution, and as above, the overbars indicate that the concentrations are expressed in moles per liter of water sorbed by polyamide. Below we provide a parallel derivation to arrive at an equivalent equation for mobile sorbed salt concentration when

$\xi < 1$.

Chemical thermodynamics dictates that at equilibrium, the activity of the salt in bulk solution must be equal to the activity of salt inside the membrane. However, due to Donnan equilibrium, the cation and anion concentrations in the membrane may not be equal, so the equality of activity between the two phases must be expressed as[11]

$$\left(\gamma_{M,+}\overline{C}_{M,+}\right)\left(\gamma_{M,-}\overline{C}_{M,-}\right) = C^2\gamma^2 \quad , \qquad \text{(A14)}$$

where γ_M refers to the activity coefficient inside the membrane, and the subscripts + and – indicate the cation and the anion, respectively. Furthermore, electroneutrality must be maintained inside the charged polymer, and thus for the case of monovalent 1:1 salts (such as the metal alkali salts studied here)

$$\overline{C}_{M,+} - \overline{C}_{M,-} + \omega\overline{C}_{FC} = 0 \quad , \qquad \text{(A15)}$$

where ω is the charge (including sign) of the fixed charged sites in the polymer. In the case of polyamide active layers the charge arises from carboxylate groups (R-COO$^-$), therefore ω = -1. Equations 14 and 15 can be combined to yield

$$\overline{C}_{M,-}(\overline{C}_{M,-} + \overline{C}_{FC})\gamma_{M,+}\gamma_{M,-} = C^2\gamma^2 \ , \qquad \text{(A16)}$$

from which the co-ion (anion) concentration in the membrane can be obtained based on the fixed charge concentration in the membrane, salt activity in solution, and ion activity coefficients in the membrane.

To obtain the ion activity coefficients inside the membrane, we turn to Manning theory. For the case when $\xi < 1$, the mean activity coefficient of mobile ions (i.e., those not associated with fixed charges) inside the membrane is given by[12]

$$(\gamma_{M,+}\gamma_{M,-})^{\frac{1}{2}} = \gamma_M = \exp\left[-\frac{1}{2}\frac{\xi\frac{\overline{C}_{FC}}{\overline{C}_M}}{\left(\frac{\overline{C}_{FC}}{\overline{C}_M}+2\right)}\right] \quad . \tag{A17}$$

In the case of monovalent salts, the co-ion concentration $\overline{C}_{M,-}$ is equal to the sorbed mobile salt concentration inside the membrane, $\overline{C}_M$. Therefore, by combining Equations 16 and 17, we obtain the expression

$$(\overline{C}_{FC}+\overline{C}_M)\overline{C}_M \exp\left[\frac{-\xi\frac{\overline{C}_{FC}}{\overline{C}_M}}{\frac{\overline{C}_{FC}}{\overline{C}_M}+2}\right] = C^2\gamma^2, \tag{A18}$$

from which the mobile salt concentration in the membrane, $\overline{C}_M$, can be determined numerically provided that the Manning parameter, the fixed charge concentration, and the bulk solution properties are known. This expression, valid for $\xi < 1$, is equivalent to Equation 13 developed by Kamcev et al. for the case when $\xi > 1$.

Prediction of salt partition coefficients. Membrane phase mobile salt concentrations, $\overline{C}_M$, were obtained by solving Equation 18 numerically via Brent's method. The solver was implemented in Python[17] using the brentq algorithm from the SciPy package[18] with an absolute tolerance of 10^{-6}. Bulk solution activity coefficients were calculated using pyEQL[19] via the Pitzer model.[20,21] The $\overline{C}_M$ results obtained from Equation 18 (which are in units of moles of mobile salt in polyamide

per liter of water sorbed by polyamide) were then converted into units of moles of mobile salt in polyamide per liter of polyamide (C_M) according to

$$C_M = \frac{\overline{C}_M V_{w,p}}{\delta(1-f_v)} \quad , \qquad \text{(A19)}$$

where C_M is equivalent to $C_{S,p}$ in the manuscript. Figure S1 compares the calculated C_M with the values measured experimentally under two scenarios. The first scenario assumes that ions inside the membrane have the same hydration number as in the bulk solution, while the second scenario treats the hydration number inside the polymer as a fit parameter. Finally, $C_M = C_{S,p}$ was divided by the bulk concentration of salt ($C_{S,bulk}$) to obtain the predicted salt partition coefficients in polyamide (K_p, see Figure 3 in the main text).

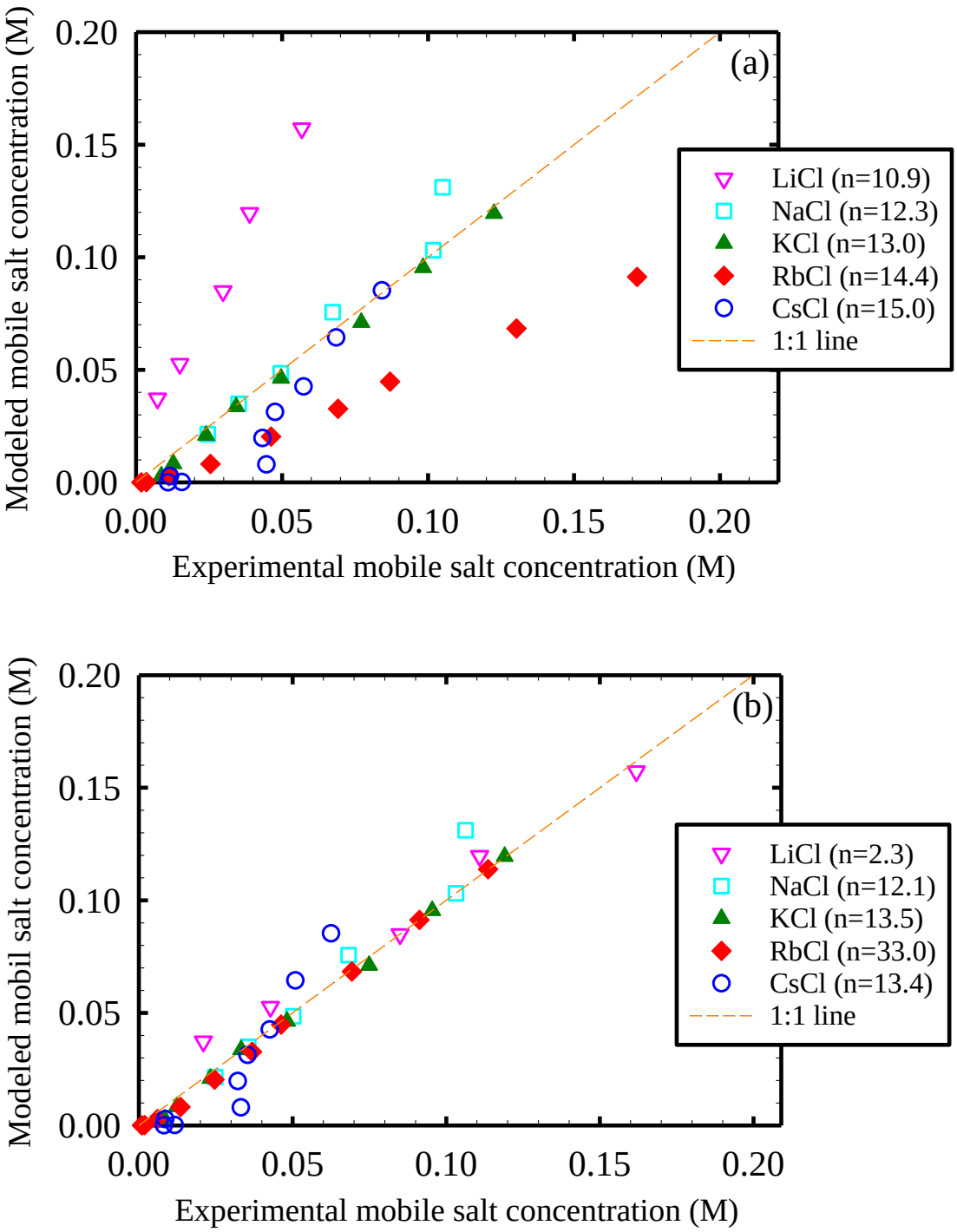

Figure S3. Parity plot comparing experimentally-determined mobile salt concentrations in the polyamide phase ($C_{S,p}$) of the active layer of the SWC4+ membrane with predictions of Donnan-Manning theory when using (a) ion hydration numbers equal to those in bulk solution (Scenario B), and (b) ion hydration numbers fitted to maximize agreement between experimental results and Donnan-Manning predictions.

Sensitivity analysis. We performed a sensitivity analysis to gain insight into which assumptions and/or measurement errors could explain deviations of the theoretical predictions from our experimental observations. Inspection of Equation 18 shows that the fixed charge concentration $\overline{C}_{FC}$ and the amount of water sorbed by the active layer (which is used to convert QCM mass data into $\overline{C}_M$ in units of moles per liter of sorbed water) are the primary variables in the Manning analysis. Therefore, both the measured water uptake and the fixed charge concentration were independently varied by +/- 20% to gauge the impact of potential measurement errors on the partition coefficients predicted by Donnan-Manning theory. The +/- 20% variation was chosen as conservative potential errors in fixed charge and water sorption values based on our studies on fixed charge[1] and water sorption[9] measurements. The partition coefficients predicted by the model for NaCl at a concentration of 0.4 M in bulk solution (considered to be representative of the other salts) were compared to the baseline predicted value.

The results summarized in Table S1 show that the maximum predicted variation of the predicted partition coefficient with respect to the baseline value was 20%. This result indicates that even after taking into account experimental uncertainties in the values of membrane properties used for K_p predictions by the Manning-Donnan theory, the predicted K_p values would still be lower than 1, consistent with the experimental K_p results. The sensitivity analysis results also show that the predicted K_p values are considerably more sensitive to the measured water uptake than to fixed charge concentration. This finding is consistent with the fact that the water uptake plays a role in the calculation of fixed charge density, hydrated polymer dielectric constant, distance between fixed charges, and Manning parameter, and is required for converting the predicted concentrations from units of moles of salt per liter of water sorbed ($\overline{C}_M$) to moles of salt per liter

of polyamide (C_M). By contrast, the fixed charge concentration impacts only the distance between charges and Manning parameter.

Table S1. Sensitivity of the partition coefficient predicted by Donnan-Manning theory for NaCl at a concentration of 0.4 M in bulk solution to water uptake and fixed charge concentration.

Scenario	**Parameter Varied**	
	Fixed Charge Concentration	**Water Absorption**
+ 20%	0.083	0.103
Baseline	0.086	0.086
-20%	0.090	0.069

Section S6. Osmotic dehydration.

We evaluated the potential impact of membrane dehydration (and thus shrinking) on the measured Δm at high salt concentrations in bulk solution. The analysis was based on results from previous studies[22,23] that measured water sorption by polyamide as a function of water activity. The water desorption results from these studies indicate that the water mass desorbed is very small at high water activities.[22,23] For example, Zhang et al. reported that the water mass desorbed from a 170-nm thick polyamide active layer when water activity was decreased from 1 to 0.95 was ~50 ng/cm^2. In our study, the average active layer thickness isolated on QCM sensors was 112 nm and the water activity in the solutions used in partitioning tests was in the range of 0.96-1 (calculated using the Pitzer model).[20,21,24] Assuming that the total amount of water desorption is proportional to active layer thickness, the maximum change in mass due to membrane dehydration in our experiments should be only ~33 ng.cm^{-2}, similar to the limit of quantification (33 ng.cm^{-2}). Moreover, given that the range of mass changes we measured at 1 M salt concentration was 246-1,668 ng.cm^{-2} and the expected error due to osmotic dehydration is less than 33 ng.cm^{-2}, then neglecting osmotic dehydration would lead to a maximum error in the calculated partition coefficients of less than 14% in all cases, as low as 2-3% for the higher molecular weight salts, and less than 7% for NaCl which is the salt of most relevance in water desalination applications. Thus, we calculated solute partition coefficients under the assumption that any potential loss of water mass by the active layer due to osmotic dehydration was negligible compared to the measured Δm.

Section S7. Analysis of partitioning of mobile salt into a membrane active layer from a 1 mM salt solution.

Table S2 shows the areal mass increase (Δm) expected in coated QCM sensors as a result of the partitioning of mobile salt into the polyamide active layer. The calculations assume 1 mM LiCl and 1 mM CsCl solutions and net partition coefficients in the active layer of $K_p = 1$ and $K_p = 5$. The results show that Δm was below the limit of quantification (33 ng.cm^{-2}, see Section S2) in all cases, and below the method detection limit (11 ng.cm^{-2}, see Section S2) for all cases except CsCl with K_p=5. Since our partitioning results showed that K_p<1 in all cases, and CsCl was the heaviest solute tested in our study, we conclude that the mass increase that resulted from the partitioning of mobile salt into the polyamide active layer from 1 mM solutions could be considered negligible in all cases.

Table S2. Areal mass increase (Δm) expected in coated QCM sensors as a result of the partitioning of mobile salt into the polyamide active layer from 1 mM salt solutions.

Mass increase (ng.cm^{-2})	$K_p = 1$	$K_p = 5$
LiCl	2.0	9.7
CsCl	4.1	18.1

Section S8. Calculation of Donnan exclusion coefficient as a function of salt concentration in bulk solution.

We calculated the dependence of the Donnan exclusion coefficient E on the salt concentration in solution using the Donnan theory for a system where a symmetrical electrolyte is at equilibrium with a charged film permeable to the electrolyte ions.[1] The Donnan exclusion coefficient E is given by

$$E = \exp(-\text{arcsinh}\,(\frac{C_{FC}}{2zC_{S,bulk}})) \quad \text{(A20)}$$

where C_{FC} (M), $C_{S,bulk}$ (M), and z (unitless) are the net volume-averaged concentration of fixed charges in the active layer, the concentration of the symmetrical electrolyte solution, and the charge of the ion of interest (-1 for chloride in our case), respectively. The concentration of fixed charges C_{FC} = 0.061±0.018 M at pH=5.3 was obtained experimentally as described in our previous work[2] and Section S1. The relationship between E and $C_{S,bulk}$ is shown in Figure S2.

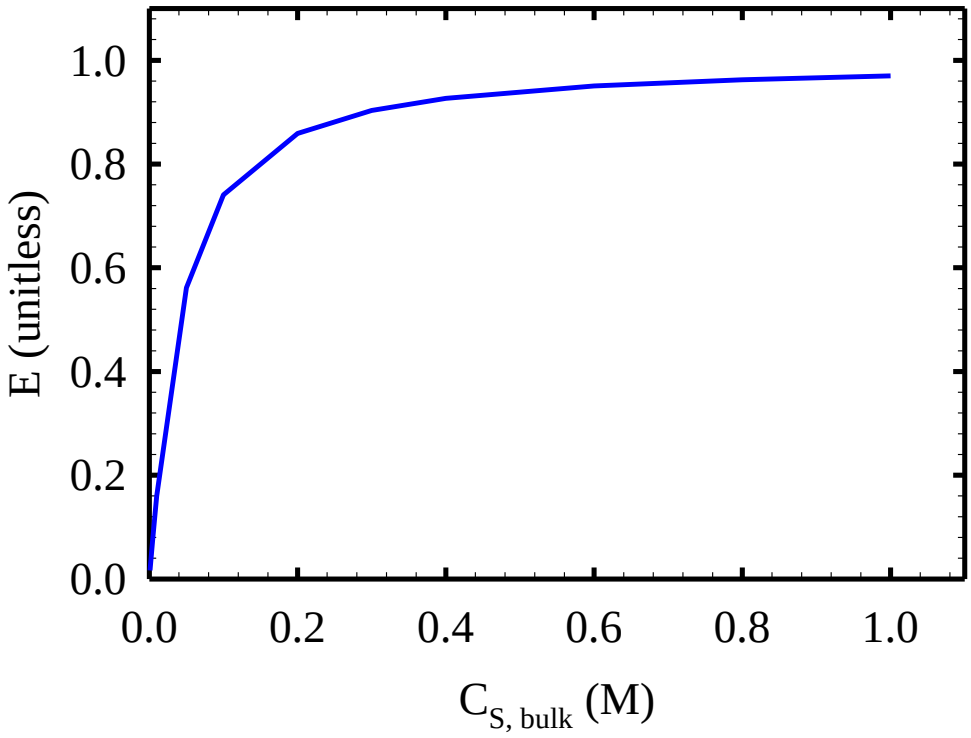

Figure S4. Dependence of Donnan exclusion coefficient (E) on salt concentration in solution ($C_{S,bulk}$) for a 1:1 symmetrical electrolyte as given by Equation 20.

Section S9. Prediction of effect of bulk solution pH on salt partitioning

We previously reported[25] that the partition coefficient of a mobile salt (K, dimensionless) in a polyamide active layer is determined by the partition coefficient of the co-ion as given by

$$K = \frac{\gamma}{\gamma_M} E \quad , \tag{A21}$$

where γ (unitless) and γ_M (unitless) are the activity coefficients of the co-ion in bulk solution and active layer, respectively, and E (unitless) is the Donnan exclusion coefficient. Note that the γ/γ_M ratio in Equation 21 above corresponds to K_p' in Equation 11 of the main manuscript. By assuming that γ_M remains approximately constant as a function of pH compared to E, the partition coefficient at pH=8.0 ($K_{pH8.0}$) was predicted based on the measured partition coefficient at pH=5.3 ($K_{pH5.3}$) using

$$K_{pH8.0} = K_{pH5.3} \frac{(\gamma E)_{pH8.0}}{(\gamma E)_{pH5.3}} \quad . \tag{A22}$$

Activity coefficients were calculated using the Pitzer model[20,21] and E was calculated as indicated in Section S8 according to

$$E = \exp(-\text{arcsinh}\,(\frac{C_{FC}}{2zC_{S,bulk}})) \quad , \tag{A23}$$

where C_{FC} (M), $C_{S,bulk}$ (M), and z (unitless) are the net volume-averaged concentration of fixed charges in the active layer at the pH of interest, the concentration of the symmetrical electrolyte solution, and the charge of the ion of interest (-1 for chloride in our case), respectively. The concentrations of fixed charges C_{FC} =0.063±0.003 M at pH=5.3 and C_{FC} =0.198±0.051 M at pH=8.0 were obtained experimentally with the procedure described in our previous work[1] and Section S1.

Section S10. Basis for assumption that ions partition into active layers with first hydration shell in Scenario B.

In the absence of a reference providing the number of molecules of hydration with which ions enter the active layer, we have as guidelines the studies from Geise et al,[26] Tansel et al,[27] and Lopez Cascales et al[28] which reported that the extent of ion hydration in a polymer/membrane is likely lower than that observed in a dilute aqueous solution, due to the ions losing water of hydration to enter the polymer film. This is intuitively consistent with the fact that RO membranes reject 99+% of salts, and therefore it is an energy consuming and partly sterically controlled process for them to move from bulk solution into the active layer. Further, while first hydration shells exist around most ions, well defined second hydration shells are common around more highly charged ions.[29] Also, given that the water molecules in the first hydration shell are electrostricted by the ion, and are the ones more firmly 'bound' to it,[30] then it is reasonable to assume that the water molecules of the first hydration shell are the most likely to move into the active layer with the ion. Note that this does not preclude the ion having a second hydration shell in the active layer, it just means that the water making up the second hydration shell in the active layer would be the water already present in the polymer. Under the assumption of hydrated ions partitioning into the active layer, the mass increase measured during partitioning tests would be due to the mass of the ions plus that of the first hydration shell. The hydration numbers used were those reported by Marcus[29] obtained using neutron diffraction.

REFERENCES

(1) Perry, L. A.; Coronell, O. Reliable , bench-top measurements of charge density in the active layers of thin-film composite and nanocomposite membranes using quartz crystal microbalance technology. *J. Membr. Sci.* **2013**, *429*, 23–33.

(2) Heyrovská, R. Ionic concentrations and hydration numbers of "supporting electrolytes." *Electroanalysis* **2006**, *18* (4), 351–361.

(3) Lin, L.; Feng, C.; Lopez, R.; Coronell, O. Identifying facile and accurate methods to measure the thickness of the active layers of thin-film composite membranes – a comparison of seven characterization techniques. *J. Membr. Sci.* **2016**, *498*, 167–179.

(4) Vanysek, P. Activity Coefficients of Acids, Bases, and Salts. In *CRC Handbook of Chemistry and Physics*; Hamner, W. M., Ed.; 2011; pp 5-104-5–105.

(5) Coronell, O.; González, M. I.; Mariñas, B. J.; Cahill, D. G. Ionization behavior, stoichiometry of association, and accessibility of functional groups in the active layers of reverse osmosis and nanofiltration membranes. *Environ. Sci. Technol.* **2010**, *44* (17), 6808–6814.

(6) Snoeyink, V. L.; Jenkins, D. *Water Chemistry*; John Wiley & Sons: United States of America, 1980.

(7) Reviakine, I.; Johannsmann, D.; Richter, R. P. Hearing what you cannot see and visualizing what you hear : interpreting quartz crystal microbalance data from solvated interfaces. *Anal. Chem.* **2011**, *83*, 8838–8848.

(8) Voinova, M. V.; Rodahl, M.; Jonson, M.; Kasemo, B. Viscoelastic acoustic response of layered polymer films at fluid-solid interfaces : Continuum mechanics approach. *Phys. Scr.* **1999**, *59*, 391–396.

(9) Lin, L.; Lopez, R.; Ramon, G. Z.; Coronell, O. Investigating the void structure of the polyamide active layers of thin-film composite membranes. *J. Membr. Sci.* **2016**, *497*, 365–376.

(10) Kamcev, J.; Galizia, M.; Benedetti, F. M.; Jang, E.-S.; Paul, D. R.; Freeman, B.; Manning, G. S. Partitioning of mobile ions between ion exchange polymers and aqueous salt solutions: importance of counter-ion condensation. *Phys. Chem. Chem. Phys.* **2016**, *18* (8), 6021-6031.

(11) Kamcev, J.; Paul, D. R.; Freeman, B. D. Ion activity coefficients in ion exchange polymers: Applicability of Manning's counterion condensation theory. *Macromolecules* **2015**, *48* (21), 8011–8024.

(12) Manning, G. S. Limiting laws and counterion condensation in polyelectrolyte solutions. III. an analysis based on the Mayer ionic solution theory. *J. Chem. Phys.* **1969**, *51* (8), 3249.

(13) Manning, G. S. Limiting laws and counterion condensation in polyelectrolyte solutions II. self-diffusion of the small ions. *J. Chem. Phys.* **1969**, *51* (3), 934–938.

(14) Wohlfarth, C. Permittivity (Dielectric Constant) of Liquids. In *CRC Handbook of Chemistry and Physics*; Haynes, W. M., Ed.; 2011; pp 6-187-6–208.

(15) Bason, S.; Oren, Y.; Freger, V. Characterization of ion transport in thin films using electrochemical impedance spectroscopy II: Examination of the polyamide layer of RO membranes. *J. Membr. Sci.* **2007**, *302* (1–2), 10–19.

(16) Szymczyk, A.; Fievet, P. Investigating transport properties of nanofiltration membranes by means of a steric, electric and dielectric exclusion model. *J. Membr. Sci.* **2005**, *252* (1–2), 77–88.

(17) Python Software Foundation, Python (version 3.5.2). 2016. http://www.python.org

(18) Jones, E.; E, O.; Peterson, P. SciPy: Open Source Scientific Tools for Python (version 0.17.1). 2016. http://www.scipy.org

(19) Kingsbury, R. S. pyEQL: A Python library for solution chemistry (version 0.4.0). 2016. https://github.com/rkingsbury/pyEQL

(20) Pitzer, K. S. *Activity Coefficients in Electrolyte Solutions*, 2nd ed.; CRC Press: Boston, 1991.

(21) Pitzer, K. S.; Mayorga, G. Thermodynamics of electrolytes II. Activity and osmotic coefficients for strong electrolytes with one or both ions univalent. *J. Chem. Inf. Model.* **1973**, *77* (19), 2300–2308.

(22) Zhang, X.; Cahill, D. G.; Coronell, O.; Mariñas, B. J. Absorption of water in the active layer of reverse osmosis membranes. *J. Membr. Sci.* **2009**, *331* (1–2), 143–151.

(23) Lee, J.; Doherty, C. M.; Hill, A. J.; Kentish, S. E. Water vapor sorption and free volume in the aromatic polyamide layer of reverse osmosis membranes. *J. Membr. Sci.* **2013**, *425–426*, 217–226.

(24) May, P. M.; Rowland, D.; Hefter, G.; Königsberger, E. A generic and updatable pitzer characterization of aqueous binary electrolyte solutions at 1 bar and 25 °C. *J. Chem. Eng. Data* **2011**, *56* (12), 5066–5077.

(25) Coronell, O.; Mi, B.; Mariñas, B. J.; Cahill, D. G. Modeling the effect of charge density in the active layers of reverse osmosis and nanofiltration membranes on the rejection of arsenic(III) and potassium iodide. *Environ. Sci. Technol.* **2013**, *47*, 420–428.

(26) Geise, G. M.; Paul, D. R.; Freeman, B. D. Fundamental water and salt transport properties of polymeric materials. *Prog. Polym. Sci.* **2014**, *39* (1), 1–24.

(27) Tansel, B.; Sager, J.; Rector, T.; Garland, J.; Strayer, R. F.; Levine, L.; Roberts, M.; Hummerick, M.; Bauer, J. Significance of hydrated radius and hydration shells on ionic permeability during nanofiltration in dead end and cross flow modes. *Sep. Purif. Technol.* **2006**, *51* (1), 40–47.

(28) Lopez Cascales, J. J.; Otero, T. F.; Lo, J. J. Molecular dynamic simulation of the hydration and diffusion of chloride ions from bulk water to polypyrrole matrix. *J. Chem. Phys.* **2004**, *120* (4), 1951–1957.

(29) Marcus, Y. Effect of ions on the structure of water: structure making and breaking. *Chem. Rev.* **2009**, *109* (February), 1346–1370.

(30) Robinson, R. A.; Stokes, R. H. *Electrolyte Solutions*, 2nd ed.; Butterworths: London, 1959.

APPENDIX B: SUPPORTING INFORMATION FOR CHAPTER 3

Section S1. Partition coefficients in polyamide phase (K_p) of NaCl in 5 tested membranes.

The K_p results reported in Table S1 and S2 correspond to those obtained at a salt concentration in bulk solution of $C_{s,bulk}$ = 0.6 M, which is representative of the ionic strength of seawater. As $C_{s,bulk}$ = 0.6 M, the Donnan exclusion coefficient is equal to E = 0.98 (Equation 9), indicating that the K_p values in Table S1 and S2 are representative of partitioning under weak electrostatic (Donnna) exclusion, and could potentially be corrected for stronger electrostatic exclusion using Equations 8-9.

Table S1. Summary of partition coefficients in polyamide phase (K_p) of NaCl in the active layer of the XLE, ESPA3, NF90, SWC4+, and homemade TFC membrane at pH 5.3, 8.0 and 10.5 (experimental data and predicted results based on Donnan theory). Scenarios A and B assume unhydrated and hydrated solutes, respectively, in the polyamide phase. Reported values and uncertainties correspond to the average and standard deviation of duplicate samples of each type membrane.

scenario	hydrated solutes?	pH	K_p of NaCl				
			XLE	ESPA3	NF90	SWC4+	TFC
A	No	5.3	0.22±0.01	0.210.03	0.34±0.04	0.14±0.01	0.15±0.00
		8.0	0.19±0.00	0.19±0.03	0.33±0.04	0.12±0.01	0.13±0.01
		8.0 prediction	0.19±0.02	0.14±0.04	0.28±0.04	0.12±0.01	0.11±0.00
		10.5	0.17±0.01	0.16±0.02	0.31±0.04	0.12±0.01	0.12±0.01
		10.5 prediction	0.16±0.01	0.12±0.05	0.27±0.07	0.09±0.00	0.12±0.01
B	Yes	5.3	0.046±0.002	0.043±0.006	0.072±0.009	0.028±0.003	0.032±0.000
		8.0	0.041±0.000	0.039±0.006	0.068±0.009	0.026±0.003	0.028±0.001
		8.0 prediction	0.040±0.003	0.028±0.008	0.059±0.008	0.024±0.002	0.023±0.000
		10.5	0.035±0.001	0.034±0.005	0.064±0.009	0.024±0.002	0.024±0.002
		10.5 prediction	0.033±0.002	0.025±0.009	0.057±0.015	0.020±0.001	0.025±0.003

Section S2. Partition coefficients in polyamide phase (K_p) of all alkali metal chlorides.

Similarly to the previous section, the K_p results reported in Table S2 correspond to those obtained at a salt concentration in bulk solution of $C_{s,bulk}$ = 0.6 M.

Table S2. Summary of partition coefficients in polyamide phase (K_p) of CsCl, RbCl, KCl, NaCl, and LiCl in the active layer of the XLE Membrane at pH 5.3 and 10.5 (experimental data and predicted results based on Donnan theory). Scenarios A and B assume unhydrated and hydrated solutes, respectively, in the polyamide phase. Reported values and uncertainties correspond to the average and standard deviation of duplicate samples of XLE membrane.

membrane	scenario	hydrated solutes?	pH	Kp				
				NaCl	LiCl	KCl	RbCl	CsCl
XLE	A	No	5.3	0.22±0.01	0.25±0.03	0.11±0.01	0.45±0.10	0.36±0.09
			10.5	0.17±0.01	0.19±0.01	0.09±0.00	0.35±0.05	0.28±0.04
			10.5 prediction	0.16±0.01	0.16±0.02	0.08±0.01	0.35±0.05	0.25±0.03
	B	Yes	5.3	0.046±0.002	0.044±0.005	0.029±0.003	0.144±0.031	0.137±0.033
			10.5	0.035±0.001	0.033±0.002	0.022±0.000	0.111±0.017	0.107±0.017
			10.5 prediction	0.033±0.002	0.029±0.004	0.021±0.001	0.110±0.019	0.098±0.012

Section S3. Cross flow filtration system for membrane performance tests.

The cross flow system (Fig. S1) consists of three stainless steel test cells connected in series to a 25L feed tank, a Hydra-Cell pump (Wanner Engineering, Minneapolis, MN) and pulsation dampener (Swagelok, Wake Forest, NC), a back pressure regulator and bypass valve (Swagelok, Wake Forest, NC) to independently control pressure (70–500 psi) and flowrate (22.5 $L.h^{-1}$), pressure transducers (Omega Engineering, Swedesboro, NJ) located immediately downstream of the pump, immediately upstream of each of the four cells and immediately downstream of the third cell, and a flow meter (King Instrument Company, Garden Grove, CA) at the end of the third cell. All wetted parts of the system are stainless steel. The feed temperature was maintained at 21.9 – 22.1 °C by circulating chilled water through a stainless steel coil in the feed tank. Each of the test cells has an active membrane surface area of 35.57 cm^2. Turbulence spacers were employed in the test cells to reduce concentration polarization. Four equally spaced bolts around the periphery of the cell secure the cell lid to the base. The permeate stream from each cell was continuously recycled to the feed tank, except during sample collection for flux and rejection measurements. Three membrane samples cut from the same area of each type membrane were used in each experiment to gauge the variability between samples. The results presented are average values obtained for the three samples, and the reported uncertainty is the standard deviation of the experimental results for the three samples.

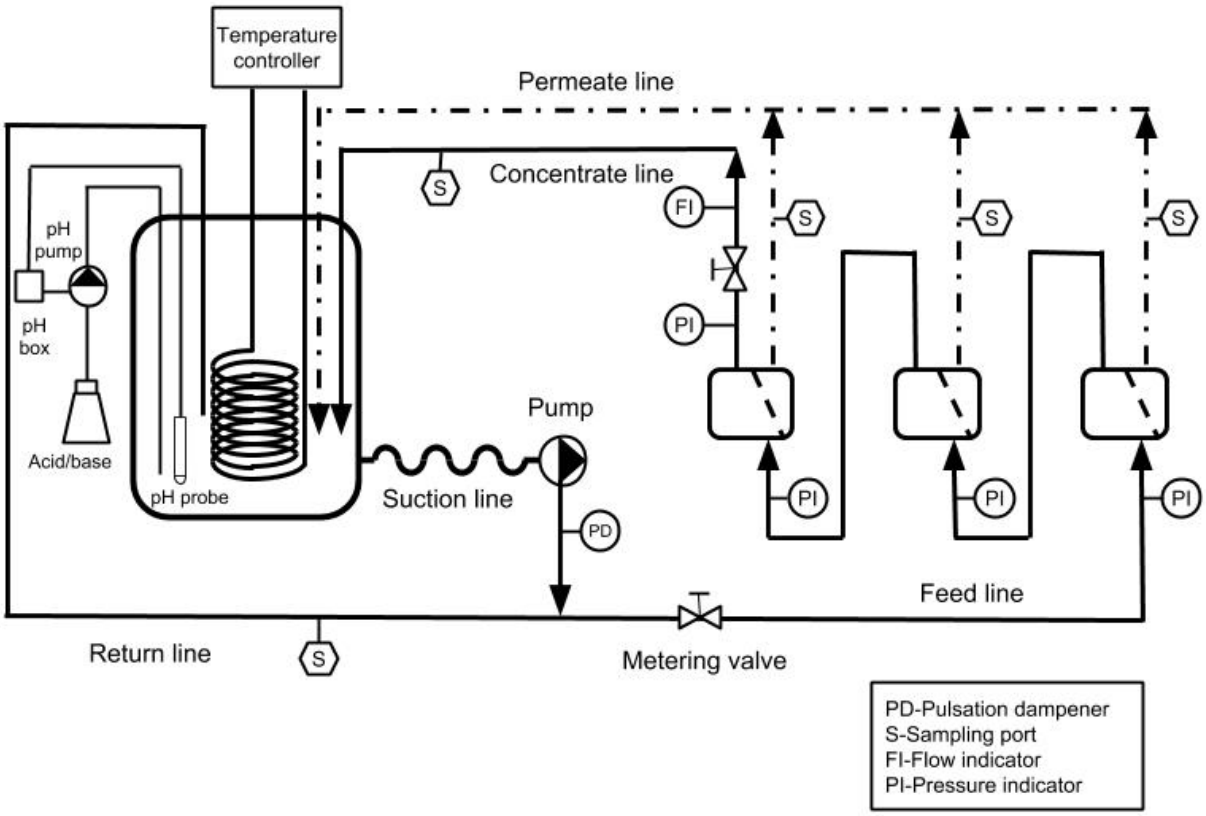

Figure B1. Schematic of cross-flow membrane filtration system used in permeation tests. Solid lines, dot-dashed lines, and dashed lines represent feed water lines, permeate lines and membranes, respectively.

APPENDIX C: SUPPORTING INFORMATION FOR CHAPTER 4

Section S1. Membrane performance tests

Table C1. Summary of salts and pH conditions evaluated for each membrane in performance tests. The concentration of salts were 0.0265M and the concentration of boron was 5mg/L as boron.

pH	LiCl	KCl	RbCl	CsCl	H_3BO_3
SWC4+	5.3	5.3	5.3	5.3	5.3, 10.5
TFC	5.3	5.3	5.3	5.3	5.3, 10.5
XLE	-	-	-	-	5.3, 10.5
ESPA3	5.3	5.3	5.3	5.3	5.3, 10.5
NF90	5.3	5.3	5.3	5.3	5.3, 10.5

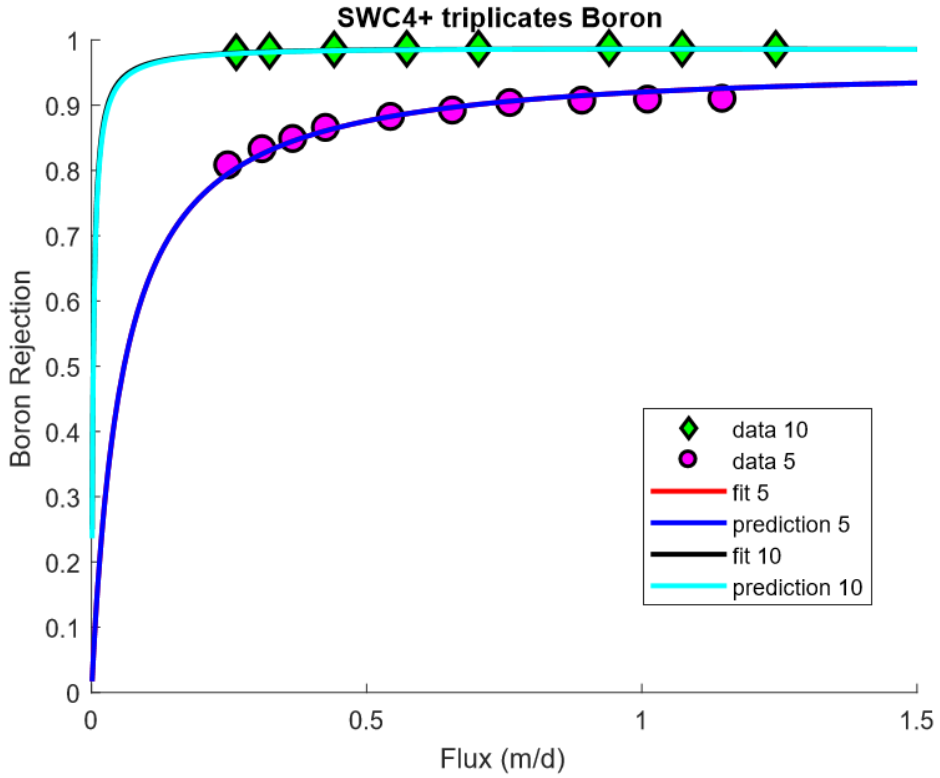

Figure C1. Rejection of boron as a function of pH by the SWC4+ membranes.

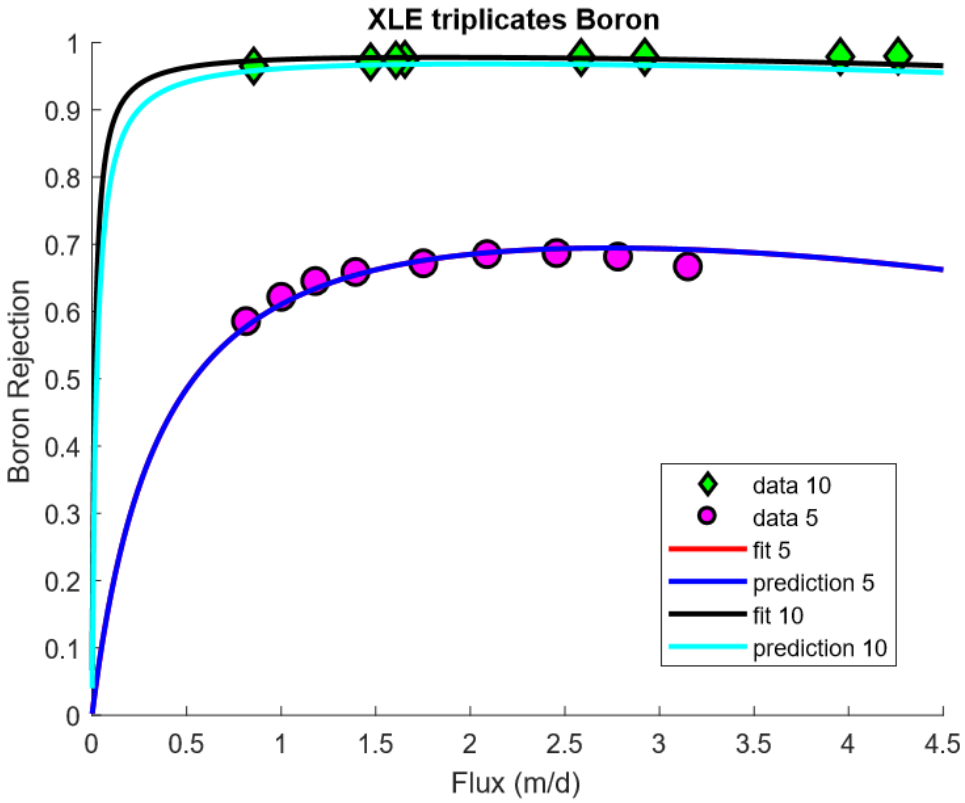

Figure C2. Rejection of boron as a function of pH by the XLE membranes.

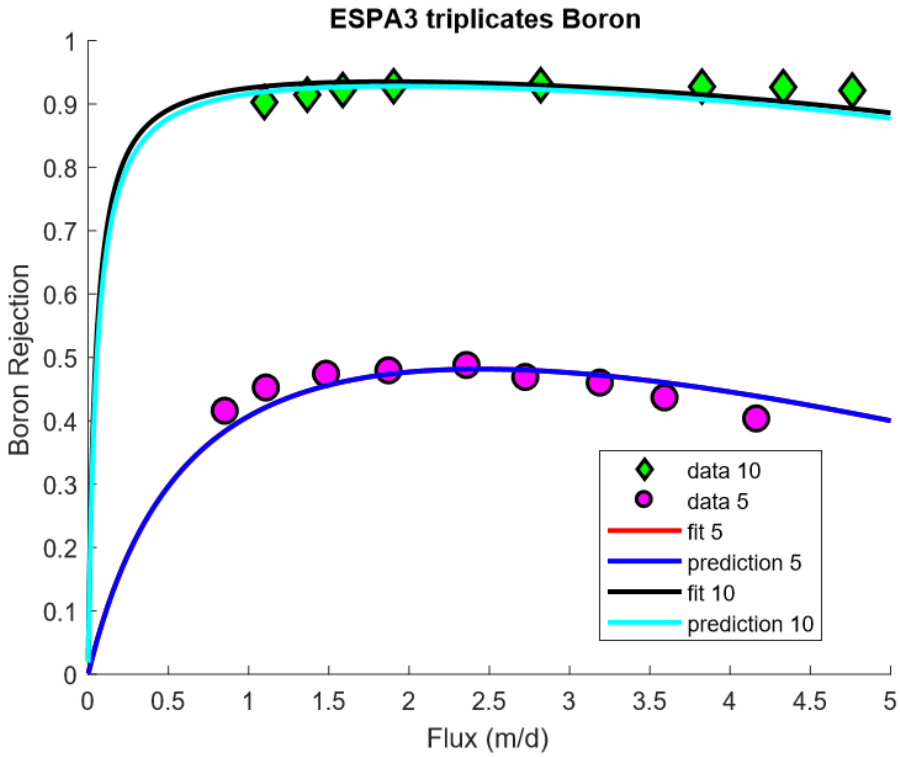

Figure C3. Rejection of boron as a function of pH by the ESPA3 membranes.

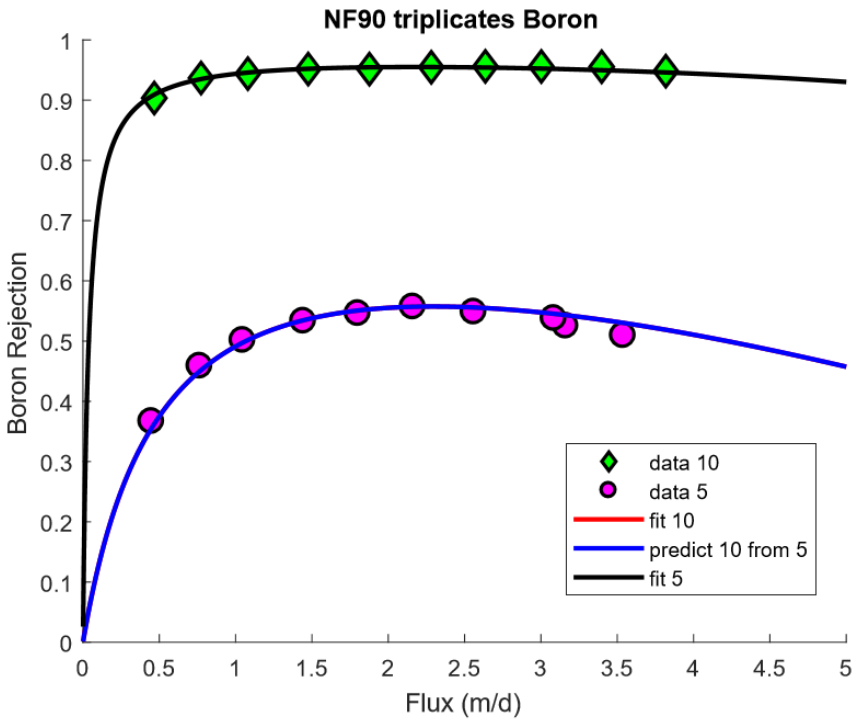

Figure C4. Rejection of boron as a function of pH by the NF90 membranes.

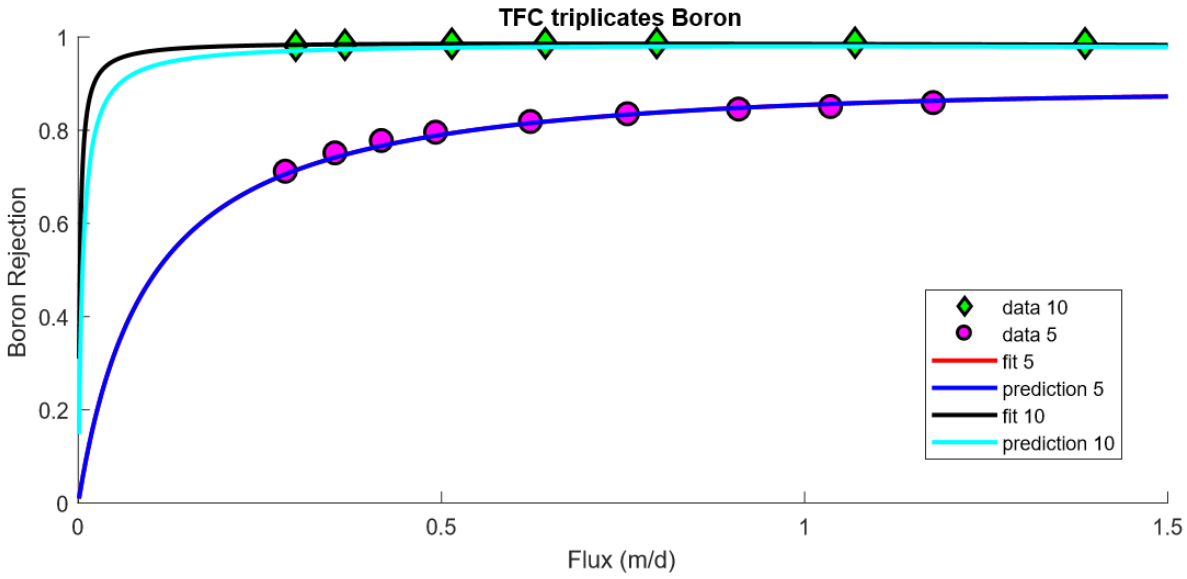

Figure C5. Rejection of boron as a function of pH by the TFC membranes.

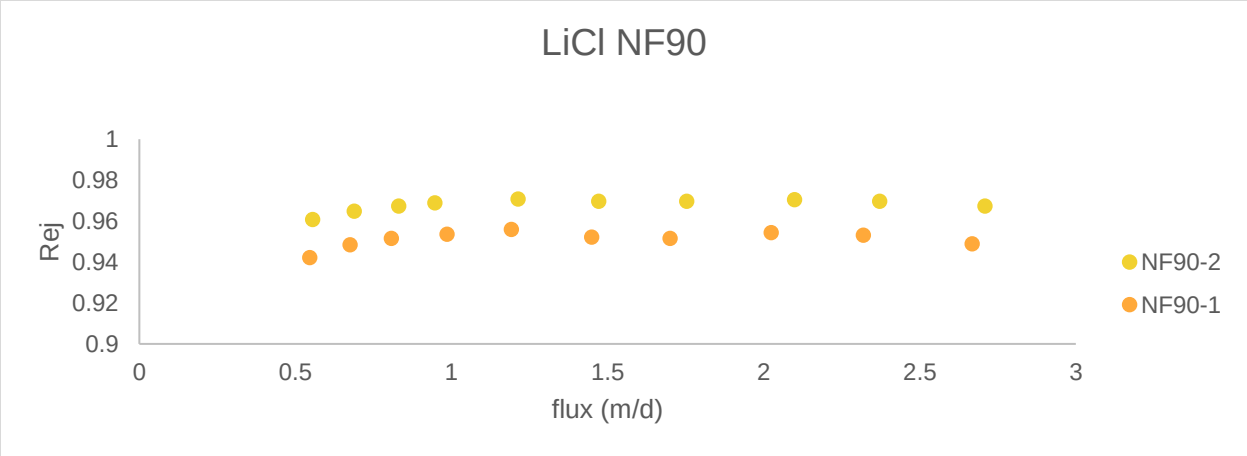
LiCl NF90
Rej
1
0.98
0.96
0.94
0.92
0.9
0
0.5
1
1.5
2
2.5
3
flux (m/d)
NF90-2
NF90-1

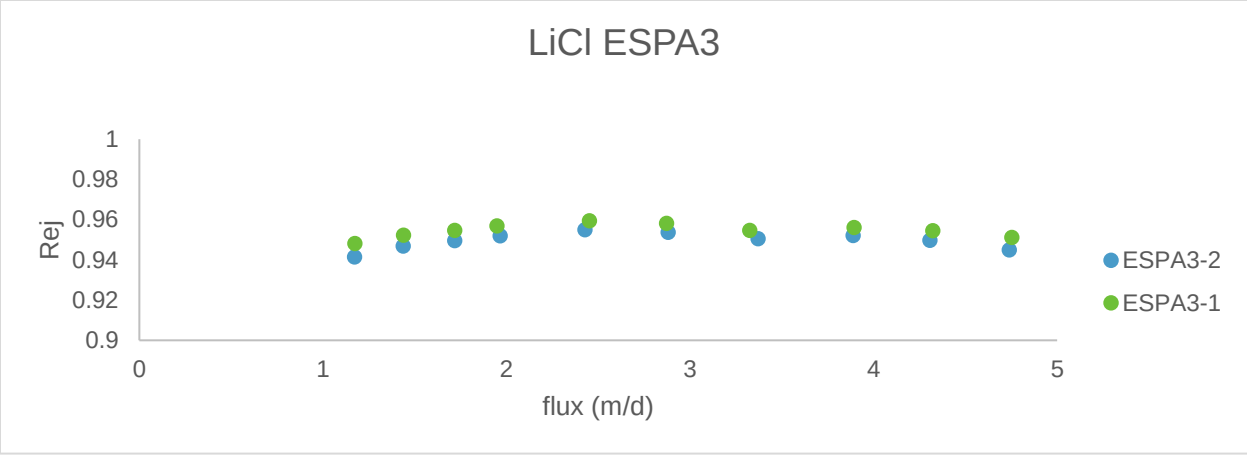
LiCl ESPA3
Rej
1
0.98
0.96
0.94
0.92
0.9
0
1
2
3
4
5
flux (m/d)
ESPA3-2
ESPA3-1

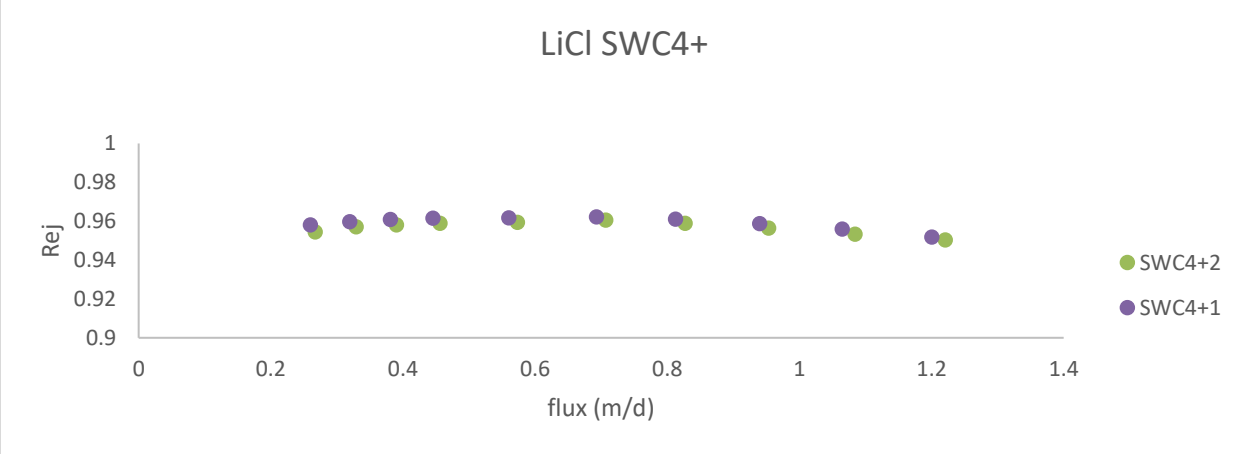
LiCl SWC4+
Rej
1
0.98
0.96
0.94
0.92
0.9
0
0.2
0.4
0.6
0.8
1
1.2
1.4
flux (m/d)
SWC4+2
SWC4+1

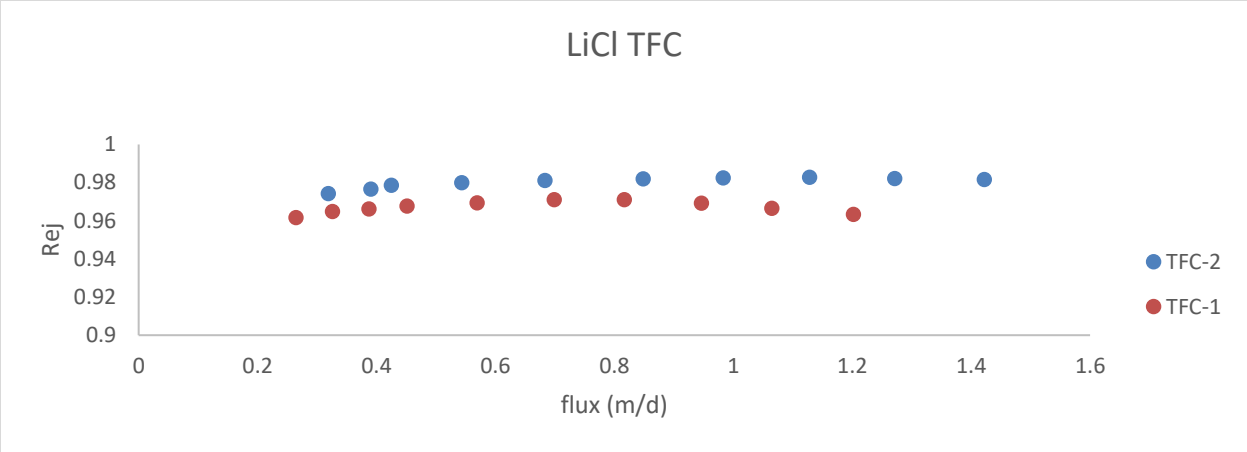
LiCl TFC
Rej
1
0.98
0.96
0.94
0.92
0.9
0
0.2
0.4
0.6
0.8
1
1.2
1.4
1.6
flux (m/d)
TFC-2
TFC-1

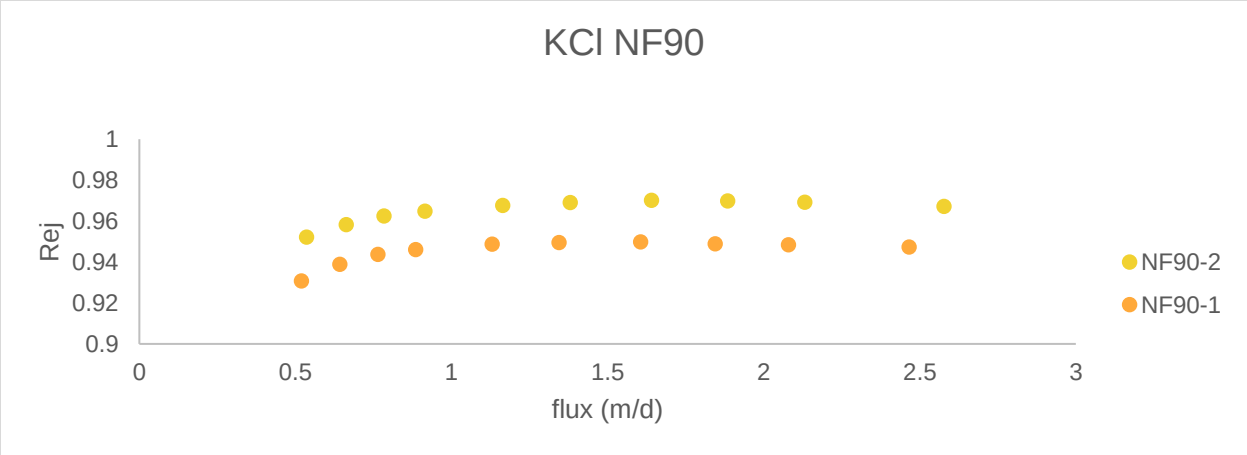
KCl NF90
Rej
1
0.98
0.96
0.94
0.92
0.9
0
0.5
1
1.5
2
2.5
3
flux (m/d)
NF90-2
NF90-1

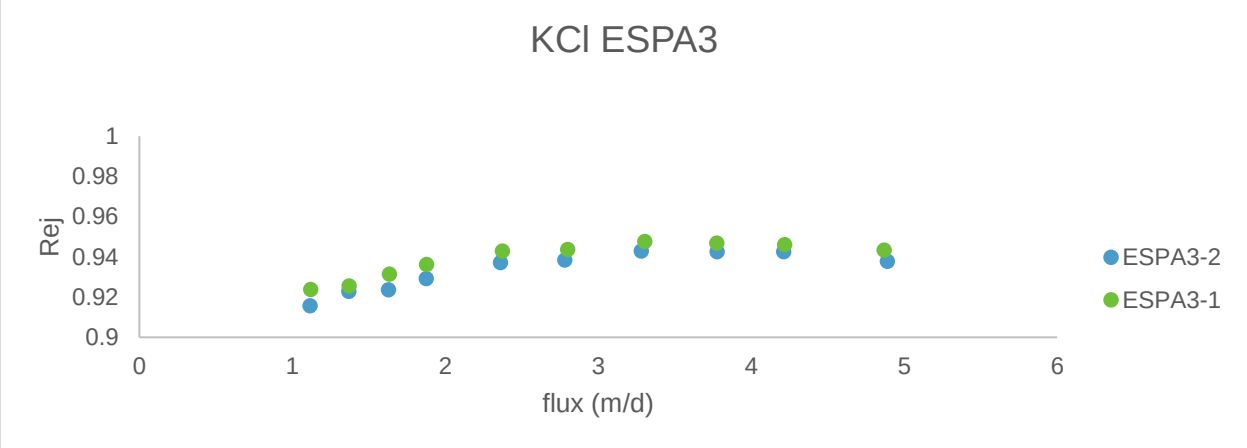
KCl ESPA3
Rej
1
0.98
0.96
0.94
0.92
0.9
0
1
2
3
4
5
6
flux (m/d)
ESPA3-2
ESPA3-1

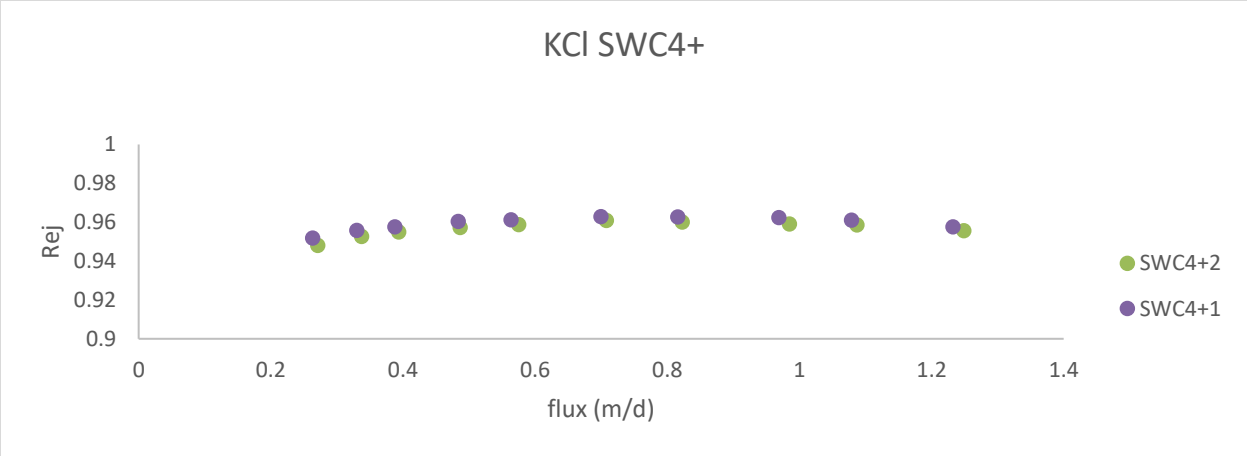
KCl SWC4+
Rej
1
0.98
0.96
0.94
0.92
0.9
0
0.2
0.4
0.6
0.8
1
1.2
1.4
flux (m/d)
SWC4+2
SWC4+1

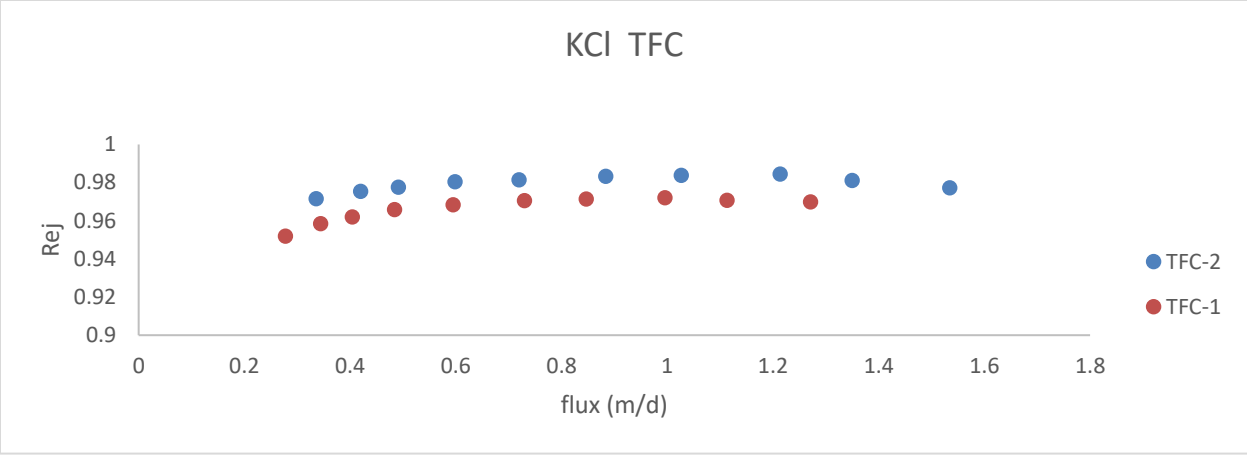
KCl TFC
Rej
1
0.98
0.96
0.94
0.92
0.9
0
0.2
0.4
0.6
0.8
1
1.2
1.4
1.6
1.8
flux (m/d)
TFC-2
TFC-1

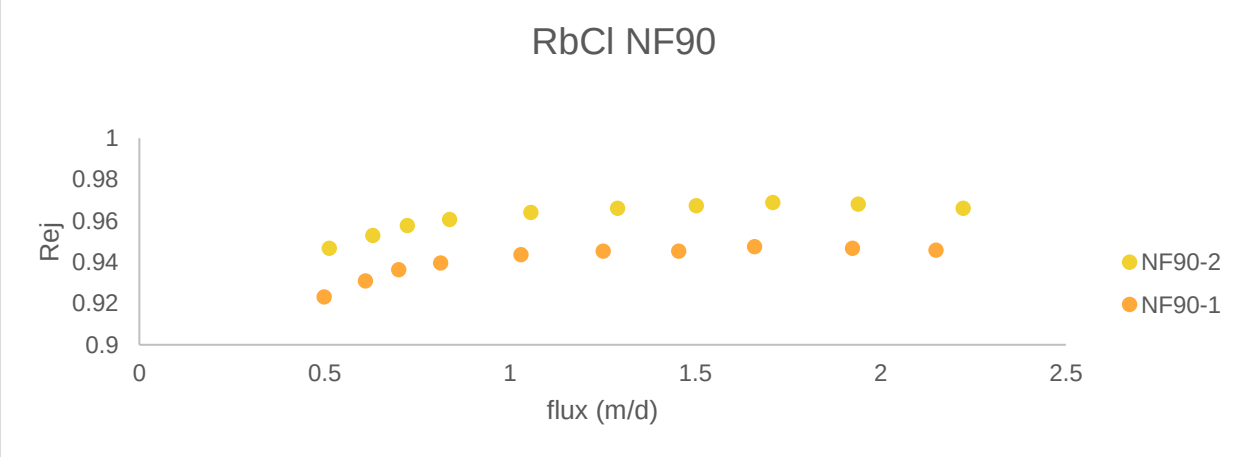
RbCl NF90
Rej
1
0.98
0.96
0.94
0.92
0.9
0
0.5
1
1.5
2
2.5
flux (m/d)
NF90-2
NF90-1

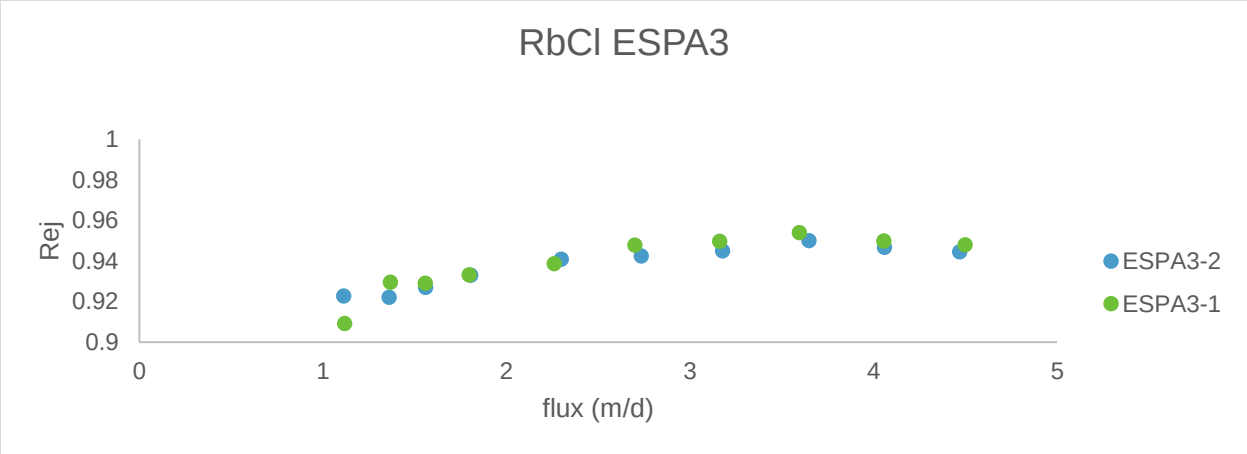
RbCl ESPA3
Rej
1
0.98
0.96
0.94
0.92
0.9
0
1
2
3
4
5
flux (m/d)
ESPA3-2
ESPA3-1

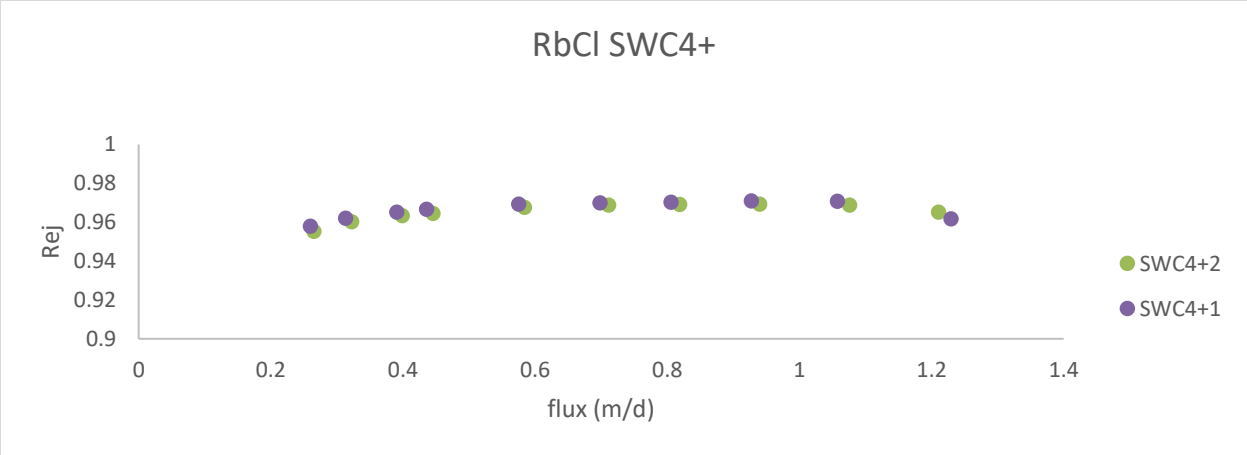
RbCl SWC4+
Rej
1
0.98
0.96
0.94
0.92
0.9
0
0.2
0.4
0.6
0.8
1
1.2
1.4
flux (m/d)
SWC4+2
SWC4+1

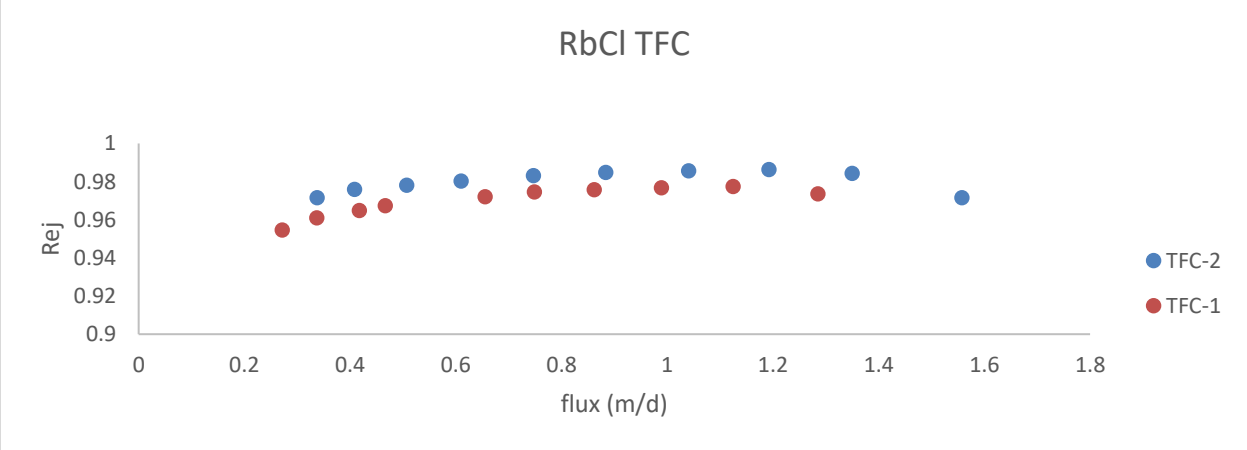
RbCl TFC
Rej
1
0.98
0.96
0.94
0.92
0.9
0
0.2
0.4
0.6
0.8
1
1.2
1.4
1.6
1.8
flux (m/d)
TFC-2
TFC-1

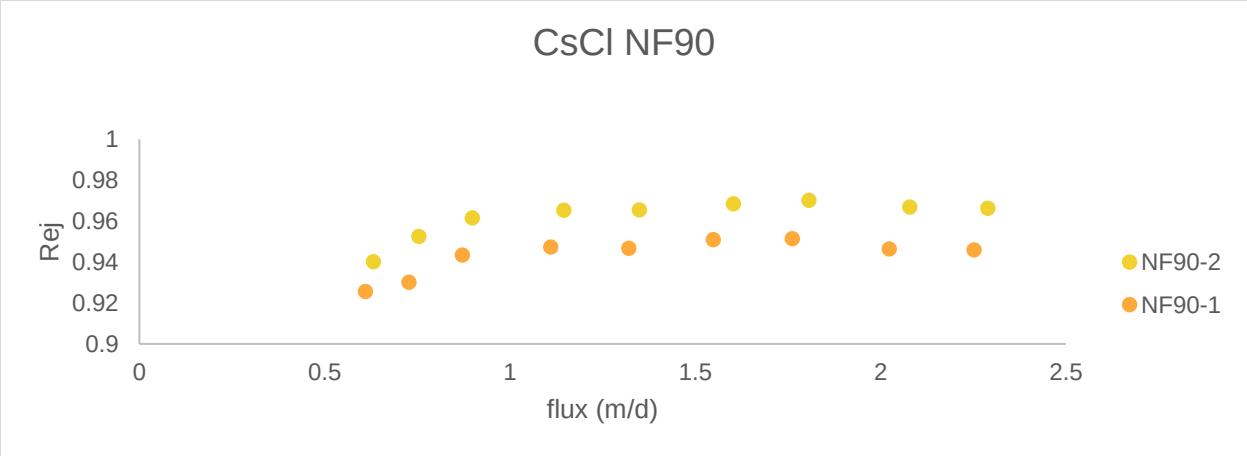
CsCl NF90
Rej
1
0.98
0.96
0.94
0.92
0.9
0
0.5
1
1.5
2
2.5
flux (m/d)
NF90-2
NF90-1

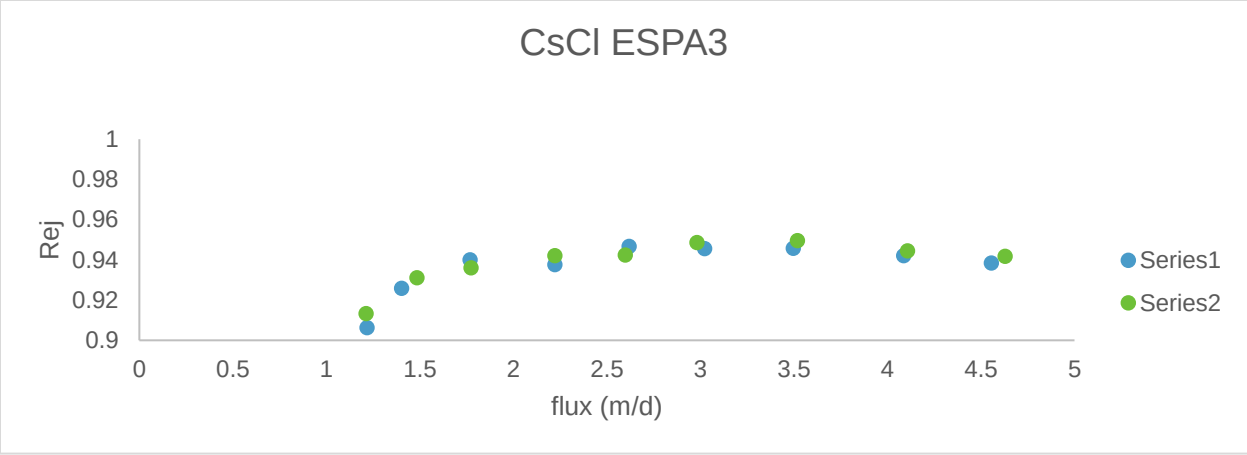
CsCl ESPA3
Rej
1
0.98
0.96
0.94
0.92
0.9
0
0.5
1
1.5
2
2.5
3
3.5
4
4.5
5
flux (m/d)
Series1
Series2

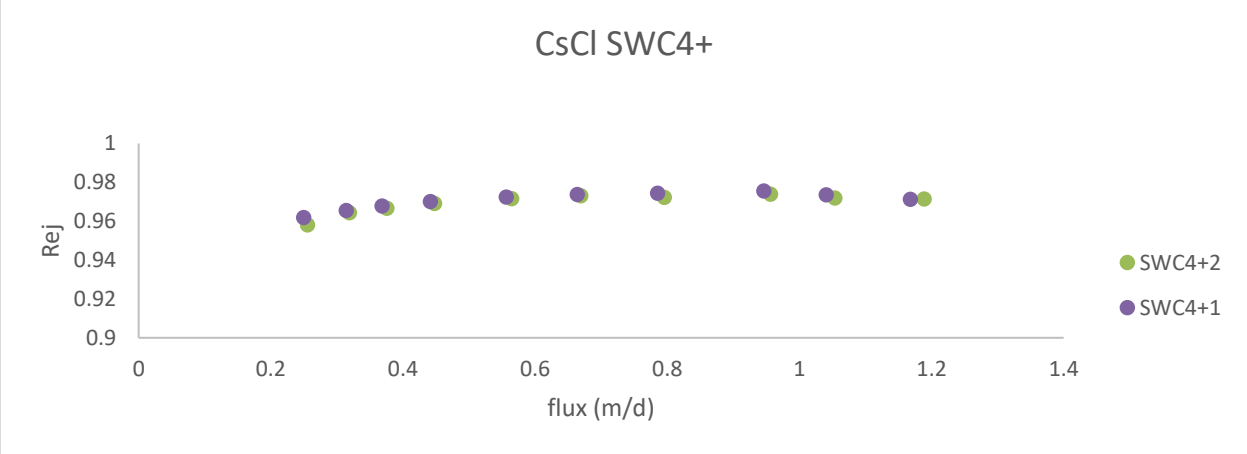
CsCl SWC4+
Rej
1
0.98
0.96
0.94
0.92
0.9
0
0.2
0.4
0.6
0.8
1
1.2
1.4
flux (m/d)
SWC4+2
SWC4+1

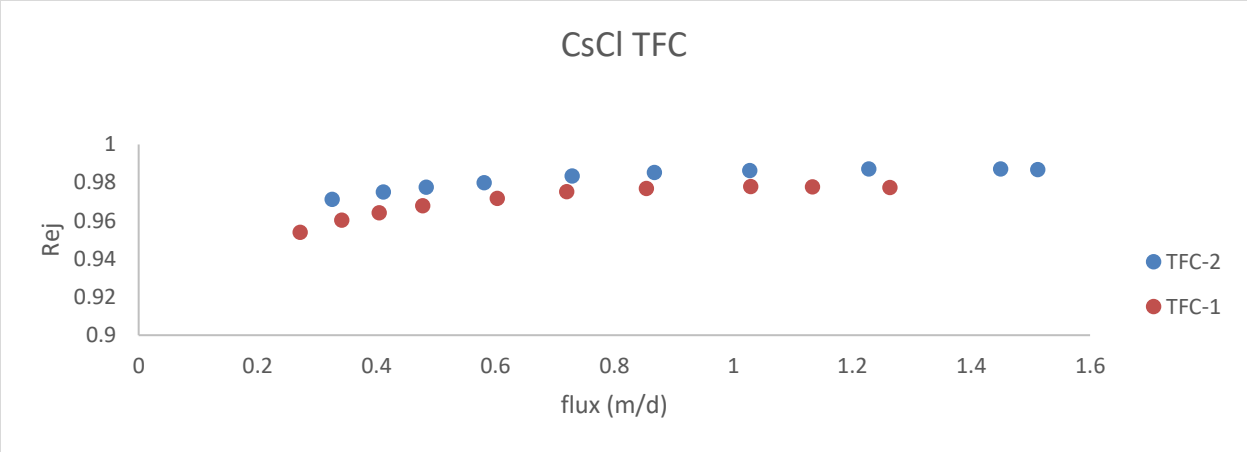

Figure C2. Rejection of LiCl, KCl, RbCl and CsCl by the SWC4+, TFC, ESPA3, and NF90, membranes.

Section S2. TFC membrane fabrication

The membrane active layer of TFC was casted on a polysulfone-polyester composite support, PS20 support. The reaction was interfacial polymerization between meta-phenylene diamine (MPD) in water at a concentration of 3.5 wt% and trimesoyl chloride (TMC) in Isopar-G^{TM} at a concentration of 0.15 wt%. The MPD solution was stirred on a stir plate at 700 rpm for ~ 3 hours and poured into a glass dish under minimal light exposure. The glass dish with the MPD solution in it was then covered with foil and stored for later use. Once the MPD and TMC casting solutions were ready, a pre-cleaned PS20 composite sheet was adhered to an 18 x18 cm^2 glass plate. The support was then exposed to the MPD solution for 2 minutes, and a squeegee was used to remove excess MPD from the support. Next, the MPD-soaked support was immersed in a TMC solution for 1 minute, which resulted in the formation of the membrane active layer. To remove unreacted TMC from the membrane active layer, the membrane was rinsed with excess n-hexanes, let dry in air for 1 minute, and thoroughly rinsed with lab grade water. The membranes were then placed in a plastic bottle filled with fresh lab grade water, and stored in the refrigerator for 24 h prior to use.

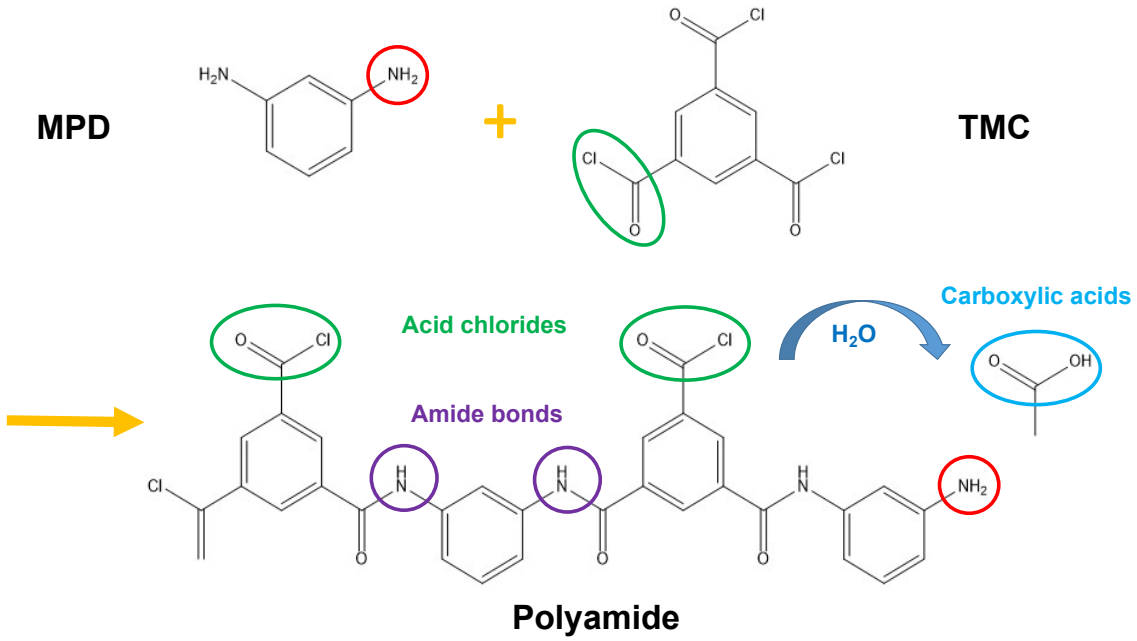

Figure C3. Polyamide formation from interfacial polymerization.

Section S3. Calculation of salt partition coefficients

The solute partition coefficient in the polymer phase, K_p, corresponds to the ratio between the concentration of solute uptake by the active layer polymer ($C_{S,p}$, M) and the concentration of solute in the bulk solution ($C_{S,bulk}$, M) as given by[1,2]

$$K_p = \frac{C_{S,p}}{C_{S,bulk}} \quad , \tag{C1}$$

where $C_{S,p}$ was calculated from

$$m_s = \delta_{AL}(C_{S,v} f MW_v + C_{S,p}(1-f) MW_p) \quad , \tag{C2}$$

where m_s (ng.cm^{-2}) is the uptake of solute by the active layer obtained from QCM tests, δ_{AL} (nm) is the total active layer thickness, $C_{s,v}$ (M) is the solute concentration in the active layer voids (equal to the solute concentration in bulk solution[2]), f (unitless) is the void fraction in the active layer,[3] and MW_v (g.mol^{-1}) and MW_p (g.mol^{-1}) are the molecular weight of the solute in the voids

and active layer, respectively. The molecular weights of solute in the voids (MW_v) and in the active layer (MW_p) were calculated as

$$MW_v = MW_{Unhydrated} \quad , \tag{C3a}$$

and

$$MW_p = MW_{Unhydrated} + n_p MW_{Water} \quad , \tag{C3b}$$

respectively, where $MW_{Unhydrated}$ (g.mol^{-1}) is the unhydrated molecular weight of the solute of interest, n_p (unitless) is the hydration number of the solute of interest in the active layer, and MW_{Water}=18.01 g.mol^{-1} is the molecular weight of water. Given that the hydration number of NaCl in the polyamide phase is unknown, two extreme cases were assumed: (i) solute in polyamide are unhydrated (n_p = 0), and (ii) the hydration number of solute in the polymer is equal to the hydration number in bulk solution.[4] The solute partition coefficients in the polyamide phase in these two scenarios were denoted as $K_{p,unhydrated}$ and $K_{p,hydrated}$, respectively.

As described above, pore structure is an important part of polyamide active layers. When immersed in solution, the pores fill with bulk solution. Thus, the net solute partition coefficient of the whole active layer $K_{AL,}$ differs from the solute partition coefficient in the polymer phase and was calculated as

$$K_{AL,unhydrated} = K_v f + K_{p,unhydrated}(1 - f) \tag{C4a}$$

$$K_{AL,hydrated} = K_v f + K_{p,hydrated}(1 - f) \tag{C4b}$$

where K_v represents the solute partition coefficient between the external solution and the solution filling up the pores. Since the solution in the pores is in equilibrium with the bulk solution in the partitioning tests, the value of K_v is 1.

REFERENCES

(1) Coronell, O.; Mi, B. Modeling the Effect of Charge Density in the Active Layers of Reverse Osmosis and Nanofiltration Membranes on the Rejection of Arsenic (III) and Potassium Iodide. *Environ. Sci. …* **2012**, *47* (Iii), 420–428.

(2) Wang, J.; Kingsbury, R. S.; Perry, L. A.; Coronell, O. Partitioning of Alkali Metal Salts and Boric Acid from Aqueous Phase into the Polyamide Active Layers of Reverse Osmosis Membranes. *Environ. Sci. Technol.* **2017**, *51* (4), 2295–2303.

(3) Lin, L.; Lopez, R.; Ramon, G. Z.; Coronell, O. Investigating the Void Structure of the Polyamide Active Layers of Thin-Film Composite Membranes. *J. Memb. Sci.* **2016**, *497*, 365–376.

(4) Marcus, Y. Effect of Ions on the Structure of Water : Structure Making and Breaking. *Chem. Rev.* **2009**, *109*, 1346–1370.